JOINT INDUSTRY PROJECT

FINAL REPORT

DEVELOPMENT OF ATTENUATION EQUATIONS FOR COMPUTING EARTHQUAKE GROUND MOTIONS AT STIFF SOIL SITES WITHIN DEEP BASINS

Submitted To:

Arco	Mobil
CNF	Shell
Exxon	Texaco
MMS	Unocal

Prepared By:

C.B. Crouse and J.W. McGuire
Dames & Moore
500 Market Place Tower
2025 First Avenue
Seattle, Washington 98121

D&M Job No.: 00216-417-004

August, 1995

Table of Contents

Development of Attenuation Equations for Computing Earthquake Ground Motions at Sites Within Deep Basins

1.0 Summary

Attenuation equations were derived for computing earthquake ground motions at stiff soil sites within deep basins. The equations are applicable to shallow crustal earthquakes with focal depths ranging from 0 to about 20 km, and moment magnitudes ranging from 5.0 to about 7.5. The ground-motion parameters predicted by the equations are peak ground acceleration (PGA) and 5%-damped pseudovelocity (PSV) response spectra at 14 oscillator periods between 0.04 and 4.0 sec; separate sets of equations were developed for the horizontal and vertical components of these parameters.

A total of 16 sets of attenuation equations were derived from nonlinear regression analyses of ground motions recorded at stiff-soil basin sites during (with one exception) California earthquakes. Each set of equations was derived for application to regions with a given amount of information known about the (1) type of earthquake mechanism (strike-slip, normal, reverse, or unknown), (2) type of site geology (stiff soil—site class B; moderately stiff soil—site class C; or, unknown, but not bedrock or soft soil), and (3) depth to basement rock beneath site (known or unknown).

The results clearly show distinct differences between the horizontal and vertical PSV response spectra predicted by the equations. For example, at short distances between the site and earthquake fault rupture, the short-period vertical PSV are similar to or greater than the horizontal PSV, whereas at longer periods greater than about 0.3 sec, the vertical PSV are less than the horizontal PSV by factors of about 2 or more.

Several other characteristics in the results were observed. First, ground motions on moderately stiff soil (site class C) are generally greater than those on stiff soil (site class B). Secondly, ground motions generated by reverse faults are greater than those generated by strike slip faults for periods of 1.0 sec or less. Finally, the results indicate that horizontal ground motions at all periods increase with increasing depth to basement rock beneath a site, whereas, the vertical motions appear to increase at short and long periods.

2.0 Introduction

This report presents the results of a joint industry project (JIP) to develop attenuation equations for computing earthquake ground motions at stiff soil sites within deep basins. The study was funded by private industry (Arco, Exxon, Texaco, Unocal, Shell, Mobil, and CNF) and federal government (Minerals Management Service), and it was motivated by the need for attenuation equations primarily oriented to offshore platform environments. During the course of the project, the Northridge, California, earthquake of moment magnitude 6.7 occurred on January 17, 1994. Because of the wealth of significant ground-motion data generated by this event, a decision was made to delay the derivation of the attenuation equations until this database became available. Although other earthquakes have occurred since then (e.g., January 17, 1995, Kobe earthquake), the data-collection phase of the project was terminated after the Northridge earthquake data were obtained to avoid further delays in disseminating the results.

The remainder of this report is organized as follows. Section 3.0 discusses the ground-motion database used in the analysis; this database is listed in Appendix A. The approach to derive the attenuation equations is described in Section 4.0, and the results are presented in Section 5.0 and Appendix B. The application of the attenuation equations in practice is discussed in Section 6.0.

3.0 Ground-Motion Database

The database is comprised of strong-motion data from 271 accelerograms recorded during the 25 earthquakes listed in Table 1. The earthquakes span the moment magnitude range $5.2 \le M_w \le 7.4$; all are shallow-crustal events, and all but one occurred in California. Only strong-motion data recorded at deep-alluvial sites within basinal environments were admitted in the database. Over half of the data are from post-1981 earthquakes not included in earlier studies of strong-motion at deep-alluvial sites (Crouse and Piazza, 1983; Crouse et al., 1985). The database listing is provided in Appendix A.

Table 1. Earthquake Catalog

Date	Name	M_w	Fault Code	No. of Records	Date	Name	M_w	Fault Code	No. of Records
1933.03.11	Long Beach	6.4	S	2	1980.01.24	Livermore	5.8	S	6
1940.05.19	Imperial Valley	7.0	S	1	1981.04.26	Westmorland	5.9	S	3
1952.07.21	Kern County	7.4	R	4	1983.05.02	Coalinga	6.4	R	20
1966.06.28	Central California	6.1	S	6	1984.04.24	Morgan Hill	6.3	S	13
1966.08.07	Baja	6.3	S	1	1986.01.26	Hollister	5.4	S	1
1968.04.09	Borrego Mountain	6.6	S	7	1986.07.08	Palm Springs	6.1	S	7
1970.09.12	Lytle Creek	5.2	R	3	1987.10.01	Whittier	6.0	R	33
1971.02.09	San Fernando	6.6	R	21	1989.10.17	Loma Prieta	7.0	S	38
1974.11.28	Central California	5.2	S	3	1990.02.28	Upland	5.6	S	2
1978.08.13	Santa Barbara	5.8	R	2	1991.06.28	Sierra Madre	5.6	R	3
1978.09.12	Tabas, Iran	7.4	R	7	1992.06.28	Landers	7.3	S	22
1979.08.06	Coyote Lake	5.8	S	5	1994.01.17	Northridge	6.7	R	37
1979.10.15	Imperial Valley	6.5	S	24					

Note: Fault Code S ⇒ *strike-slip fault event,* R ⇒ *reverse fault event*

Local geotechnical and regional geologic characteristics for each of the recording station sites were included in the database. These data were derived from soil boring logs, shear-wave velocity profiles, geologic maps, other ground-motion studies, and the results of geophysical investigations. The site classification system of Boore et al. (1993) was used to characterize the local geotechnical environment of the station sites as either site class B (soft rock or stiff soil) or site class C (medium-stiff soil). According to Boore et al. (1993), class B sites have an average shear-wave velocity, $\overline{v}_s$, in the upper 30 m of 366 to 762 m/sec; class C sites range between 183 and 366 m/sec. Only data recorded at sites with average shear-wave velocities falling within the range encompassed by classes B and C were included in the database. Of the 271 records, 112 were recorded at sites identified as class B (class B records), and

132 were recorded at sites identified as class C (class C records). The proper classification of the remaining 27 records could not be established, although they were recorded at sites known to fall within the range spanned by the two classes (class B/C records).

Regional geologic sources were used to determine whether station sites were within a basinal environment, and, when available, the depth to basement rock (alluvial depth) at the site. Only data recorded at sites within basins were included in the database. Alluvial depths were determined at sites recording 146 of the 271 records in the database. Basin boundary information was inadequate to derive other basin and site/basin characteristics that might be correlated with ground motion, such as basin size and site-to-basin edge distance.

Figure 1 shows the distribution of the 271 records in magnitude–distance (*M*–*R*) space, where the characteristic magnitude, *M*, is moment magnitude, M_w, and the characteristic source-to-site distance, *R*, is the closest distance from the site to the fault rupture surface. Note that the majority of data are within the region, $6.0 \leq M \leq 7.5$ and $10 \leq R \leq 80$ km, and that the data are fairly evenly distributed between strike-slip and reverse events.

4.0 Database Analysis

The ground-motion parameters, *Y*, investigated were peak ground acceleration (*Y* = PGA) and pseudo-velocity (*Y* = PSV), the latter at fourteen periods *T* of an oscillator with 5%-of-critical damping: *T* = 0.04, 0.10, 0.15, 0.20, 0.30, 0.40, 0.50, 0.60, 0.80, 1.00, 1.50, 2.00, 3.00, and 4.00 seconds. The 4.00 second upper period bound was determined by the long-period cutoff of the filters used to remove noise in the processing of the accelerograms in the database. Both horizontal and vertical components of the ground-motion parameters were investigated; for the horizontal component investigation, the ground-motion parameter *Y* of each record was defined as the geometric mean of the record's two horizontal component motions.

The independent variables used in the investigation characterized the earthquake (magnitude, *M*, defined as the moment magnitude, M_w, and fault-type, *F*, a binary variable used to distinguish between strike-slip and reverse events), the source-to-site distance (*R*, the closest distance from the site to the fault rupture surface), the local geotechnical environment (*S*, a binary variable used to distinguish between class B and class C sites), and the regional basin geology (*D*, the depth of alluvium at the site).

All of the ground-motion parameters were investigated by means of regression analysis. A number of regression models were investigated to determine appropriate functional relationships between the ground-motion parameter, *Y*, and the independent variables (*M*, *R*, *S*, *F*, and *D*) under a variety of ground-motion modeling scenarios that may be encountered in seismic hazard analysis. The following equation depicts the general form of these models.

$$\ln Y \;=\; p_1 \;+\; f_1(M) \;+\; f_2(R,M) \;+\; f_3(F,R) \;+\; f_4(S,R,M) \;+\; f_5(D) \qquad (1)$$

where

p_1 ≡ constant
$f_1(M)$ ≡ magnitude scaling function
$f_2(R,M)$ ≡ magnitude-dependent distance attenuation function
$f_3(F,R)$ ≡ distance-dependent fault-type scaling function
$f_4(S,R,M)$ ≡ distance- and magnitude-dependent site class scaling function
$f_5(D)$ ≡ alluvial depth scaling function

Different forms of the model resulted depending upon which, if any, of the fault-type, site class, or alluvial depth scaling functions were included in the model. Furthermore, the regressions of models which include one or more of these terms were necessarily on only those records for which the proper values of the associated variables (F, S, and/or D) were known. For models which were to include the dependence of ground-motion upon the local geotechnical environment, two approaches were adopted. In the first approach, a site-class scaling function $f_4(S,R,M)$ was included in the models, and the regressions were performed on those records in the database for which the class B/class C distinction was known. In the second approach, no site-class scaling function was used in the models, but the regressions were performed on class B records and on class C records separately, resulting in independent models for the two site classes.

As noted, the different models required analysis of different subsets of the database. Table 2 illustrates the eight different database subsets which were used; Figures 2 and 3 show the distribution of the data

Table 2. Database Subsets

Database Subset Number	Criteria for Inclusion in Database Subset: Site Classification				Alluvial Depth		Number of Records in Subset	
	B	C	B/C		unknown	known	H comp.	V comp.
1	(◆	or ◆	or ◆)	and	(◆	or ◆)	271	269
2	(◆	or ◆	or ◆)	and		◆	146	146
3	(◆	or ◆)		and	(◆	or ◆)	244	242
4	(◆	or ◆)		and		◆	139	139
5	◆			and	(◆	or ◆)	112	111
6	◆			and		◆	50	50
7		◆		and	(◆	or ◆)	132	131
8		◆		and		◆	89	89

within each subset in magnitude–distance (M–R) space. Within each database subset, each record was assigned a weight according to its location in M–R space. Referring to Figures 2 and 3, magnitude and distance intervals were defined, and the weighting scheme gave the recordings in each of the populated magnitude–distance bins the same total weight.

The regressions were performed by the BMDP Statistical Software program 3R (Dixon, 1992). The program provides as output the parameter values of the input ground-motion function that afford the best fit (in the least squares sense) between the function and the (weighted) data. It also calculates the standard error of the regression, the asymptotic standard deviation of the parameter value estimates, and the asymptotic parameter correlation matrix.

5.0 Regression Results

The regressions results (i.e., the resulting ground-motion equations) were analyzed to determine the goodness of fit between the equations and the data, to test the reasonableness of the ground-motion predicted by the equations (especially at close distances where data were less abundant), and to detect trends in the ground-motion data with respect to the independent variables. Based on these analyses, the following general regression model which was judged most appropriate.

$$ln\,Y \;=\; p_1 + p_2 M + p_3 ln\left(R + p_4 exp\{p_5 M\}\right) + p_6 S + p_7 F + p_8 D \tag{2}$$

where

- $Y \equiv$ ground-motion parameter—either PGA or PSV
- $M \equiv$ moment magnitude, M_w
- $R \equiv$ closest distance from the site to the fault rupture surface in km
- $S \equiv$ site classification code: $S = 0$ for site class B, $S = 1$ for site class C
- $F \equiv$ fault-type code: $F = 0$ for strike-slip, $F = 1$ for reverse
- $D \equiv$ depth to basement rock (alluvial depth) in km
- $p_i \equiv$ regression coefficients, $i = 1$ to 8

The equation terms involving the coefficients p_2 through p_5 proved adequate to model the magnitude scaling and the magnitude-dependent distance attenuation that were observed in the data. Simple linear site class, fault-type, and alluvial depth scaling terms are used; more complex, multivariate functions were not found to be warranted by the data.

Because strong motion data were relatively scarce for small distances–large magnitudes, it was anticipated that it might be necessary to impose constraints on some of the coefficients to ensure that the ground-motion parameter Y predicted by the regression model was an increasing function of magnitude M for all distances R. Therefore, two additional coefficients were defined:

$$q_1 \equiv {p_2}/{p_3} \qquad \text{and} \qquad q_2 \equiv -(q_1 + p_5) \tag{3}$$

The addition of these dependent regression coefficients allowed the regression equation (2) to be recast in a form more amenable to the imposition of the constraints within the 3R program:

$$ln\,Y \;=\; p_1 + p_3\left\{q_1 M + ln\left(R + p_4 exp\{p_5 M\}\right)\right\} + p_6 F \tag{4}$$

This equivalent expression was used in the regression analyses, along with the following coefficient constraints.

$$q_1 \le 0, \quad p_3 \le 0, \quad p_4 \ge 0, \quad \text{and} \quad q_2 \ge 0 \tag{5}$$

These constraints enforce the physical expectation that Y is an increasing function of M and a decreasing function of R for all positive M and R. Coefficient definitions (3) were used to convert raw regression results to the form of the general regression model, equation (2). All regression results herein are reported in terms of equation (2), unless otherwise indicated.

In application, a number of ground-motion modeling scenarios arise because it is not always possible to assign appropriate values to the site class, fault-type, and alluvial depth variables (S, F, and D). To provide ground-motion equations appropriate for these different modeling scenarios, a total of 16 variations of equation (2) were developed. Table 3 indicates the database subset which was utilized to develop each equation, the modeling scenarios for which it is applicable, and which (if any) of the terms of the general regression model are not present.

Table 3. Ground-Motion Equation Sets

Regression Equation Set No.	Database Subset No.	Applicable Ground-Motion Modeling Scenario										Term Present, Eqn. (2)					
		Site Class (within B–C range)					Fault-Type			Alluvial Depth		p_6S		p_7F		p_8D	
		Unknown	Class B		Class C		Unknown	Known		Unknown	Known	n	y	n	y	n	y
1	1	◆				and	◆		and	◆		◆		◆		◆	
2	2	◆				and	◆		and		◆	◆		◆			◆
3	1	◆				and		◆	and	◆		◆			◆	◆	
4	2	◆				and		◆	and		◆	◆			◆		◆
5	3		(◆	or	◆)	and	◆		and	◆			◆	◆		◆	
6	4		(◆	or	◆)	and	◆		and		◆		◆	◆			◆
7	3		(◆	or	◆)	and		◆	and	◆			◆		◆	◆	
8	4		(◆	or	◆)	and		◆	and		◆		◆		◆		◆
9	5		◆			and	◆		and	◆		◆		◆		◆	
10	6		◆			and	◆		and		◆	◆		◆			◆
11	5		◆			and		◆	and	◆		◆			◆	◆	
12	6		◆			and		◆	and		◆	◆			◆		◆
13	7				◆	and	◆		and	◆		◆		◆		◆	
14	8				◆	and	◆		and		◆	◆		◆			◆
15	7				◆	and		◆	and	◆		◆			◆	◆	
16	8				◆	and		◆	and		◆	◆			◆		◆

Note: Database Subset No. *refers to designation assigned in Table 2*

Each equation set provides horizontal- and vertical-component ground-motion equations for PGA and for PSV at fourteen periods T in the band $0.04 \le T \le 4.00$ sec. The values of the parameters p_i in the general equation (2) to be used with each equation set are provided in Appendix B, along with the standard errors of the regressions.

To test the validity of the ground-motion equations' representation of the data, plots of the normalized regression residuals were prepared. The normalized residual of the i^{th} datum of a regression, ϕ_i, is defined as:

$$\phi_i \equiv \frac{\left(\ln Y_i^{\text{observed}} - \ln Y_i^{\text{predicted}} \right)}{\sigma_{\ln Y}} \qquad (6)$$

where Y_i^{observed} is the i^{th} observed value of the ground-motion parameter Y, $Y_i^{\text{predicted}}$ is the corresponding value predicted by the regression equation, and $\sigma_{\ln Y}$ is the standard error of the regression. Figures 4 through 7 provide normalized residual plots for horizontal PGA and horizontal PSV at period $T = 1.00$ second, for ground-motion equation sets 1 and 12. The top frame of each plot shows the residuals plotted versus magnitude, M, and the bottom frame shows the residuals plotted versus distance, R. Ground-motion equation set 1 resulted from regression analyses of database subset number 1, which contains 271 horizontal-component records (see Table 2); ground-motion equation set 12 resulted from regression analyses of database number 6, which contains 50 horizontal-component records. The residuals from both equation sets are uniformly distributed about zero with respect to both magnitude and distance (i.e., the averages of the residuals are close to zero for small and large magnitudes and for short and long distances), which indicates that the equations model the data reasonably well. Note also that the dispersion of the residuals about the mean does not appear to vary between small and large magnitudes; this indicates that the standard error of the regression is not magnitude-dependent, as some researchers have found (Geomatrix, 1992; Idriss, 1993). Similar plots were generated for other periods and different equations, yielding similar results.

A number of plots of horizontal ground-motion attenuation and of response spectra were generated to test the reasonableness and consistency of the ground-motions predicted by the various equation sets. Figure 8 compares median horizontal ground-motion (PGA and PSV at period $T = 1.0$ sec) predicted by equation sets 3 and 8. Equation set 3 was developed using database subset 1, which contains 271 horizontal-component records (see Table 2); as shown in Table 3, the equation does not include a site-class or alluvial depth term, but does include a fault-type term. Equation set 8 was developed using database subset 4, which contains 139 horizontal-component records, approximately half the size of database subset 1; it includes site-class, fault-type, and alluvial depth terms. To compare the predicted ground-motions for similar conditions, the fault-type parameter value $F = 0$ (strike-slip), was used in both equation sets. For equation set 8, the site-class parameter value $S = 0.5$ was used. This is appropriate for comparing equation set 8 to equation set 3, since the latter neglects site class distinction and was derived from a database subset which is approximately evenly split between site classes B and C. For similar reasons, the alluvial depth parameter value $D = 3.0$ km was used in equation set 8, as this was approximately the median depth observed in database subset 4.

The plots in Figure 8 show close agreement between the two equation sets at magnitudes $M = 6.5$ and 7.5 over the distance range spanned by the data. Similar plots in Figures 9 and 10 demonstrate this consistency across database subsets and equation sets for site class B ground-motions (equation sets 8 and 12, using database subsets 4 and 6, respectively) and site class C ground-motions (equation sets 8 and 16, using database subsets 4 and 8, respectively). The consistency demonstrated in Figures 8, 9, and 10 is important because it demonstrates that the results of seismic hazard analyses using the present study are not especially sensitive to the choice of one equation set over another, provided the analysis scenario is consistent with the equation set modelling assumptions. It also indicates that ground-motion trends which are observed in the larger database subsets are present in the smaller subsets as well, permitting greater assurance that the size of the smaller subsets is adequate to develop valid inferences to trends not obtainable from the larger subsets (such as alluvial depth-dependency).

Several horizontal ground-motion trends are observed in Figures 8, 9, and 10. (1) The ground-motion attenuates more slowly for longer periods. However, the most rapid attenuation was observed at periods between $T = 0.10$ and 0.20 sec, and was slightly slower for shorter periods and for PGA. This is consistent with the findings of Boore et al. (1995), who show the greatest attenuation rate at periods $T = 0.12$ and 0.13 sec. (2) The magnitude scaling increases with increasing period, which is consistent with Boore et al. (1995) and Campbell (1990). (3) The attenuation of ground-motion with distance is slower with increasing magnitude. This trend is contrary to Boore et al. (1994), who found no statistically significant difference in magnitude scaling between data recorded within 10 km of the surface projection of fault rupture and magnitude scaling in the database as a whole. The reduction in attenuation rate with increasing magnitude is more pronounced for PGA and shorter periods, which is in general agreement with Campbell (1990), who predicts complete "saturation" at zero distance of PGA and PSV at periods $T \leq 0.30$ sec. However, only a few of the equation sets in the present study predict zero-distance ground-motion saturation, and then only at periods $T = 0.10$ and 0.15 sec. Saturation is predicted by six of the 16 equation sets for ground-motion at period $T = 0.10$ sec; saturation at $T = 0.15$ sec is predicted by only one the 16 equation sets.

Figures 11 through 14 explore the difference between site class B and class C response spectra, and compare the site class-dependency predicted by different equation sets. The top frame of each figure plots the median site class B and class C horizontal pseudo-spectral acceleration, PSA (by definition, $\text{PSA} \equiv \text{PSV} \cdot 2\pi/T$) predicted by equation set 8, which assumes a constant ratio of site class B to class C ground-motion at each period. The bottom frame of each figure plots site class B and class C PSA predicted by equation sets 12 and 16, respectively. Equation sets 12 and 16, by contrast, assume that class B and C ground-motions are independent of each other. Together, the four figures plot the equations at magnitudes $M = 6.5$ and 7.5, and distances $R = 1.0$ and 10.0 km.

It may be observed in Figures 11 through 14 that site class C ground-motions are generally greater than site class B ground-motions. This is consistent with the findings of Boore et al. (1995). The only notable exception appears in the bottom frame of Figure 12; for magnitude $M = 7.5$ and distance $R = 1.0$ km, the site class B PSA at period $T = 0.80$ sec is approximately 40 percent greater than the class C PSA. This result is probably an aberration caused by the extreme scarcity of large-magnitude, short-distance data in the database subsets used to produce equation sets 12 and 16. Comparing this plot with the equation set 8 plot in the top frame, and with the spectral shapes at the other magnitudes and distances, it is seen that at this particular magnitude–distance combination, (a) the class C PSA shows a peak at $T = 0.60$ sec and a dip at $T = 0.80$ sec, relative to other class C PSA, while (b) the class B PSA shows a dip at $T = 0.80$ sec, relative to other class B PSA. As the magnitude–distance combination moves in M–R space towards regions with more data, the PSA plots of Figures 11 through 14 become progressively smoother. Additionally, the consistency improves between equation sets 8 and 12 class B PSA, and between equation sets 8 and 16 class C PSA.

Figures 15 and 16 compare the median horizontal and vertical PSV predicted by equation set 3. It may be noted that the shapes of the horizontal and vertical PSV are significantly different, with the vertical PSV plots showing a shift in frequency content towards shorter periods, relative to the horizontal PSV. Specifically, the greatest vertical spectral accelerations occur at shorter periods ($T \leq 0.20$ sec) than the horizontal spectral acceleration peaks. For magnitudes greater than $M = 6.5$ and distances less than 10 to 30 km, the vertical spectral response at these shorter periods can be significantly greater than the corresponding horizontal response, this trend increasing with increasing magnitude and decreasing distance. At periods greater than about 0.10 to 0.20 sec however, the vertical response is approximately constant in spectral velocity and, in general, is significantly less than the horizonatal response. Below magnitude $M = 6.0$, or beyond distance $R = 30$ km, the vertical spectral response is less than the horizontal response at all periods studied.

Figures 17 through 19 show ground-motion attenuation, and compare the median horizontal ground-motion predicted by the present study with those predicted by other researchers. Figures 17 and 18 compare equation set 7 and Boore et al. (1995) ground-motions for site class B and class C conditions, respectively. Figure 19 compares equation set 4 and Campbell (1990) ground-motions. The forms of the Boore et al. and Campbell equations are as follows.

Boore et al. (1995):
$$\begin{aligned} \log Y = \; & b_{SS}G_{SS} + b_{RS}G_{RS} + b_2(M-6) + b_3(M-6)^2 \\ & + b_4R + b_5\log R + b_6G_B + b_7G_C \end{aligned} \tag{7}$$

where
- $Y \equiv$ ground-motion parameter—either PGA (in g) or PSV (in cm/sec)
- $G_{SS}, G_{RS} \equiv$ fault-type codes: $G_{SS} = 1$ for strike-slip, $G_{SS} = 0$ otherwise; $G_{RS} = 1$ for reverse, $G_{RS} = 0$ otherwise
- $M \equiv$ moment magnitude, M_w
- $R \equiv$ characteristic distance in km, $R \equiv (d^2 + h^2)^{1/2}$
- $d \equiv$ closest horizontal distance, in km, from the site to the vertical projection of the fault rupture onto the earth's surface
- $G_B, G_C \equiv$ site classification codes: $G_B = 1$ for site class B, $G_B = 0$ otherwise; $G_C = 1$ for site class C, $G_C = 0$ otherwise
- $b_i, h, b_{SS}, b_{RS} \equiv$ regression coefficients, $i = 2$ to 7

Campbell (1990):
$$\begin{aligned} \ln Y = \; & c_1 + c_2M + c_3\ln\left(R + c_4\exp\{c_5M\}\right) + c_6F \\ & + c_7\tanh\left(c_8\{c_9 + M\}\right) + c_{10}\tanh\left(c_{11}D\right) + \sum q_jK_j \end{aligned} \tag{8}$$

where
- $Y \equiv$ ground-motion parameter—either PGA (in g) or PSV (in cm/sec)
- $M \equiv$ magnitude: $M \equiv$ Richter local magnitude, M_L, for magnitudes < 6.0; $M \equiv$ surface-wave magnitude, M_S, for magnitudes ≥ 6.0
- $R \equiv$ closest distance from the site to the seismogenic rupture in km
- $F \equiv$ fault-type code: $F = 0$ for strike-slip, $F = 1$ for reverse
- $D \equiv$ depth to basement rock (alluvial depth) in km
- $K_j \equiv$ structure codes characterizing structure which houses the recording instrument, $j = 1$ to 3; $K_j = 0$ for typical instrument shelter
- $c_i, q_j \equiv$ regression coefficients, $i = 1$ to 11, $j = 1$ to 3

Equation sets 7 and 4 were selected for the comparisons since their assumed ground-motion functional dependence on the variables S, F, and D most closely resembled that of the Boore et al. and Campbell models, respectively. Both Boore et al. and equation (2) define the characteristic magnitude, M, as the moment magnitude, M_w. Characteristic magnitudes assigned by Campbell's definition are approximately the same as moment magnitude below a moment magnitude of about 8.0 (Joyner and Boore, 1988), so the characteristic magnitude definitions of the three models may be assumed to be essentially identical.

However, the definitions of the characteristic distance, R, are somewhat different between the three models, that of Boore et al. being the least like Campbell's or the present study. For the purposes of comparison, the approximate equivalence of the distance variable, R, of equation (2), and the variables d and R of equations (7) and (8), respectively, is assumed to be adequate.

Figures 17 and 18 show reasonably close agreement between the ground-motions predicted by equation set 7 and by Boore et al. (1995). Notable differences include (1) the slower attenuation of equation set 7 for shorter distances (especially for PSV at period $T = 1.00$ sec), and the faster attenuation for larger distances (especially for PGA), the transition occurring at approximately 40 to 50 km distance; and (2) the lesser magnitude scaling of equation set 7 at shorter distances and the greater magnitude scaling at larger distances, the transition occurring between approximately 10 and 30 km distance. The agreement between equation set 7 and Boore et al. is greater for magnitude $M = 6.5$ than $M = 7.5$, and for PGA than PSV ($T = 1.00$ sec). Magnitude $M = 7.5$ ground-motion at distances less than 10 km predicted by equation set 7 is less than that of Boore et al., most significantly for site class C PSV ($T = 1.00$ sec), where the difference at 1.0 km is approximately a factor of 2.5.

Figure 19 shows reasonably close agreement between the ground-motions predicted by equation set 4 and by Campbell (1990) for distances $R \leq 50$ km, the maximum record distance admitted in Campbell's database. The attenuation of equation set 4 is slower than that of Campbell, especially for PSV ($T = 1.00$ sec). The difference in magnitude scaling between short and large distances is greater for Campbell, especially of PGA, for which Campbell predicts magnitude saturation at zero distance. The slower attenuation of equation set 4 yields lesser ground-motions than Campbell for distances less than 10 km (especially for magnitude $M = 6.5$), and greater ground-motions for distances larger than 20 km (especially for magnitude $M = 7.5$). Figures 17, 18 and 19 show that equation sets 7 and 4, which display close agreement with each other, consistently predict lesser ground-motion at magnitude $M = 7.5$ than either Boore et al. or Campbell at distances less than 10 km; however, the severity of the difference varies significantly. Apart from this, differences in PGA and PSV ($T = 1.00$ sec) between the present study and the two other researchers do not appear to be consistent across magnitude or distance.

Figures 20 through 23 compare response spectra predicted by equation set 7 with that of Boore et al. for site classes B and C, at magnitudes $M = 6.5$ and 7.5, and distances $R = 1.0$ and 10.0 km. Close agreement is observed between the two ground-motion models except for magnitude $M = 7.5$ at distance $R = 1.0$ km. As shown in the bottom frames of Figures 20 and 22, the equation set 7 PSA is significantly less than that of Boore et al. for periods greater than $T = 0.30$ sec. This is consistent with the observations made earlier in comparing the attenuation of PSV ($T = 1.00$ sec) of the two models; refer to the bottom frames of Figures 17 and 18.

Figures 24 and 25 compare response spectra predicted by equation set 4 with that of Campbell (1990) at the same magnitude and distance combinations used in Figures 20 through 23. The close agreement between the PGA and PSV ($T = 1.00$ sec) predictions of the two models at distance $R = 10$ km noted earlier in conjunction with Figure 19 is readily apparent in Figure 25 across the entire period range. At magnitude $M = 6.5$, the slower attenuation of all periods of equation set 4 is observed, producing a PSA spectra at distance $R = 1.0$ km uniformly less than Campbell (1990). The ratio of Campbell PSA to equation set 4 PSA in the top frame of Figure 24 varies between approximately 1.5 and 2.5. However, the agreement in the bottom frame (magnitude $M = 7.5$) is greater; PSA predicted by equation set 4 is still generally less (except for periods between $T = 0.50$ and 0.80 sec) than that predicted by Campbell, but the difference is smaller, and is negligible for periods greater than $T = 2.50$ sec.

6.0 Application to Practice

The attenuation equations in this report were derived from predominantly California strong motion data. Therefore, the question arises whether these equations are applicable in other regions. In the absence of information to the contrary, the equations are recommended for shallow crustal earthquakes in plate-boundary regions, including those where plate subduction is occurring. However, the equations are not recommended for computing ground motions from interplate or intraplate subduction earthquakes; the ground motions from these events are different from those generated by shallow crustal earthquakes. Attenuation equations are available for computing ground motions from subduction earthquakes (e.g., Crouse, 1991a,b; Youngs et al., 1988).

In relatively stable continental interiors, such as eastern North America, the equations in this report also may not be appropriate. Attenuation in the eastern North America is different than in the western United States based on analysis of intensity and ground motion data recorded in both regions.

Assuming the equations in this report are judged to be applicable in a given region, the user must select one or more of the 16 sets of equations that are provided in Appendix B. Tables 2 and 3 were developed to assist in the selection. For example, if no information is known other than the fact the site is comprised of moderately stiff to stiff soil, then equation set 1 would be appropriate. On the other hand, if the site class, fault type, and alluvial depth are known, then one or two equation sets could be selected. For example, if the site class is B, then either equation set 8 or equation set 12 is appropriate; if the site class is C, then equation set 8 or equation set 16 could be used. In fact, when the site class is known, there are two equations that can be selected: one that contains a site term and one that was derived from data recorded at stations in the same site class.

Situations may arise where the fault-type is known to be normal (e.g., in the Basin and Range province of the western United States). The database used to derive the equations does not contain any records from normal-fault earthquakes (see Table 1). For this case, the user could select the set of equations for unknown fault-type, or known fault-type with $F = 0$ or $F = 0.5$. The use of $F = 1$ (reverse faults) is considered too conservative.

Other situations may arise where the locations of a comparable number of reverse and strike-slip faults are known, but the information on their seismic activity is not sufficient to model them as individual sources. In this case, the user may elect to model the tectonic province in which the faults are located as one seismic source and select the set of equations based on the assumption that the fault-type is unknown.

7.0 References

Campbell, K.W. (1990). "Empirical Prediction of Near-Source Soil and Soft-Rock Ground Motion for the Diablo Canyon Power Plant Site, San Luis Obisbo County, California," *Dames and Moore Report*, prepared for Lawrence Livermore Laboratory, September, 110 pages.

Boore, D.M., W.B. Joyner, and T.E. Fumal (1993). "Estimation of Response Spectra and Peak Accelerations from Western North American Earthquakes: An Interim Report," *U.S. Geological Survey Open-File Report 93-509*, 72 pages.

Boore, D.M., W.B. Joyner, and T.E. Fumal (1994). "Estimation of Response Spectra and Peak Accelerations from Western North American Earthquakes: An Interim Report Part 2," *U.S. Geological Survey Open-File Report 94-127*, 40 pages.

Boore, D.M., W.B. Joyner, and T.E. Fumal (1995). "Ground Motion Estimates for Strike- and Reverse-Slip Faults," U.S. Geological Survey, 4 pages.

Crouse, C.B., and M. Piazza (1983). "Development of Attenuation Equations for the Santa Barbara Channel," *Earth Technology Report*, prepared for Exxon Production Research Co., November.

Crouse, C.B., N. Moeen-Vaziri, Y. Vyas, and L. Yau (1985). "Analysis of Vertical Components of Near-Field Earthquake Ground Motion," *Earth Technology Report*, prepared for Exxon Production Research Co., January.

Crouse, C.B. (1991a). "Ground Motion Attenuation Equations for Earthquakes on the Cascadia Subduction Zone," *Earthquake Spectra*, Vol. 7, pp. 201–236.

Crouse, C.B. (1991b). Errata to Crouse (1991a). *Earthquake Spectra*, Vol. 7, p. 506.

Dixon, W.J. (editor) (1992). *BMDP Statistical Software Manual*, Manual to accompany *BMDP Release 7*, University Press of California, 1500 pages.

Geomatrix Consultants (1992). "Ground Motion Study for West San Francisco Bay Bridge," *Geomatrix Consultants Report*, prepared for Caltrans, Division of Structures, Sacramento, California, December.

Idriss, I.M. (1993). "Procedures for Selecting Earthquake Ground Motion at Rock Sites," *Report No. NIST GCR 93-625*, National Institute of Standards and Technology.

Joyner, W.B., and D.M. Boore (1988). "Measurement, Characterization, and Prediction of Strong Ground Motion," *Earthquake Engineering and Soil Dynamics II; Recent Advances in Ground Motion Evaluation*, ASCE Special Geotechnical Publication No. 20, pp. 43–102.

Youngs, R.R., S.M. Day, and J.L. Stevens (1988). "Near Field Ground Motions on Rock for Large Subduction Earthquakes," *Earthquake Engineering and Soil Dynamics II; Recent Advances in Ground Motion Evaluation*, ASCE Special Geotechnical Publication No. 20, pp. 445–462.

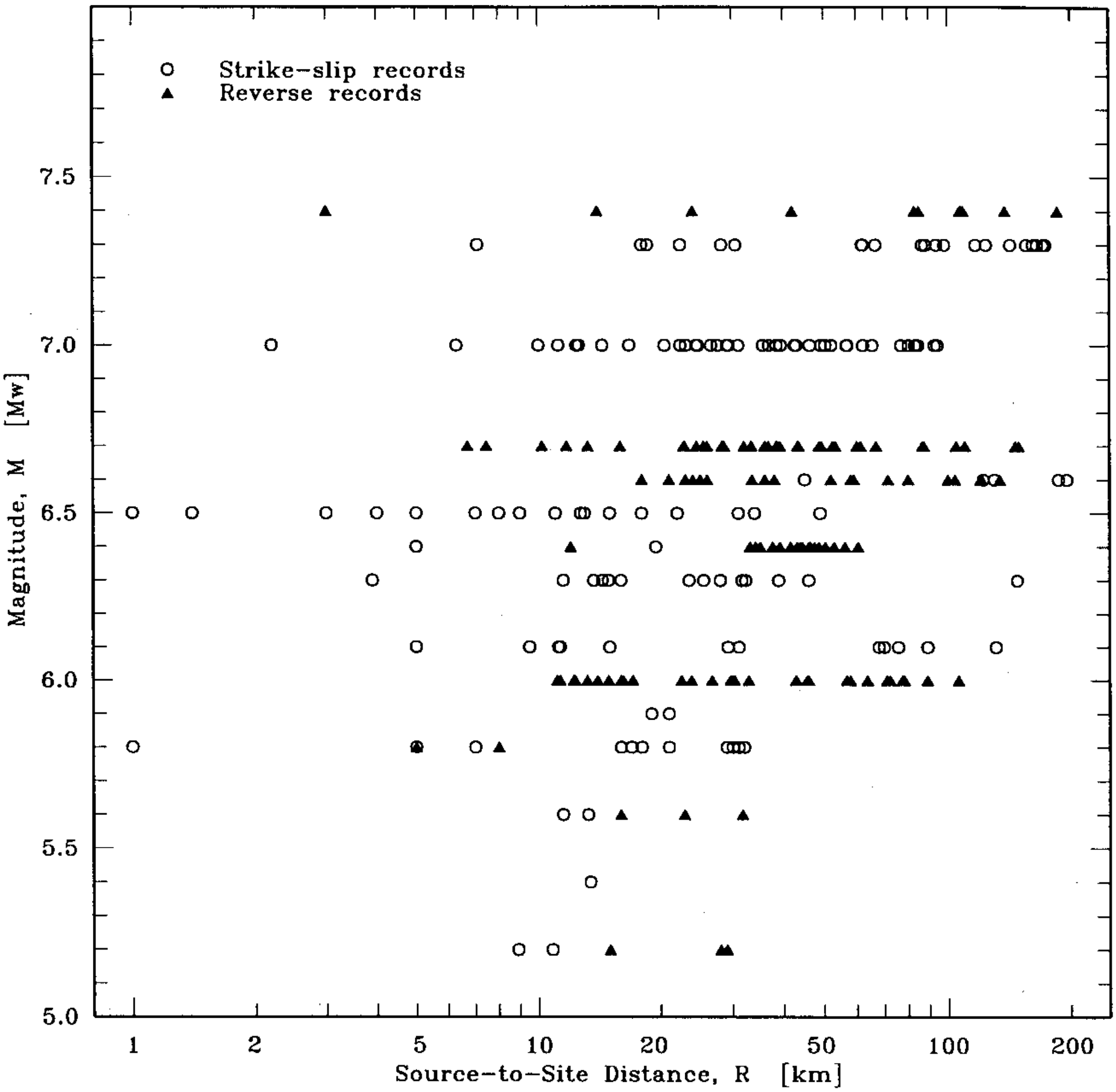

Figure 1. Distribution of database records in Magnitude–Distance (*M–R*) space.

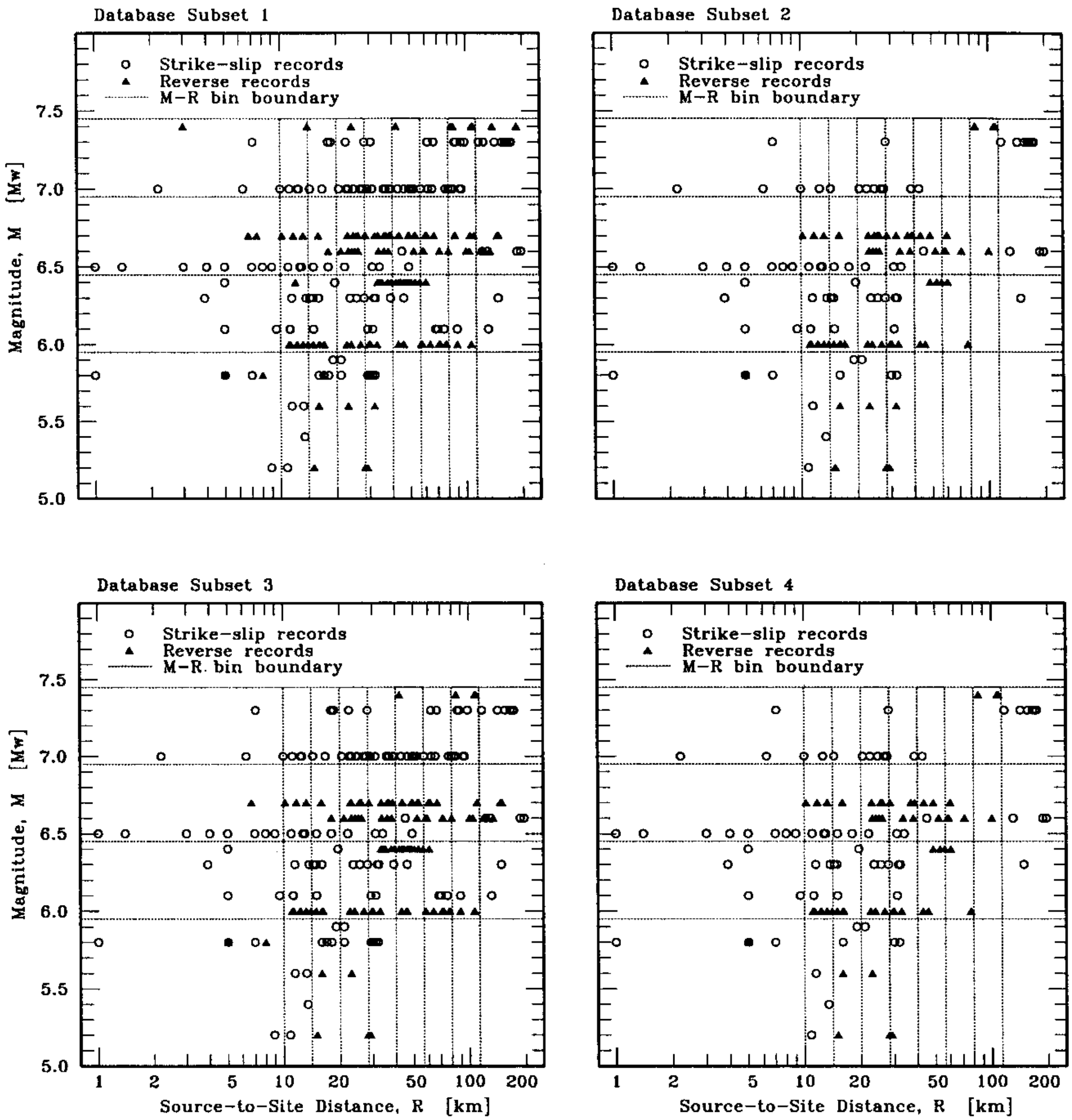

Figure 2. Magnitude–distance distribution of records in database subsets 1 through 4.

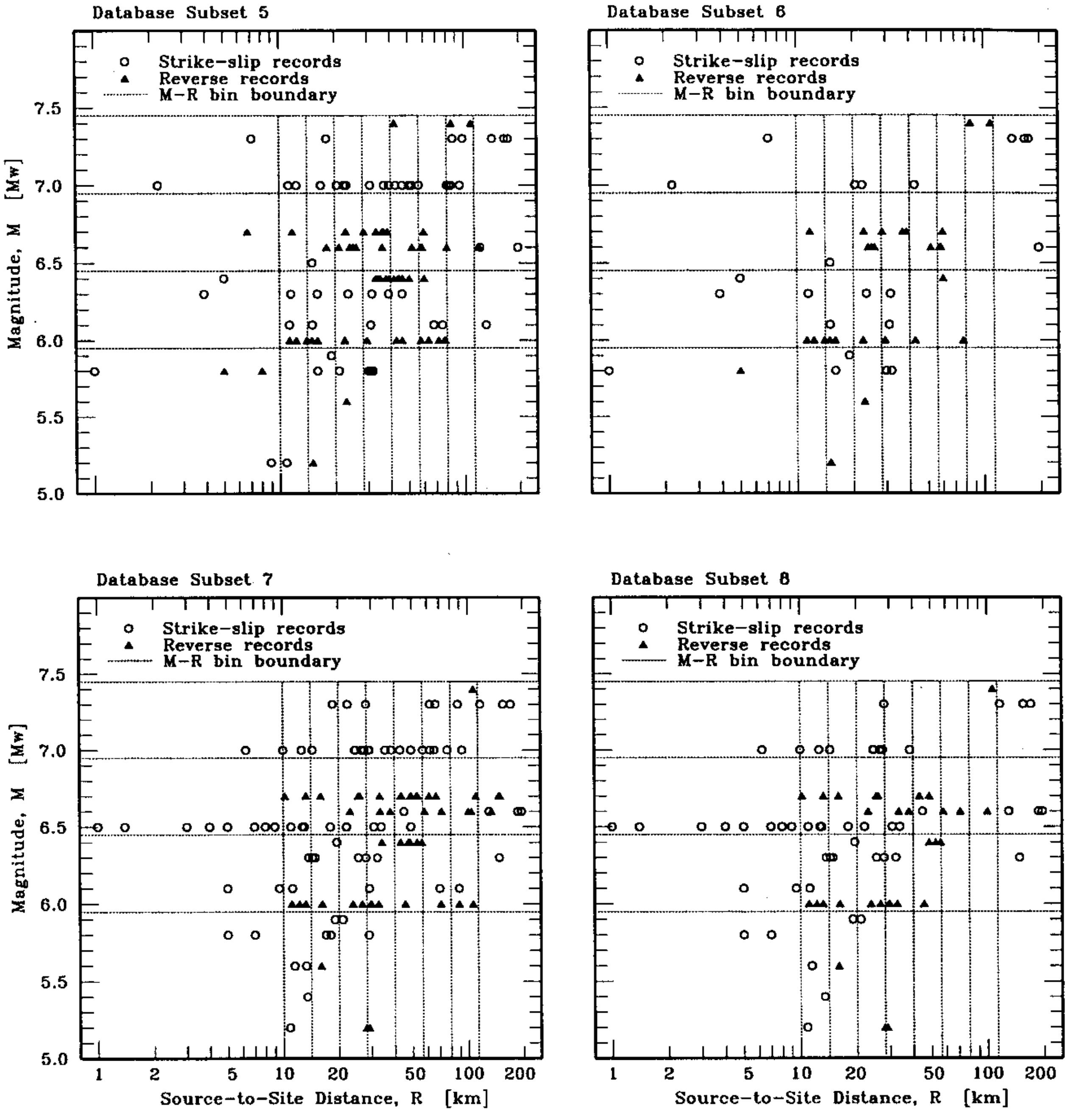

Figure 3. Magnitude–distance distribution of records in database subsets 5 through 8.

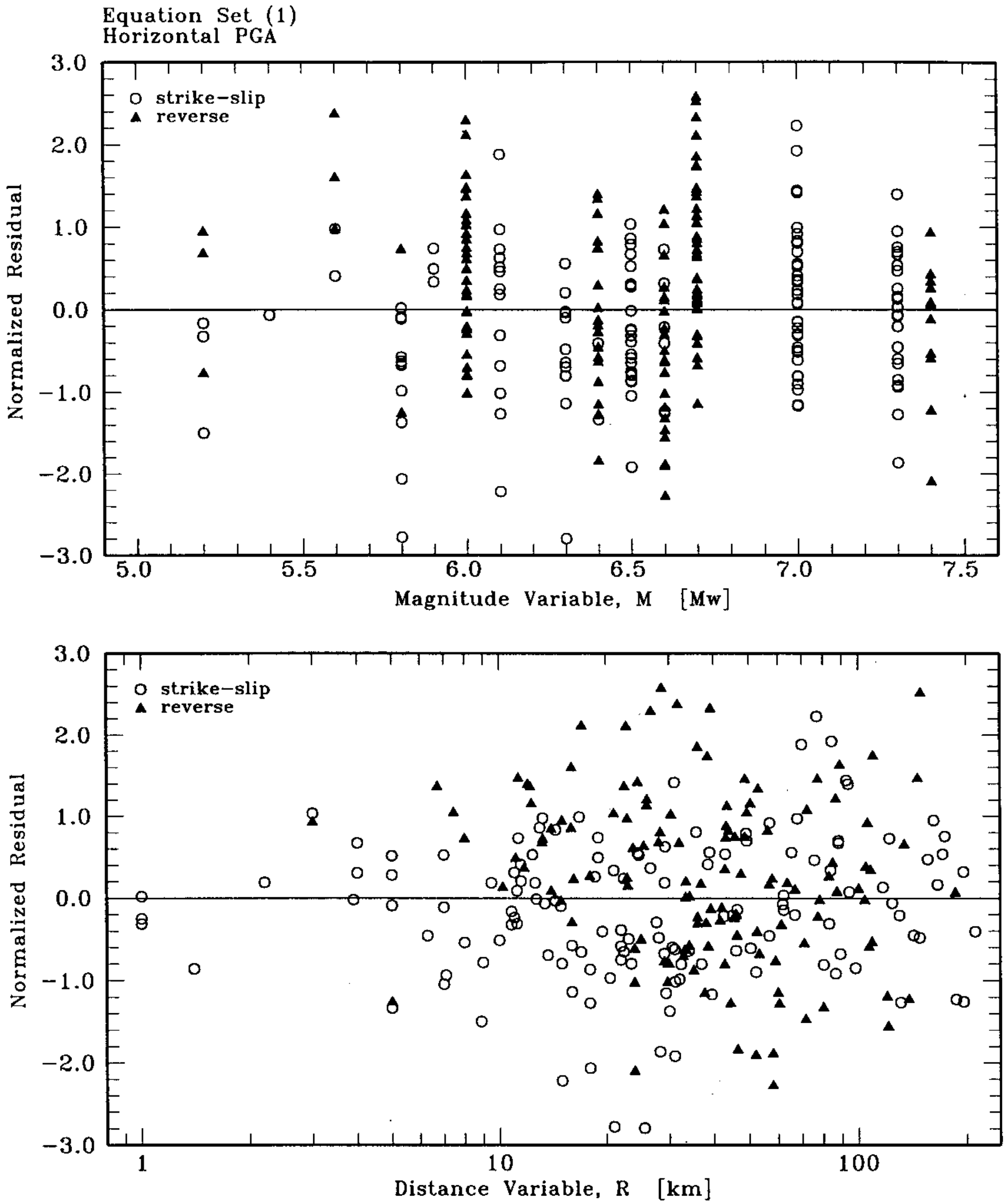

Figure 4. Plots of equation set 1 horizontal PGA residuals versus magnitude and distance.

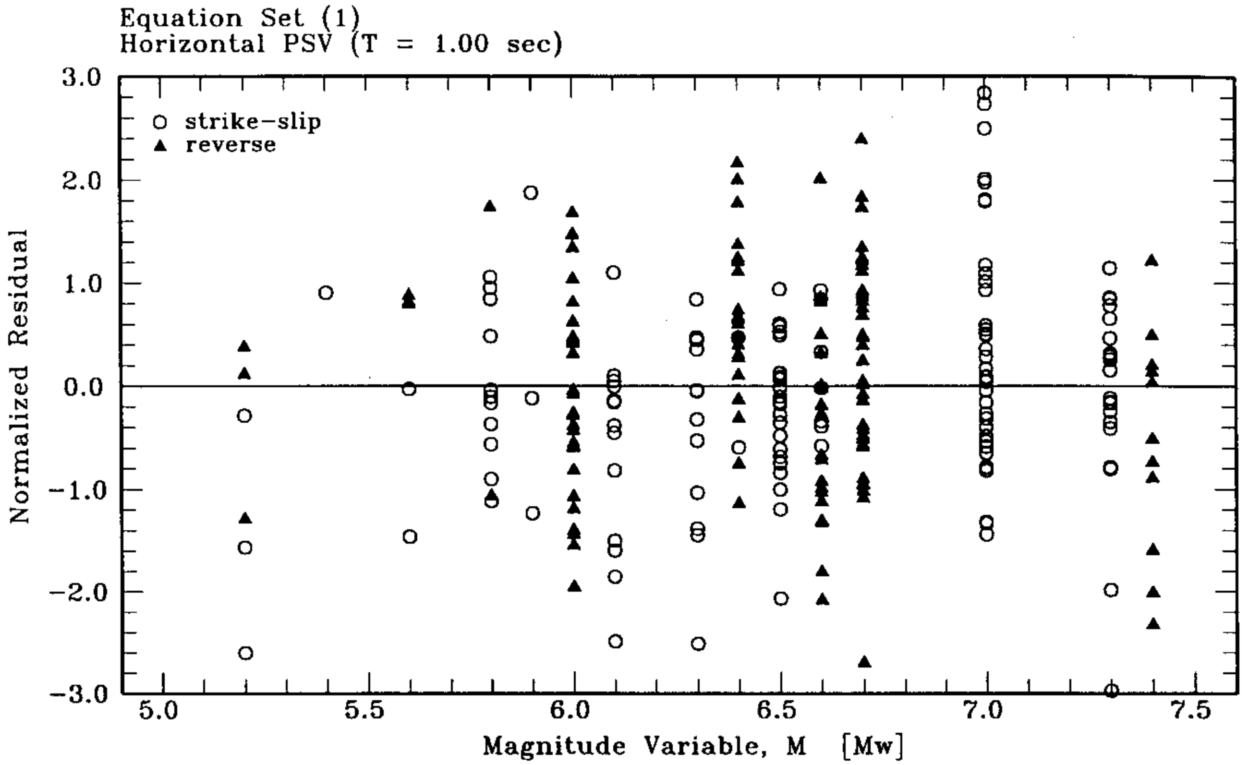

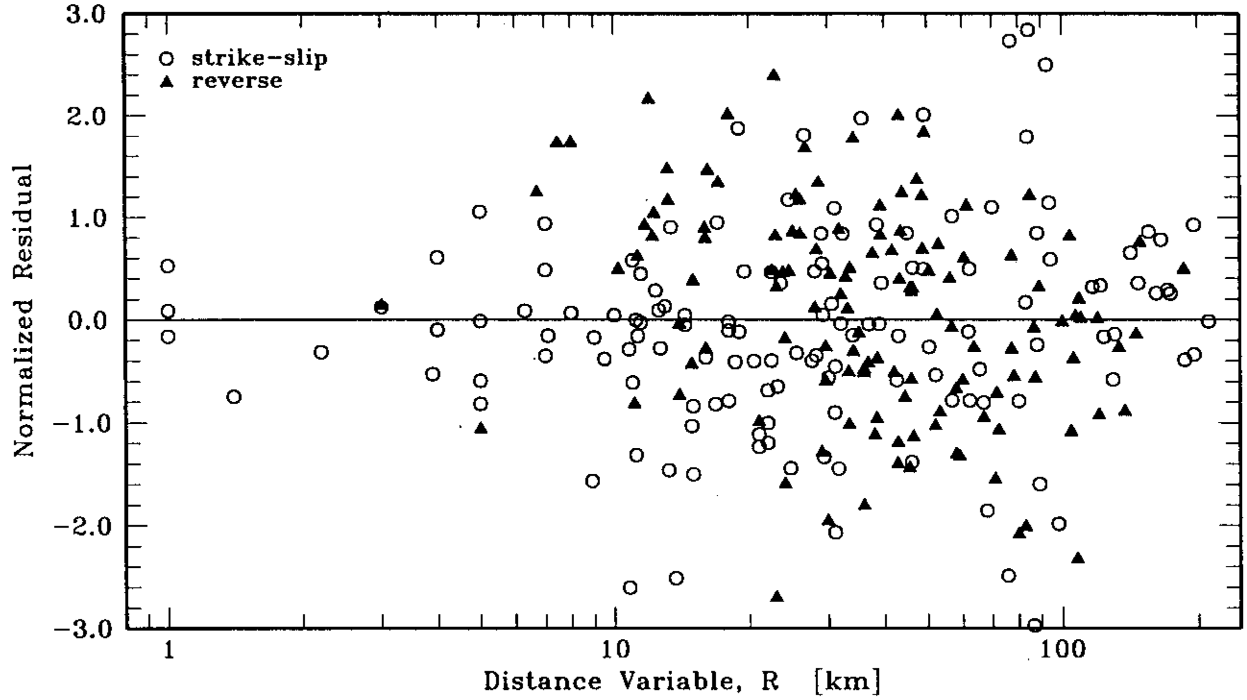

Figure 5. Plots of equation set 1 horizontal PSV (period $T = 1.0$ sec) residuals versus magnitude and distance.

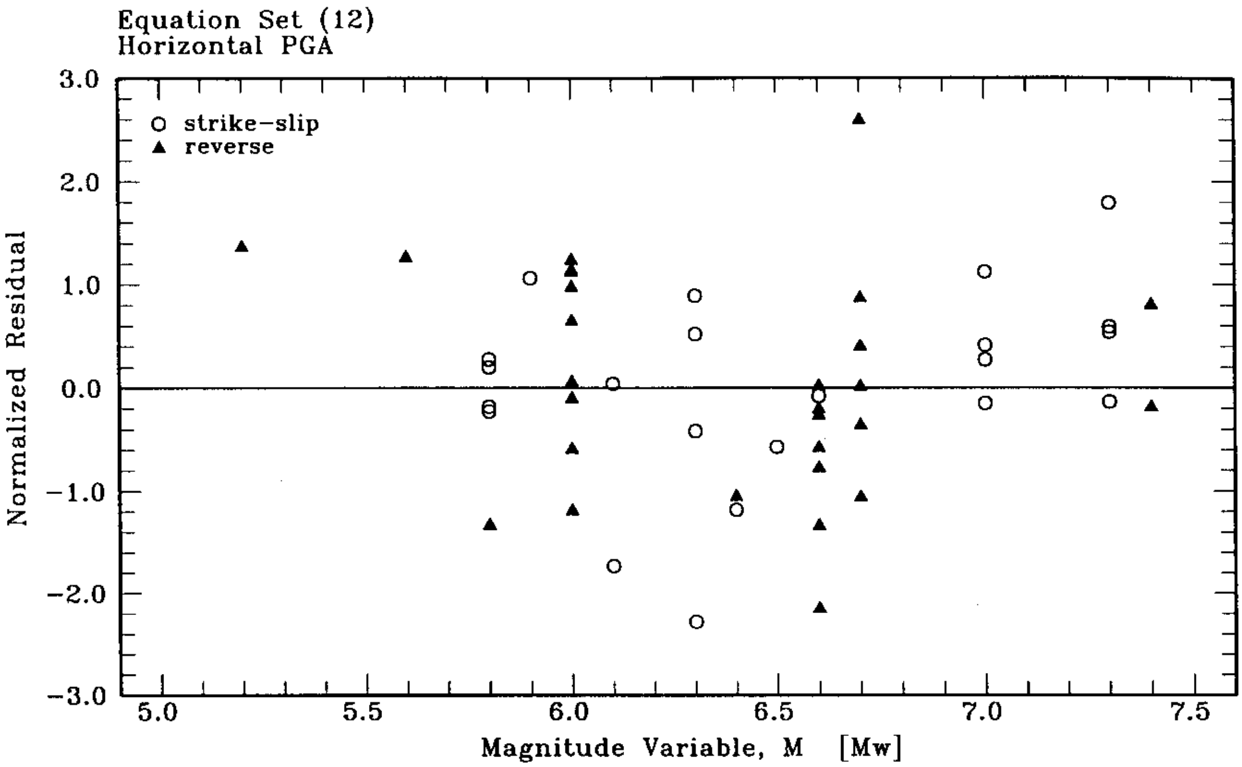

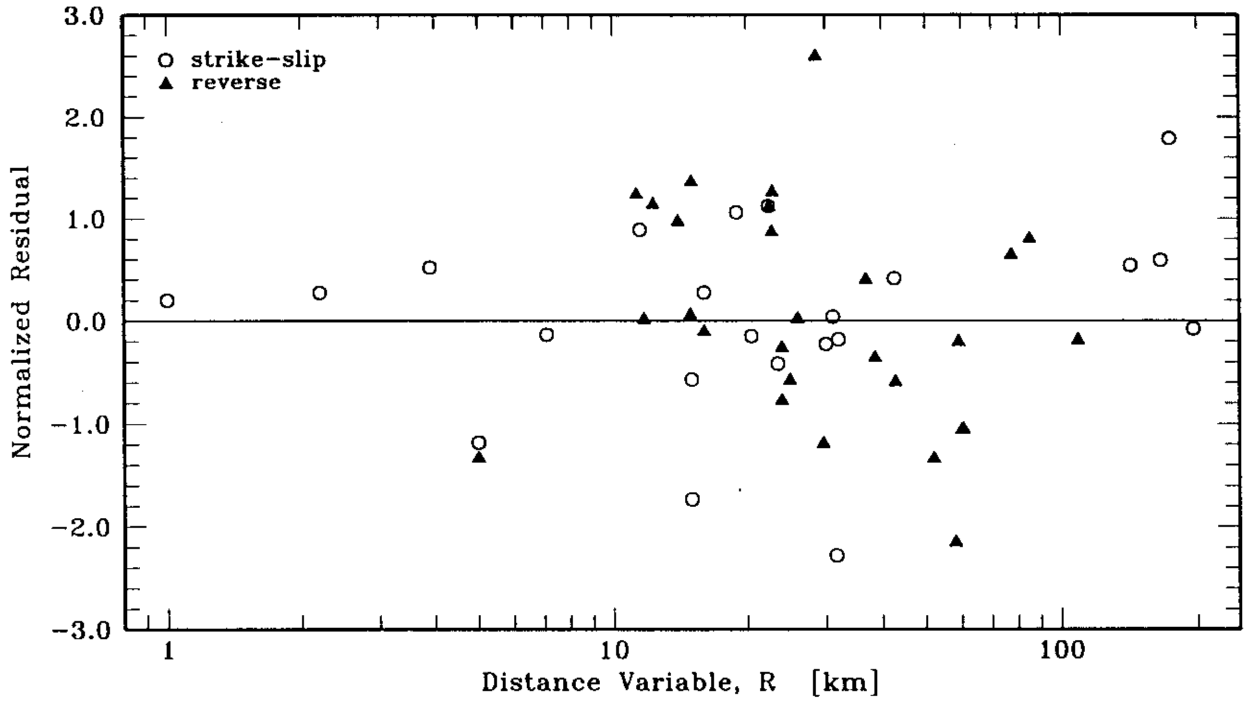

Figure 6. Plots of equation set 12 horizontal PGA residuals versus magnitude and distance.

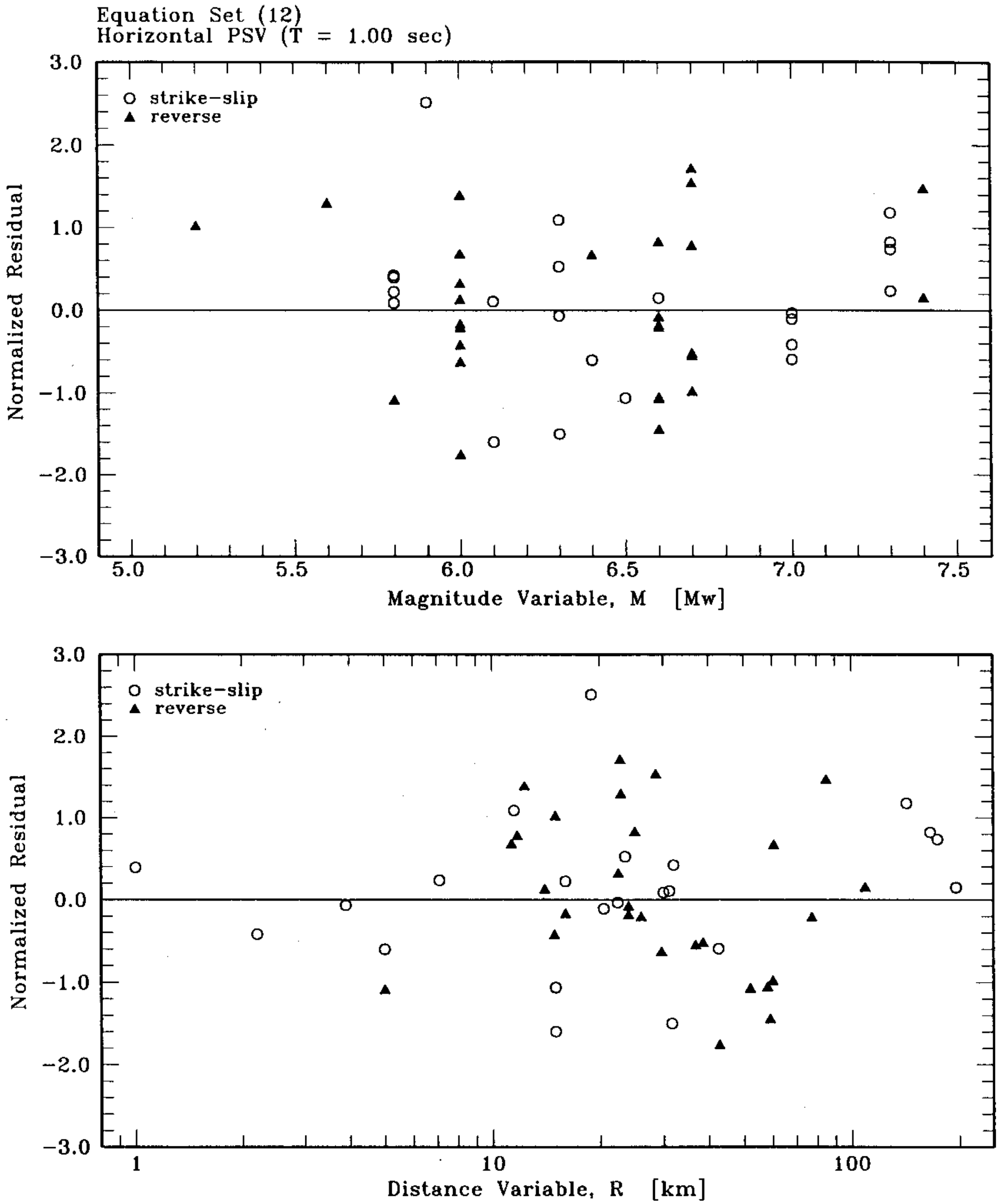

Figure 7. Plots of equation set 12 horizontal PSV (period $T = 1.0$ sec) residuals versus magnitude and distance.

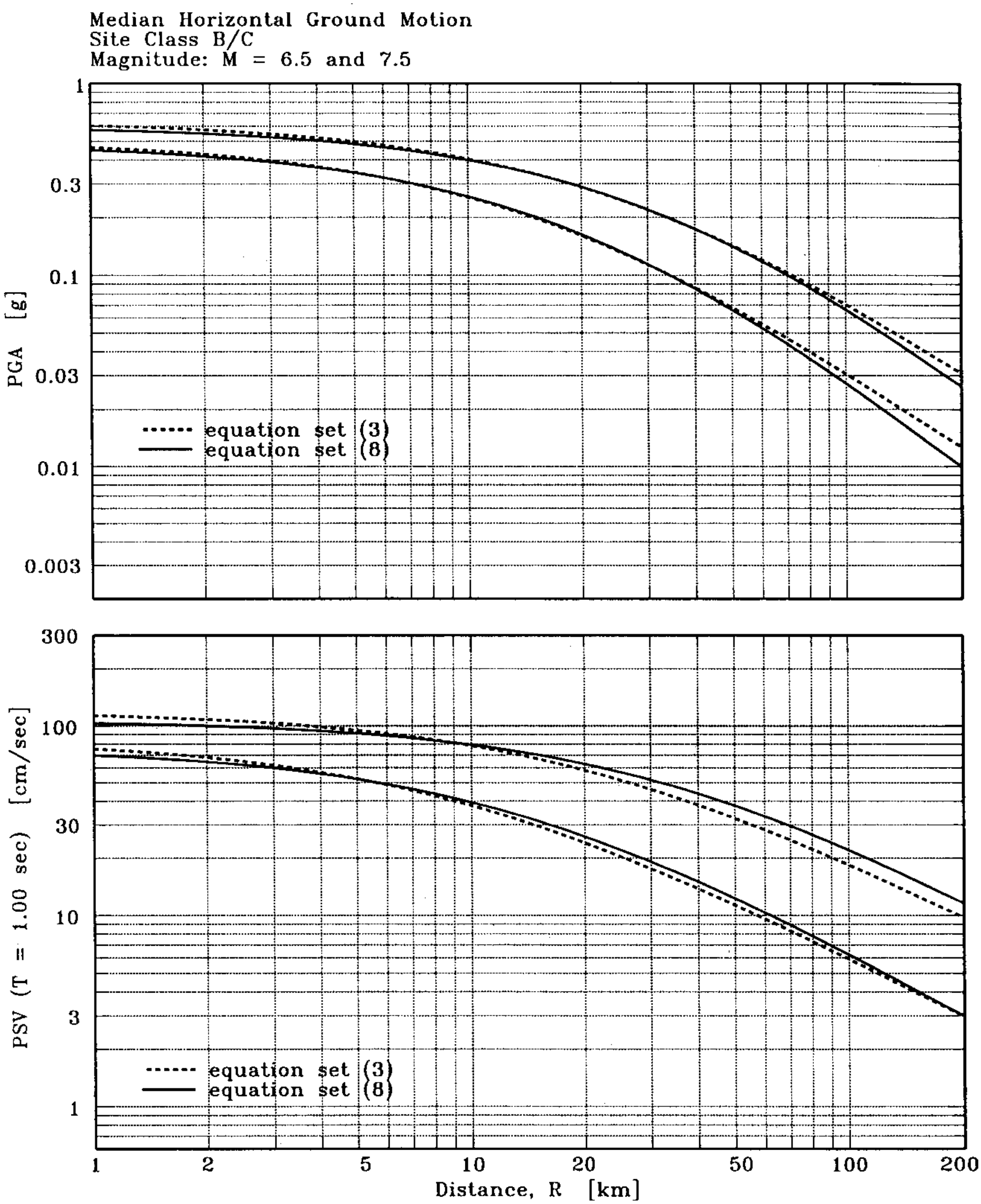

Figure 8. Median horizontal PGA and PSV (period $T = 1.0$ sec) attenuation plots. Plots compare ground-motions at magnitudes $M = 6.5$ and 7.5 predicted by equation sets 3 and 8 for site class B/C, strike-slip conditions. For equation 8, $S = 0.5$ (class B/C) and $D = 3.0$ km (database median depth).

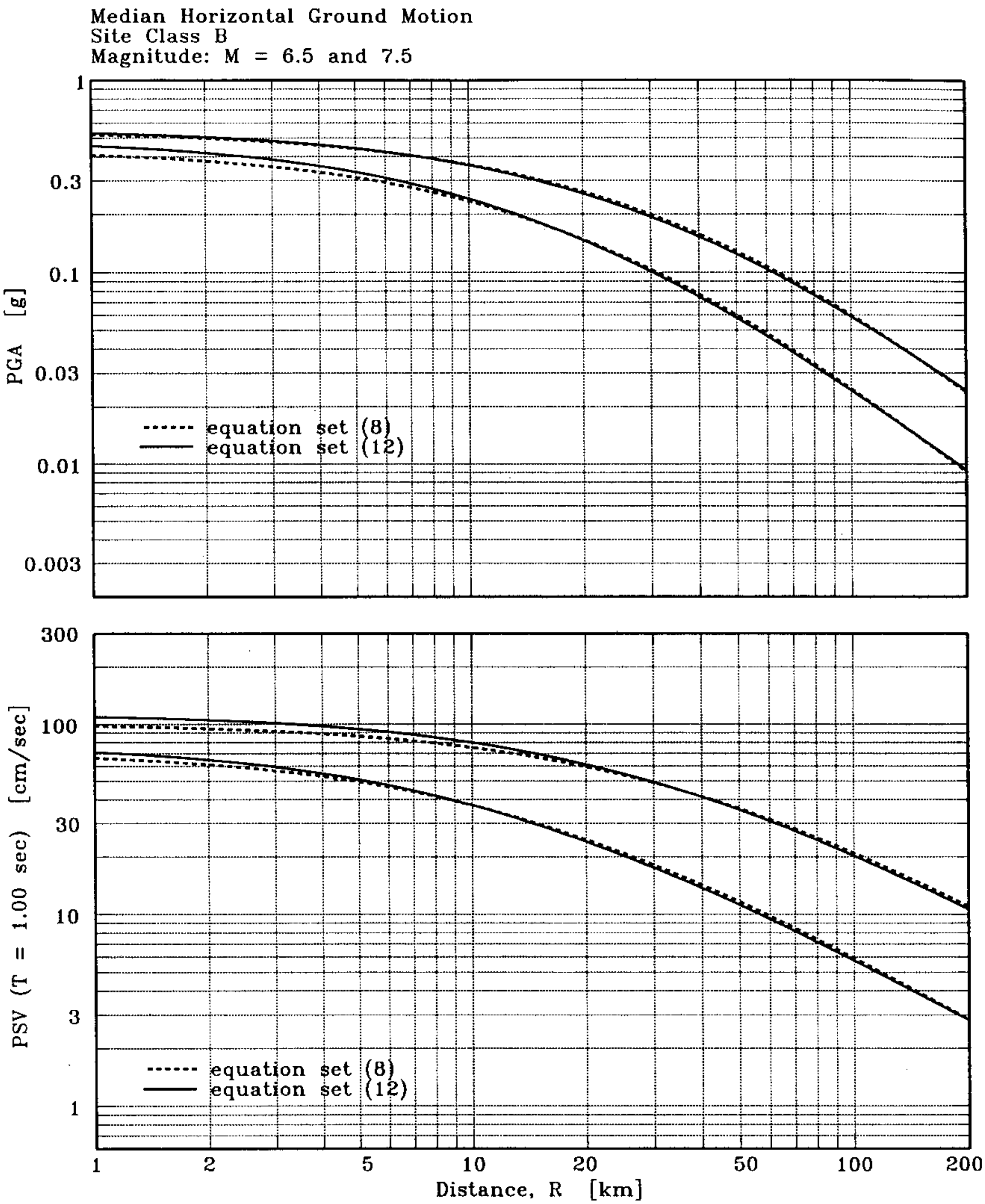

Figure 9. Median horizontal PGA and PSV (period $T = 1.0$ sec) attenuation plots. Plots compare ground-motions at magnitudes $M = 6.5$ and 7.5 predicted by equation sets 8 and 12 for site class B, strike-slip conditions. For both equations, $D = 3.0$ km (database median depth).

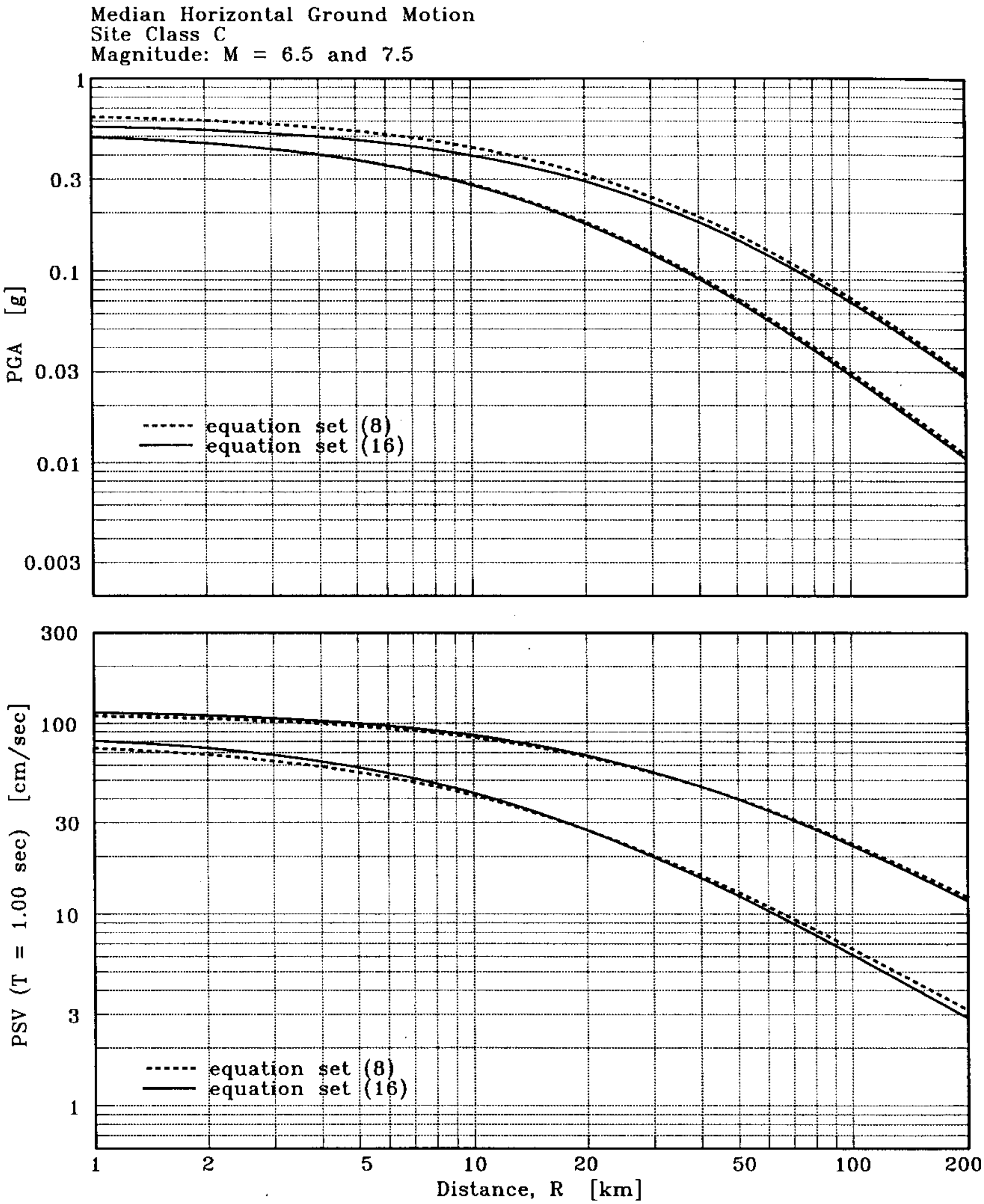

Figure 10. Median horizontal PGA and PSV (period T = 1.0 sec) attenuation plots. Plots compare ground-motions at magnitudes M = 6.5 and 7.5 predicted by equation sets 8 and 12 for site class C, strike-slip conditions. For both equations, D = 3.0 km (database median depth).

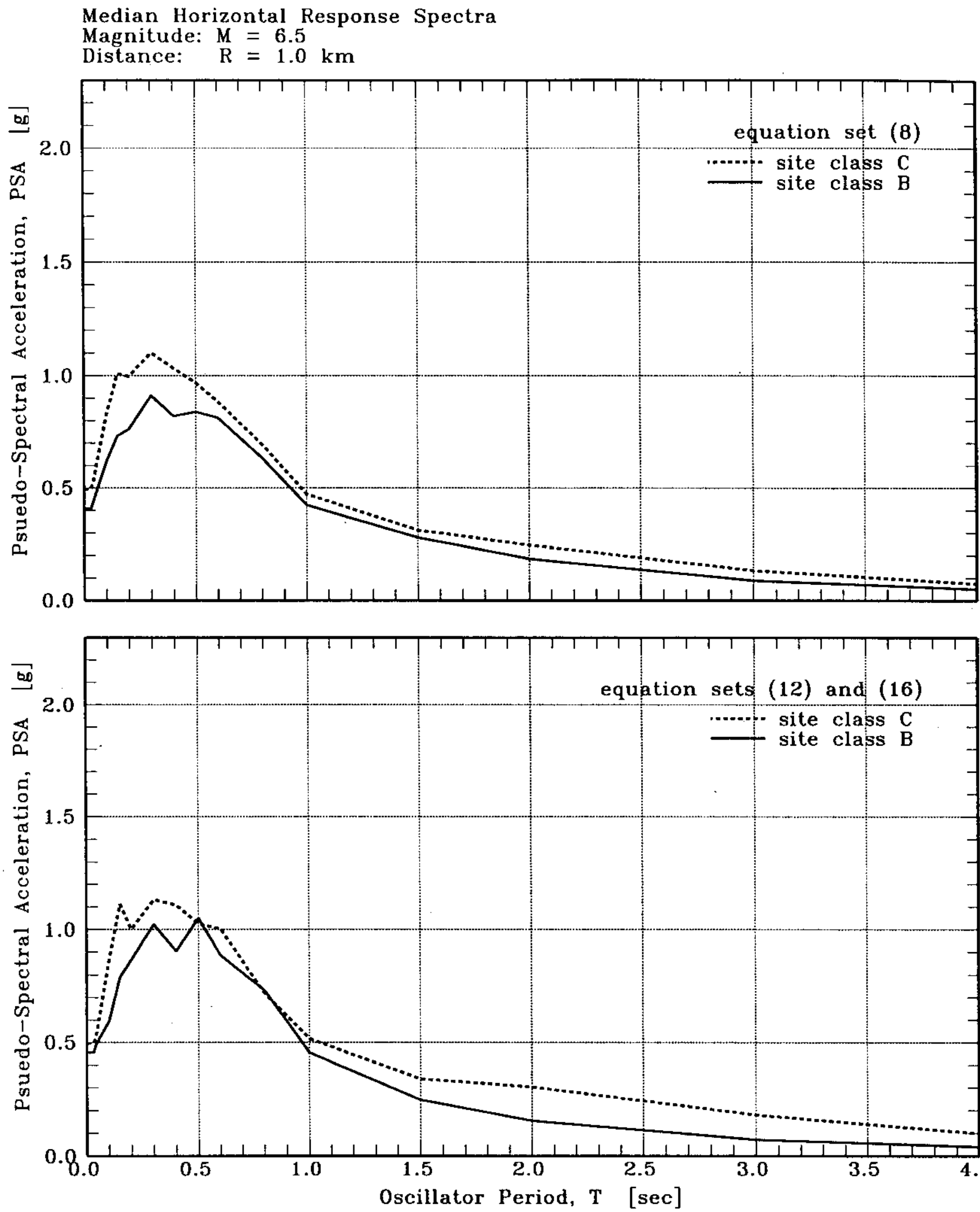

Figure 11. Median horizontal response spectra plots. Plots compare site class B and C response spectra at magnitude $M = 6.5$ and distance $R = 1.0$ km for strike-slip events. The top frame plots equation 8; the bottom frame plots equations 12 and 16. Depth $D = 3.0$ km is used for all equations.

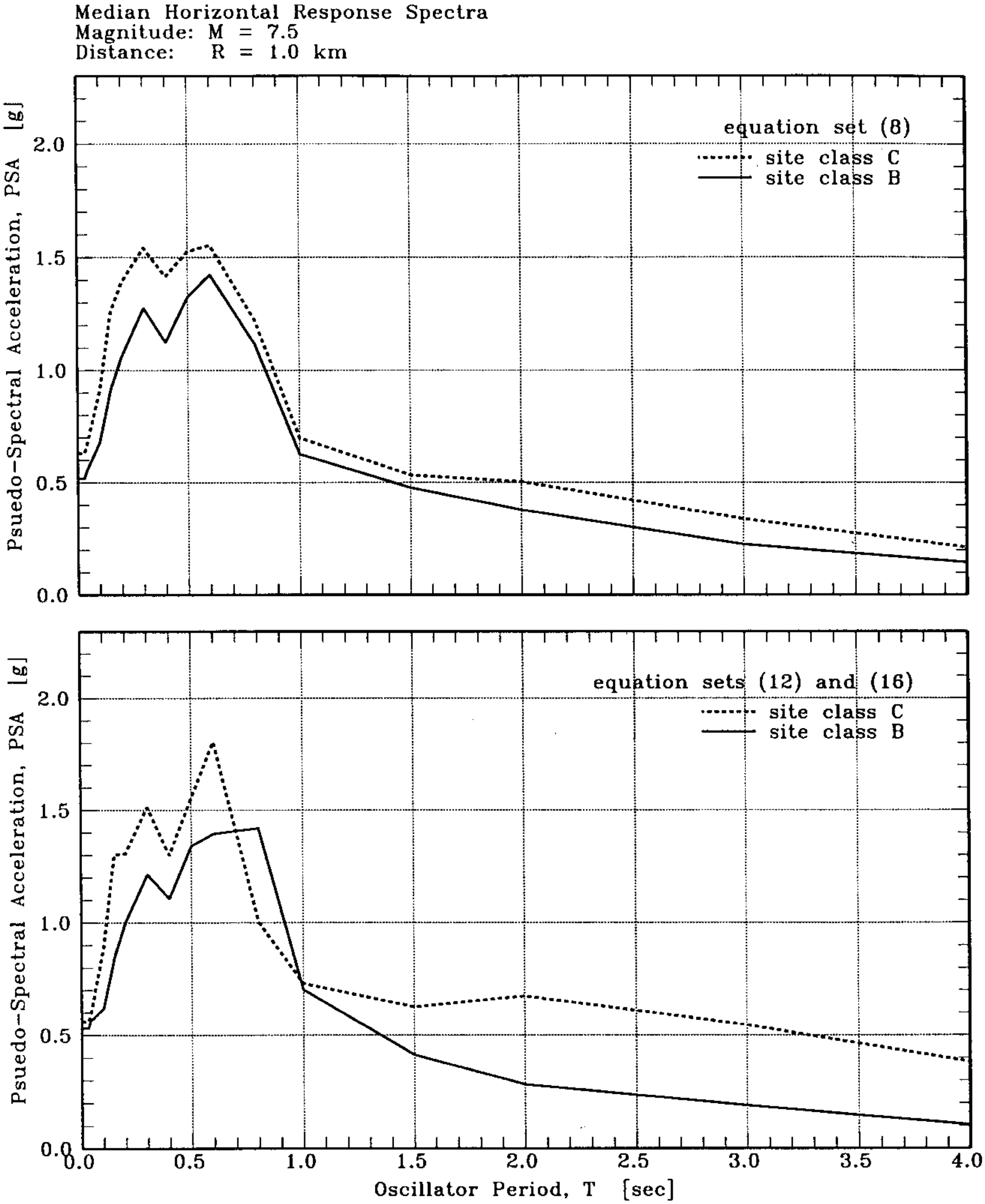

Figure 12. Median horizontal response spectra plots. Plots compare site class B and C response spectra at magnitude M = 7.5 and distance R = 1.0 km for strike-slip events. The top frame plots equation 8; the bottom frame plots equations 12 and 16. Depth D = 3.0 km is used for all equations.

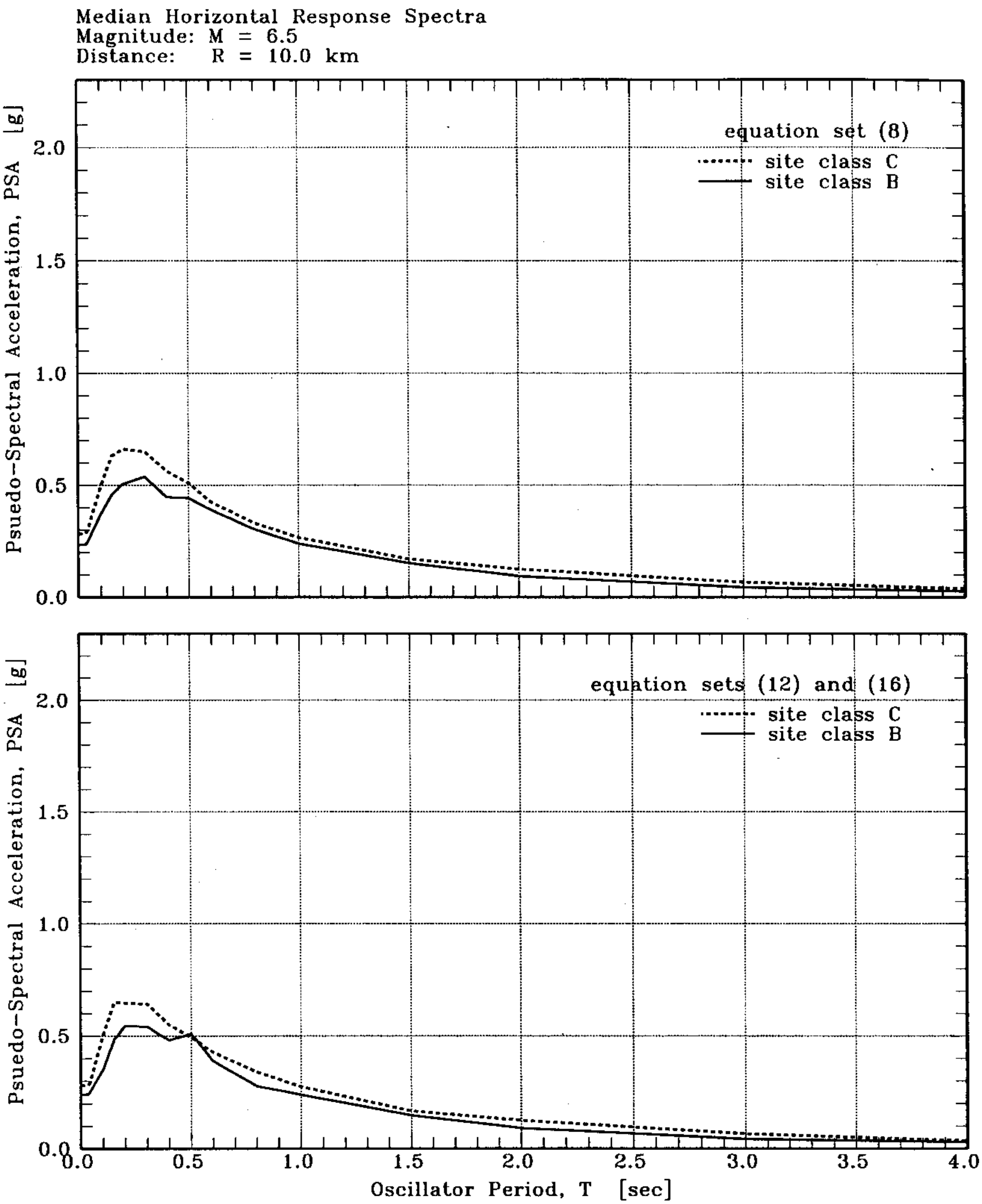

Figure 13. Median horizontal response spectra plots. Plots compare site class B and C response spectra at magnitude $M = 6.5$ and distance $R = 10.0$ km for strike-slip events. The top frame plots equation 8; the bottom frame plots equations 12 and 16. Depth $D = 3.0$ km is used for all equations.

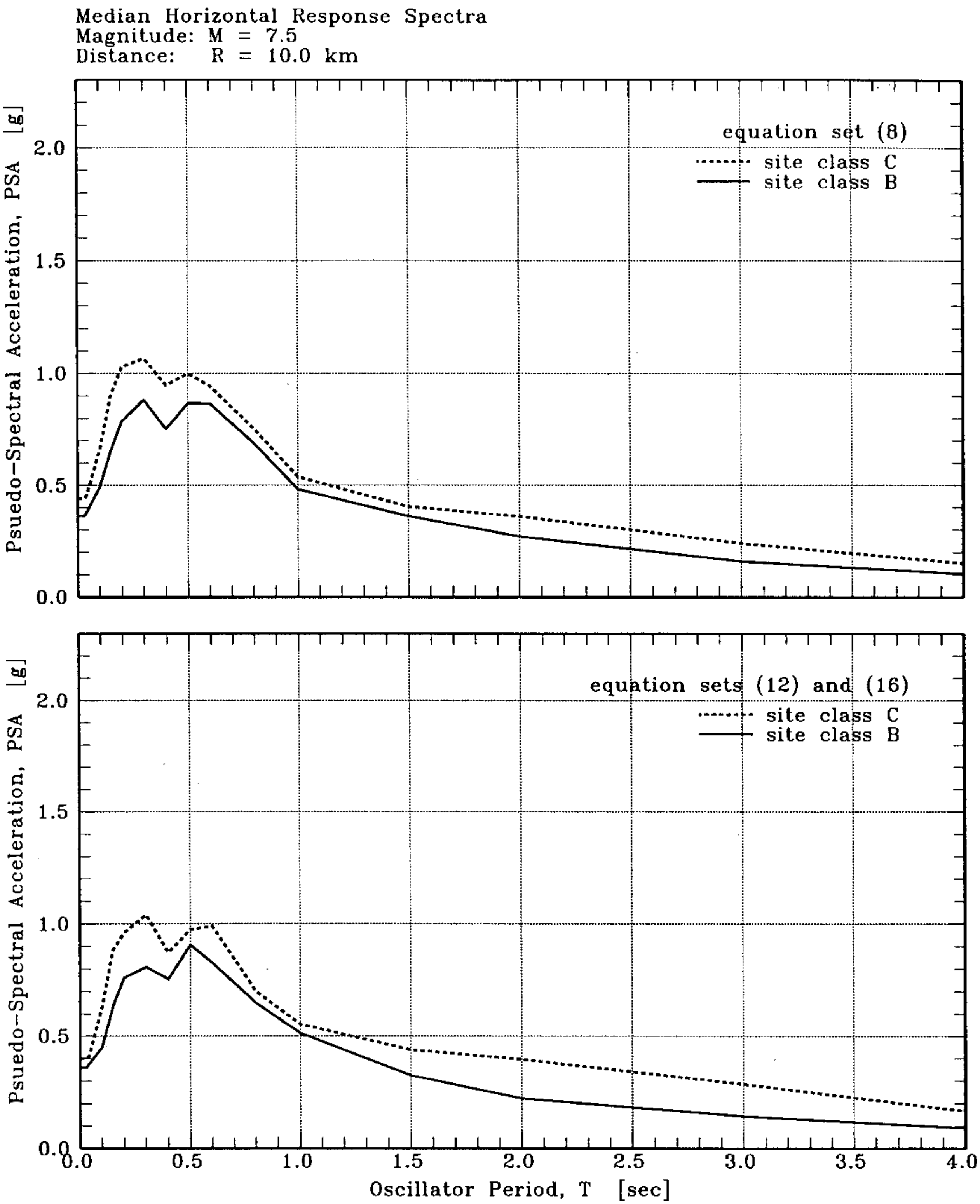

Figure 14. Median horizontal response spectra plots. Plots compare site class B and C response spectra at magnitude M = 7.5 and distance R = 10.0 km for strike-slip events. The top frame plots equation 8; the bottom frame plots equations 12 and 16. Depth D = 3.0 km is used for all equations.

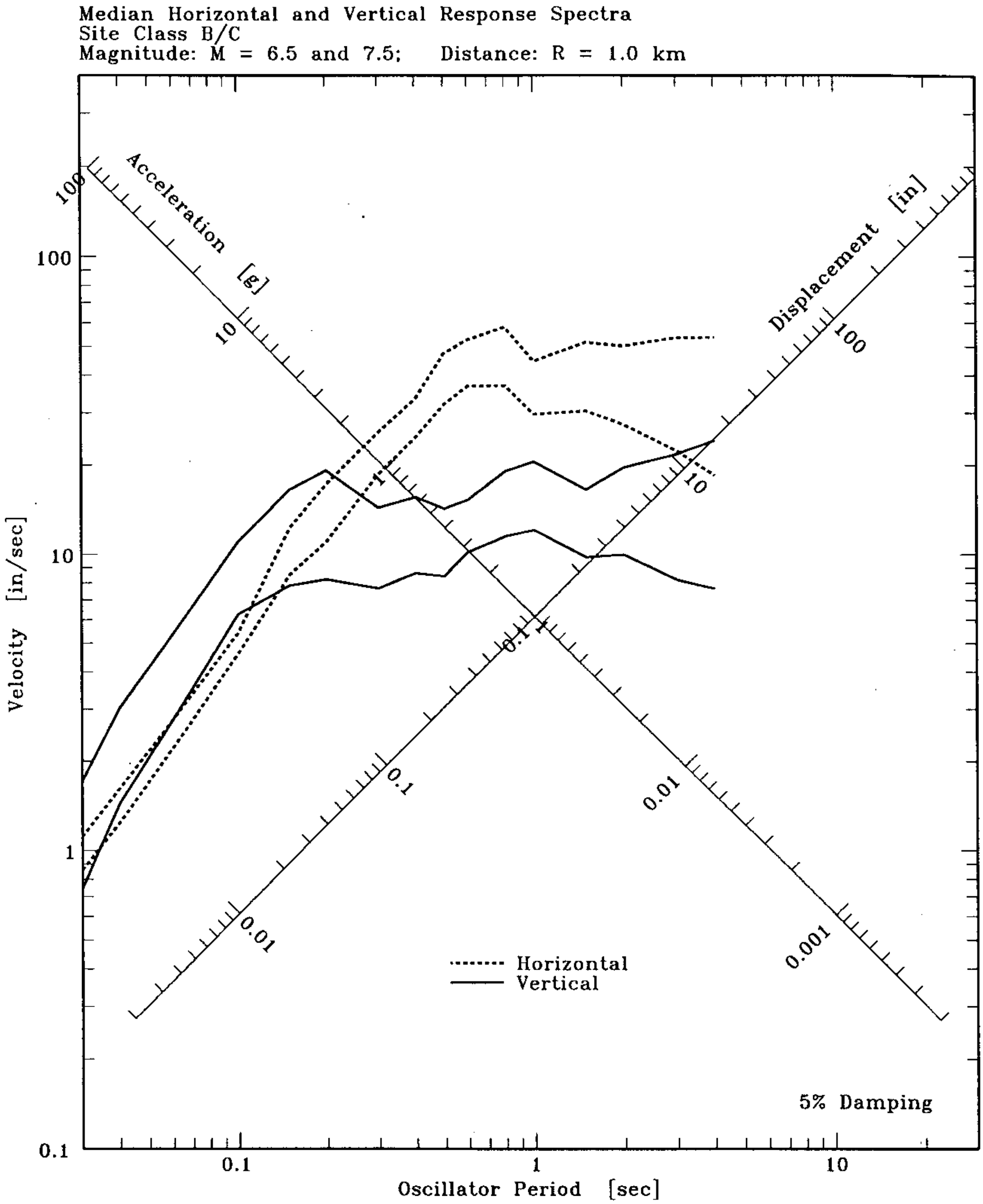

Figure 15. Median horizontal and vertical response spectra plots. Plots compare horizontal and vertical response spectra predicted by equation set 3 for site class B/C, strike-slip conditions, for magnitudes $M = 6.5$ and 7.5 at distance $R = 1.0$ km.

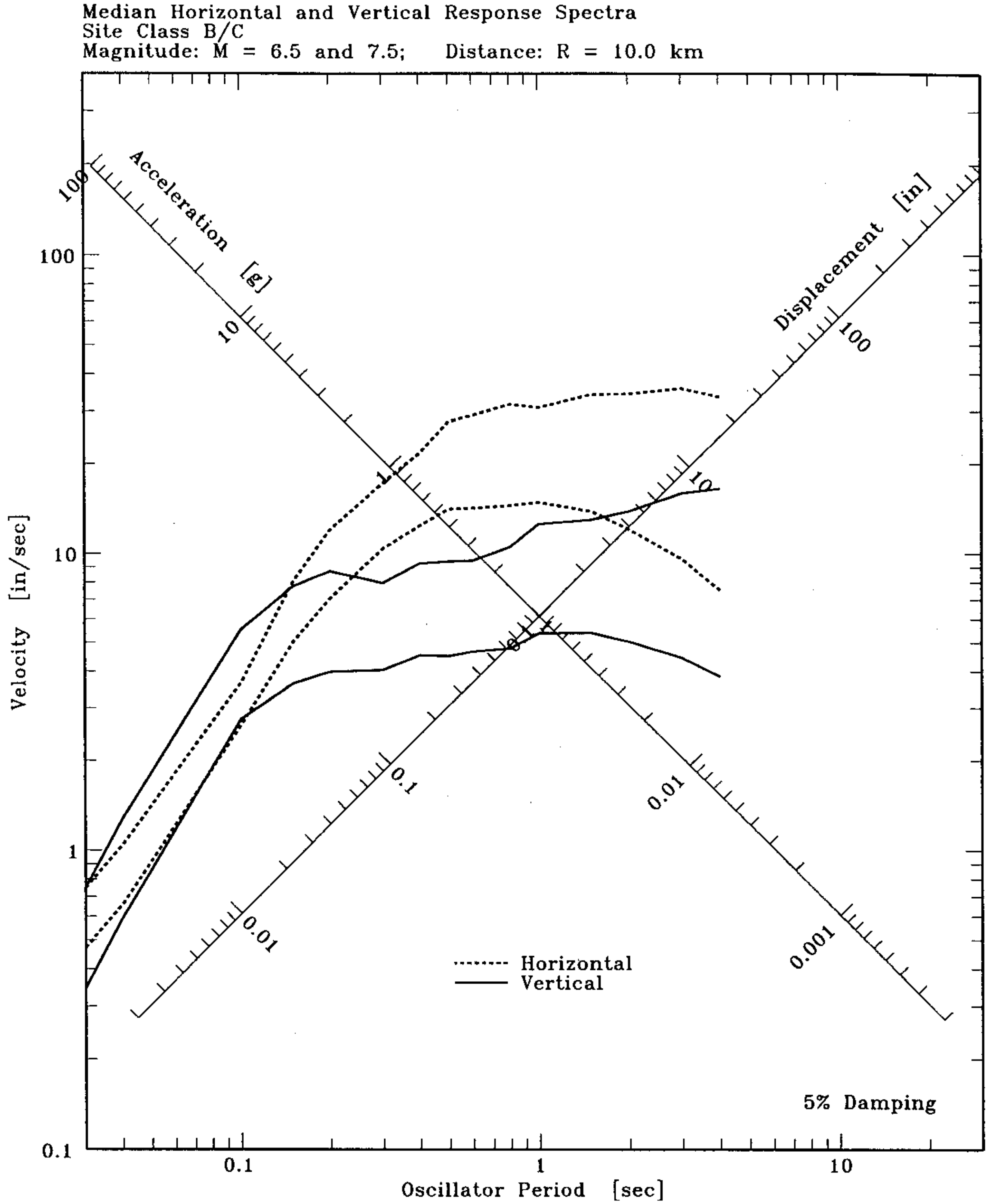

Figure 16. Median horizontal and vertical response spectra plots. Plots compare horizontal and vertical response spectra predicted by equation set 3 for site class B/C, strike-slip conditions, for magnitudes M = 6.5 and 7.5 at distance R = 10.0 km.

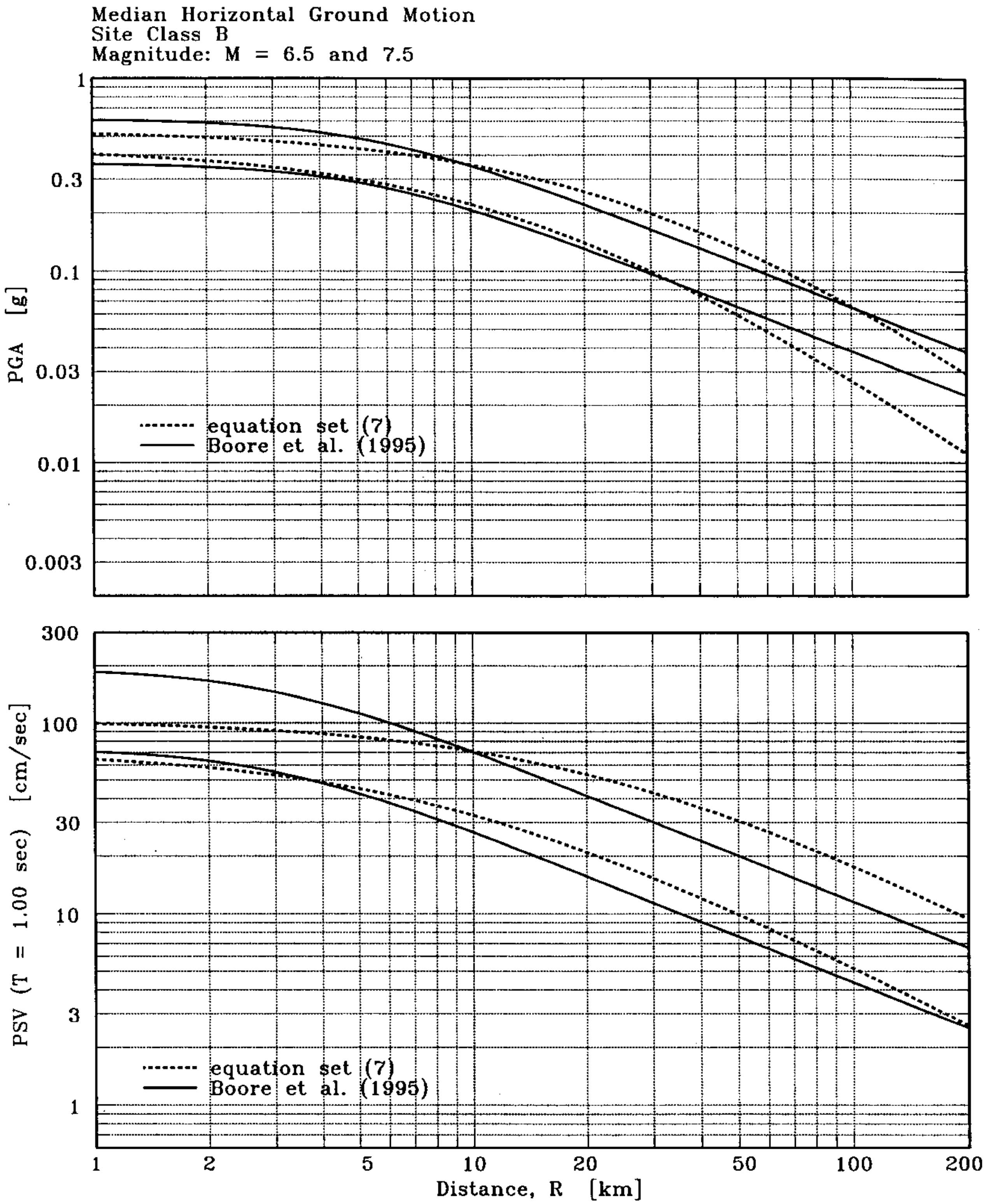

Figure 17. Median horizontal PGA and PSV (period $T = 1.0$ sec) attenuation plots. Plots compare ground-motions at magnitudes $M = 6.5$ and 7.5 predicted by equation set 7 and by Boore et al. (1995) for site class B, strike-slip conditions.

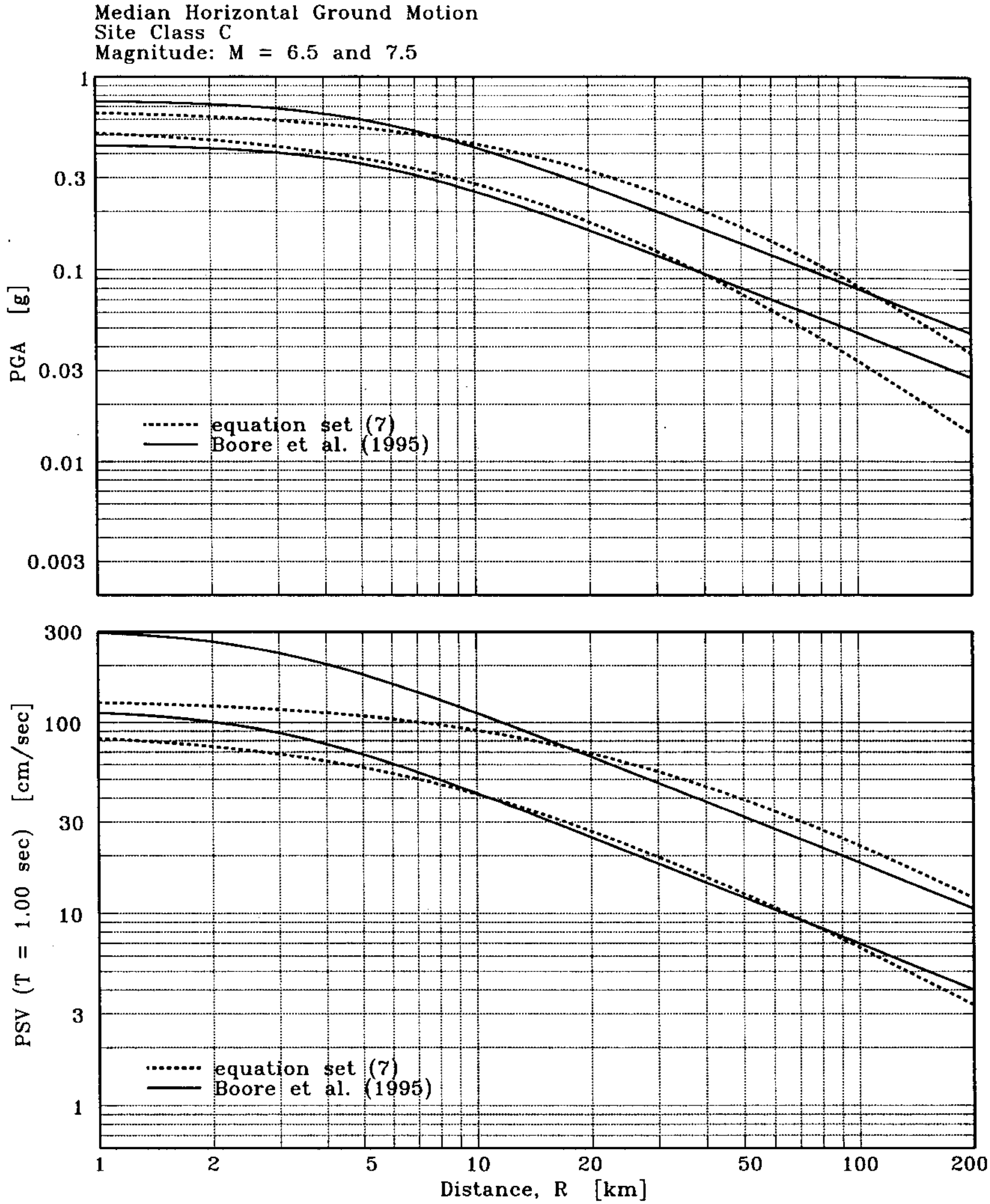

Figure 18. Median horizontal PGA and PSV (period $T = 1.0$ sec) attenuation plots. Plots compare ground-motions at magnitudes $M = 6.5$ and 7.5 predicted by equation set 7 and by Boore et al. (1995) for site class C, strike-slip conditions.

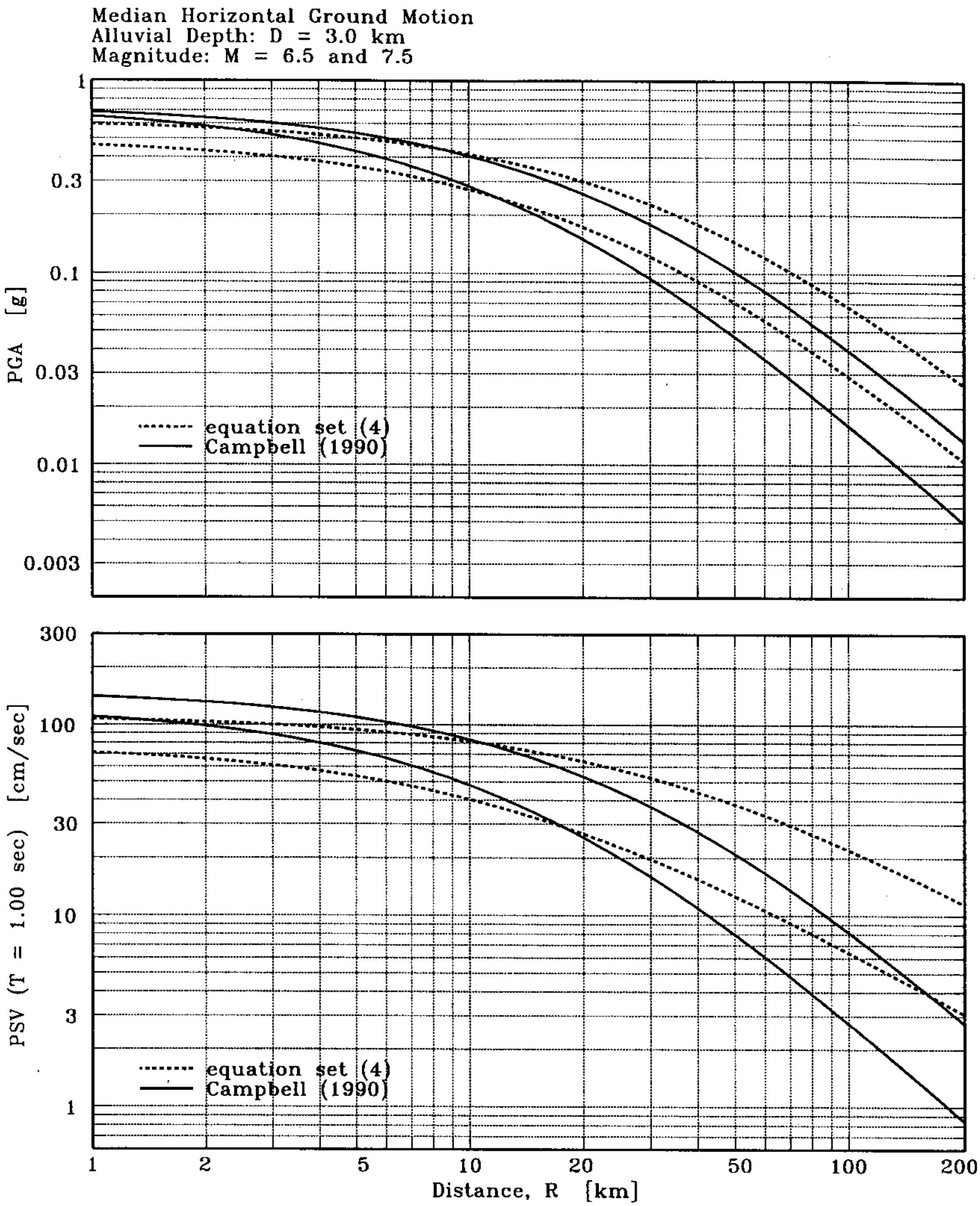

Figure 19. Median horizontal PGA and PSV (period $T = 1.0$ sec) attenuation plots. Plots compare ground-motions at magnitudes $M = 6.5$ and 7.5 predicted by equation set 4 and by Campbell (1990) for strike-slip conditions with alluvial depth $D = 3.0$ km (database median depth).

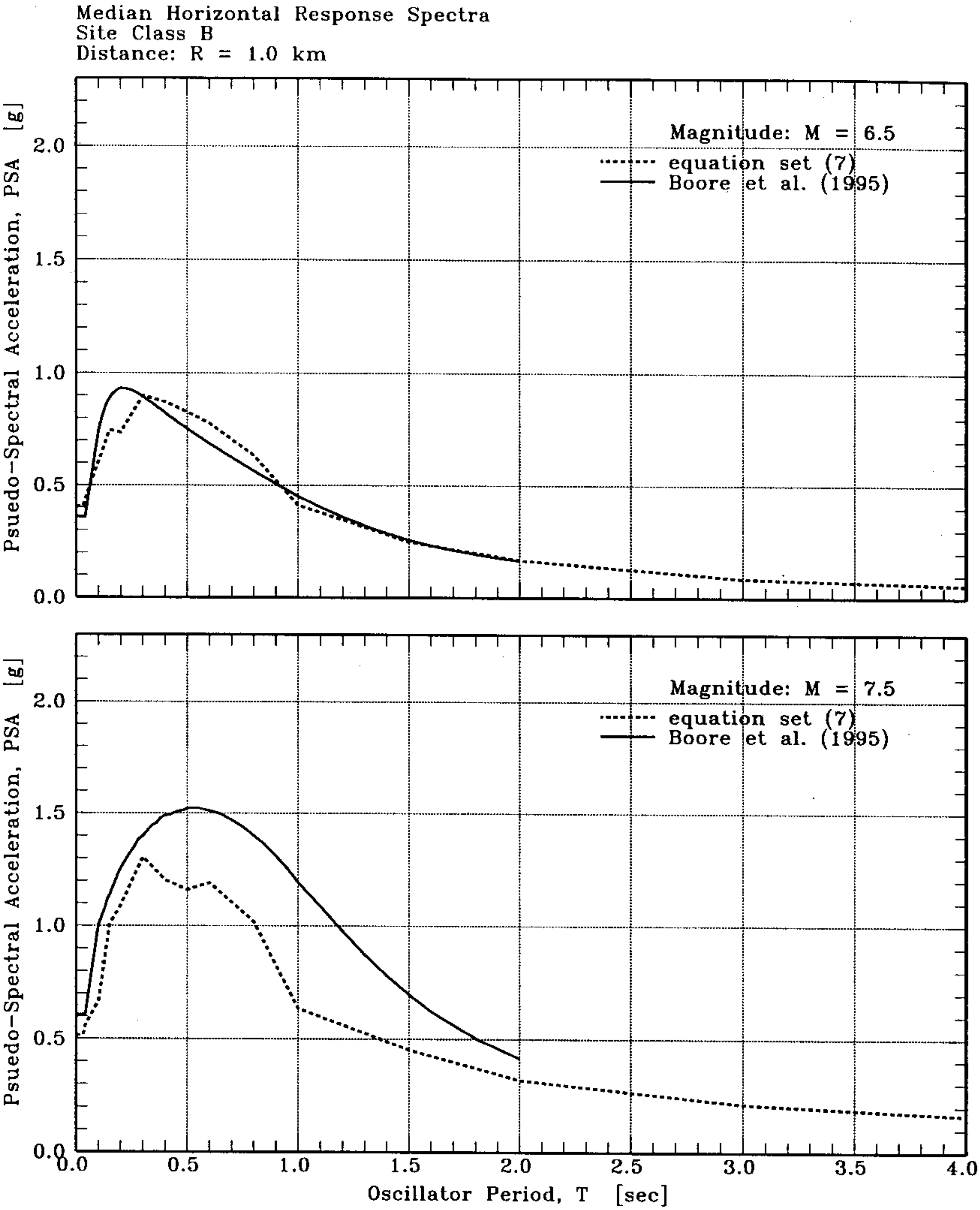

Figure 20. Median horizontal response spectra plots. Plots compare response spectra predicted by equation set 7 and by Boore et al. (1995) for magnitudes M = 6.5 and 7.5 at distance D = 1.0 km for site class B, strike-slip conditions.

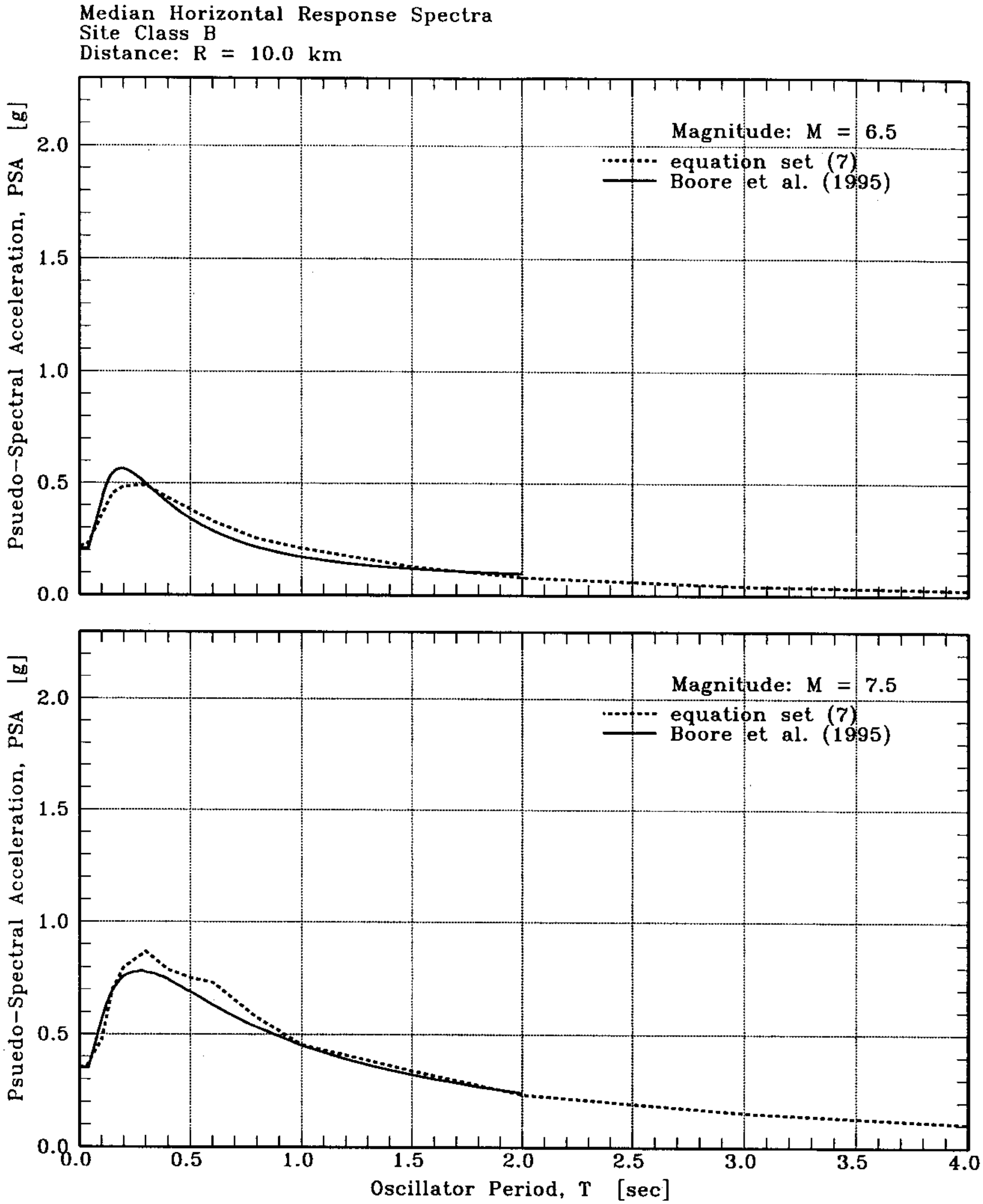

Figure 21. Median horizontal response spectra plots. Plots compare response spectra predicted by equation set 7 and by Boore et al. (1995) for magnitudes M = 6.5 and 7.5 at distance D = 10.0 km for site class B, strike-slip conditions.

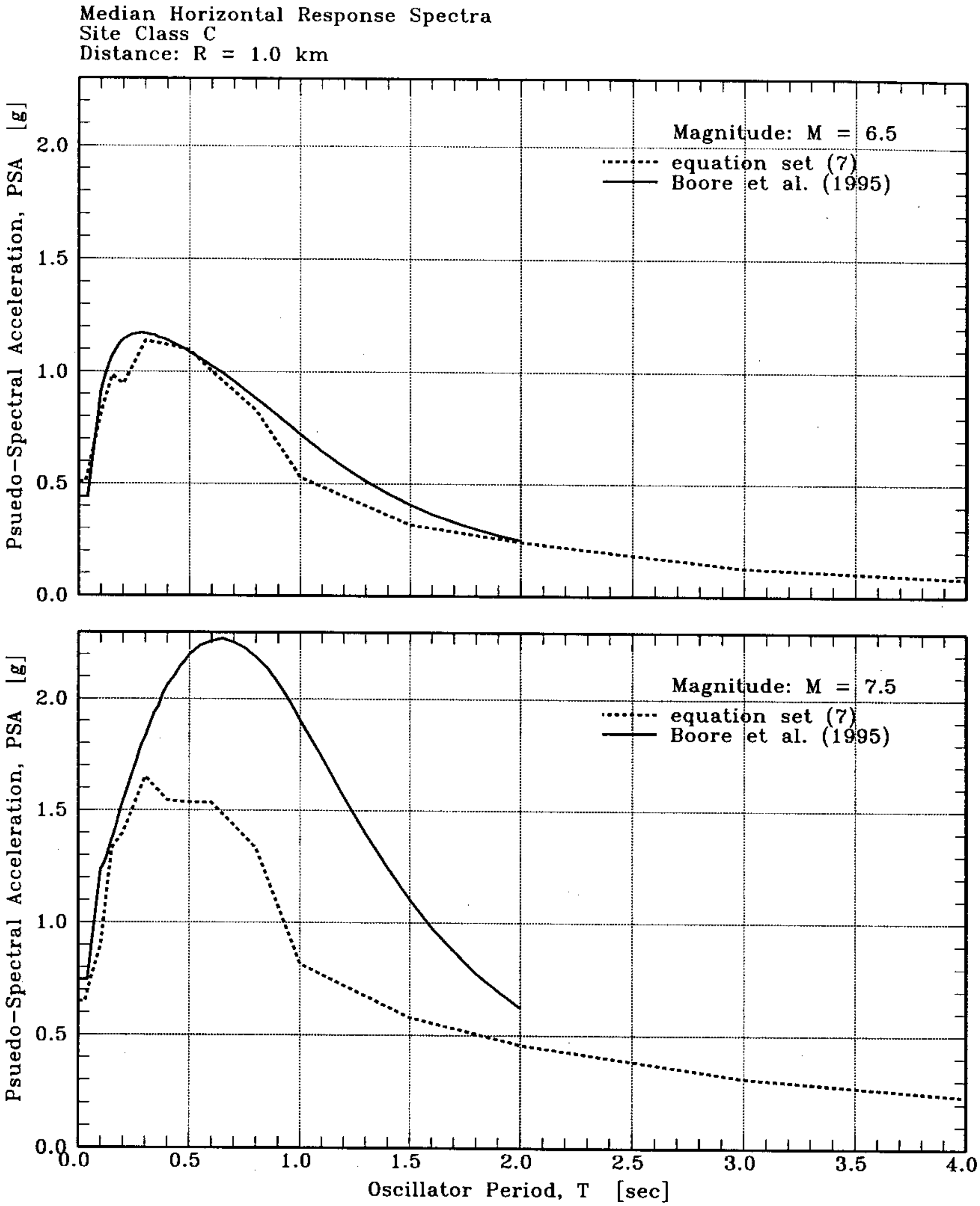

Figure 22. Median horizontal response spectra plots. Plots compare response spectra predicted by equation set 7 and by Boore et al. (1995) for magnitudes M = 6.5 and 7.5 at distance D = 1.0 km for site class C, strike-slip conditions.

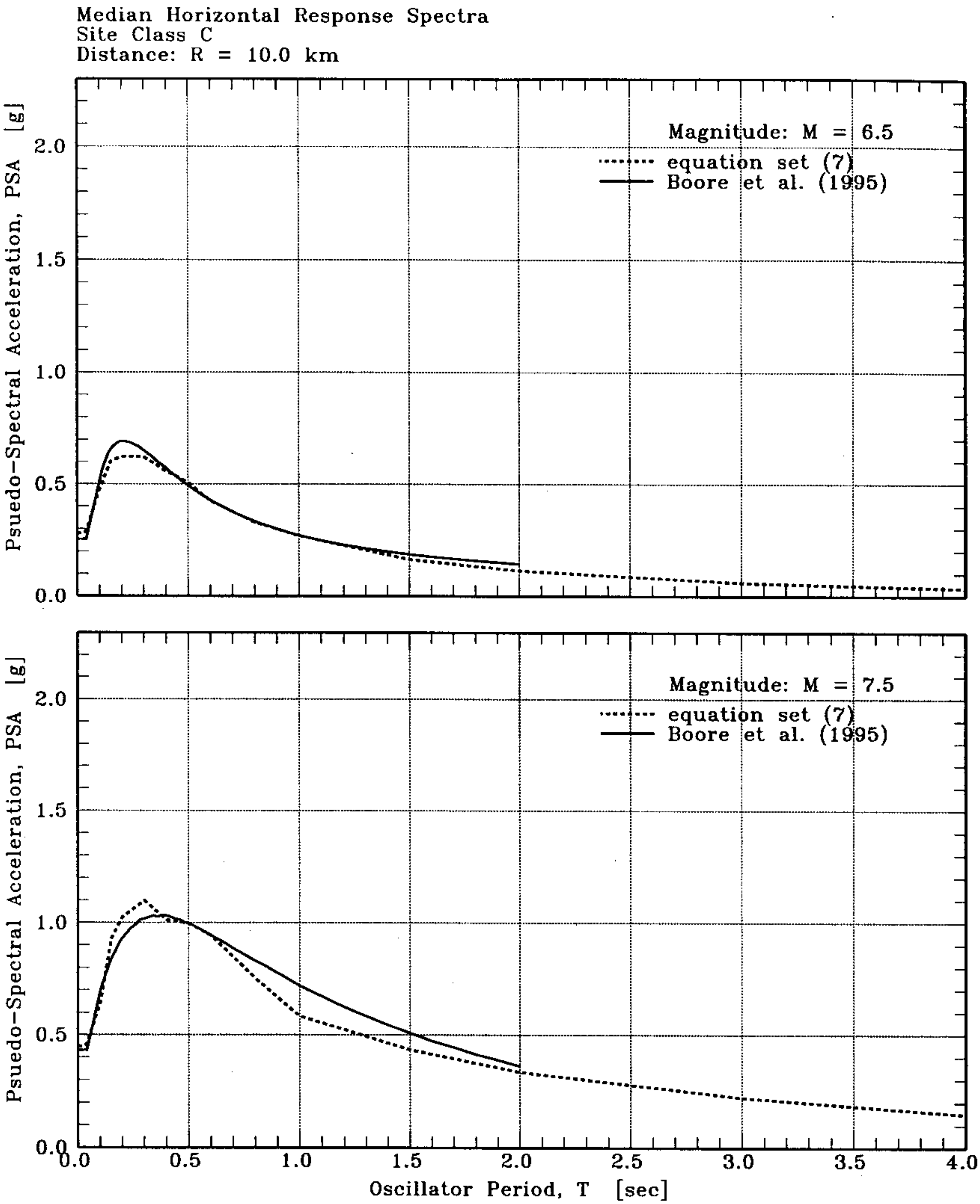

Figure 23. Median horizontal response spectra plots. Plots compare response spectra predicted by equation set 7 and by Boore et al. (1995) for magnitudes $M = 6.5$ and 7.5 at distance $D = 10.0$ km for site class C, strike-slip conditions.

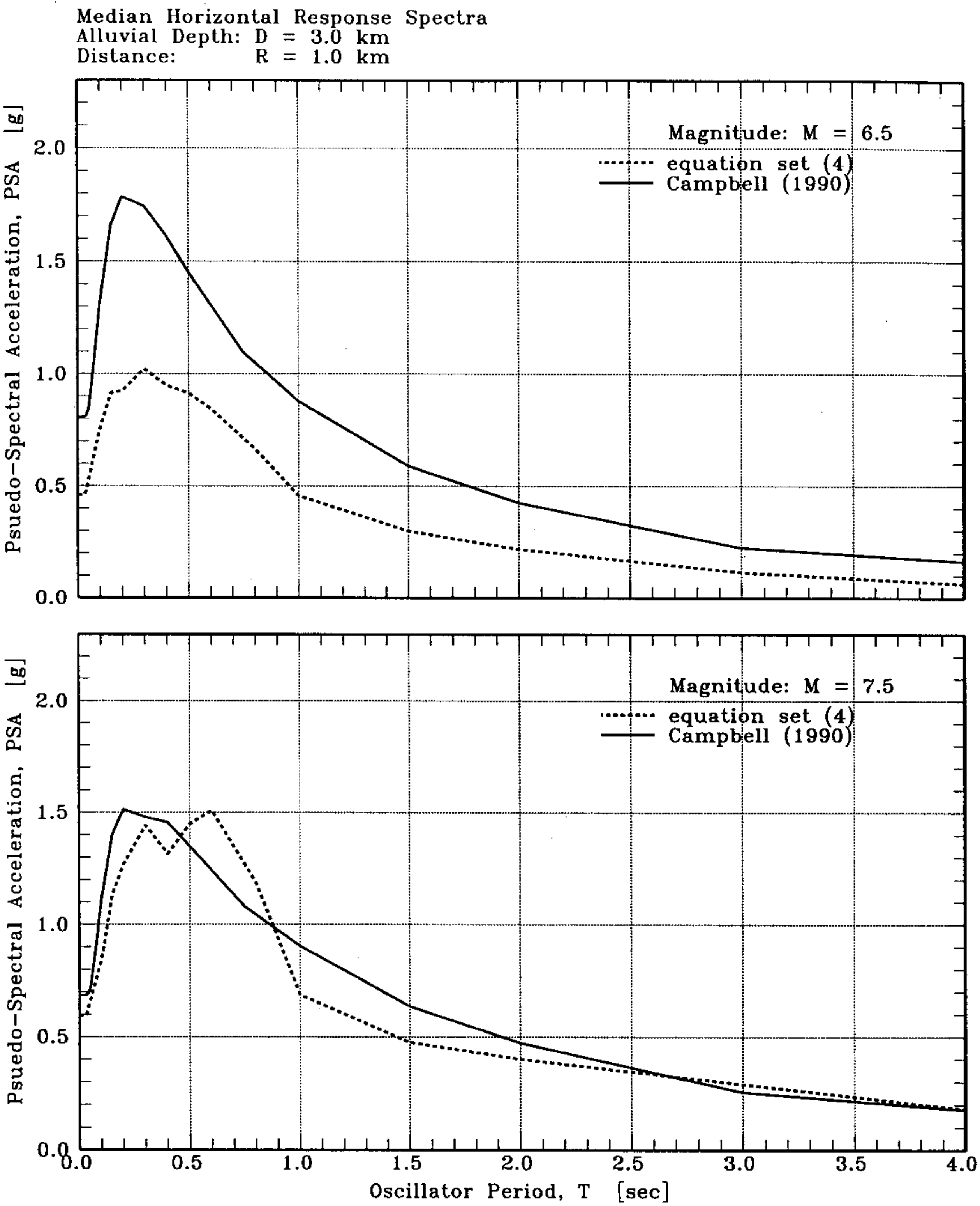

Figure 24. Median horizontal response spectra plots. Plots compare response spectra predicted by equation set 4 and by Campbell (1990) for magnitudes $M = 6.5$ and 7.5 at distance $D = 1.0$ km for strike-slip conditions with alluvial depth $D = 3.0$ km (database median depth).

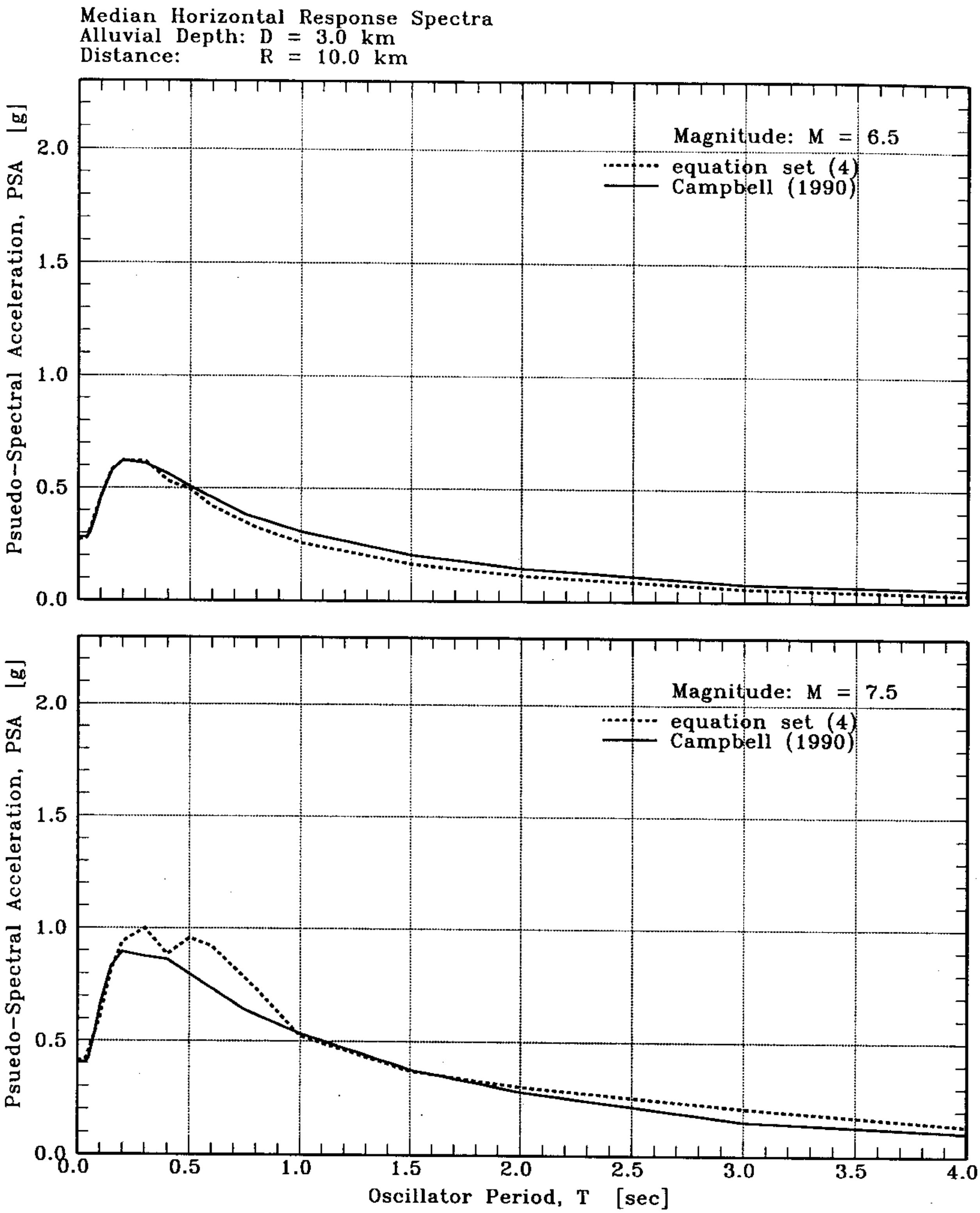

Figure 25. Median horizontal response spectra plots. Plots compare response spectra predicted by equation set 4 and by Campbell (1990) for magnitudes $M = 6.5$ and 7.5 at distance $D = 10.0$ km for strike-slip conditions with alluvial depth $D = 3.0$ km (database median depth).

Appendix A. Ground-Motion Database

Table A-1 on the following pages lists the ground-motion records used in the analysis. The table provides (1) the date, name, moment magnitude, and fault-type of the causative earthquake; (2) the station code, name, structure type, geographic coodinates, site classification, and depth-to-basement; (3) the source-to-site distance of the record; (4) the horizontal and vertical peak ground acceleration values; (5) references for geotechnical/geologic and strong-motion data sources; and (6) a list, for each record, of the databases within which the record is used. The following definitions and notes apply to Table A-1:

Mw	Earthquake moment magnitude
Fault Type	Code indicating the earthquake focal mechanism; $S \Rightarrow$ strike-slip, $R \Rightarrow$ reverse-slip
Station Desig.	U.S. Geological Survey station number, California Division of Mines and Geology station number, or an assigned alpha-numeric code
Structure Code	Code describing the structure housing the instrument (e.g. “3/1” refers to a 3-story structure with 1 sub-ground level; “3/” refers to a structure with either no sub-ground levels, or an unknown number of sub-ground levels; no entry indicates an instrument shelter in most cases, but may refer to a small structure)
Site Class	Entry is either “B”, “C”, or “B/C”; see the report text for the associated site class definitions
Alluvial Depth	Depth to basement rock at the recording station site; depth is reported in km.
Geologic Reference	Refer to the “Geologic References” list that follows Table A-1 for the complete citation corresponding to the given reference number
Closest Approach Distance	Closest distance from the recording station to the earthquake fault rupture surface; distance is reported in km
PGA	Peak ground accelerations recorded for the horizontal (*H1* and *H2*) and vertical (*V*) components; reported in units of *g*
Strong-Motion Data Source	Refer to the “Strong-Motion Data Sources” list that follows Table A-1 for complete citation corresponding to the given reference number
Database Subsets	A list of the database subsets within which the record is used; the database subsets are identified in Table 2, which is repeated below

Table 2. Database Subsets

Database Subset Number	Criteria for Inclusion in Database Subset									Number of Records in Subset	
	Site Classification						Alluvial Depth				
	B		C		B/C		unknown		known	H comp.	V comp.
1	(◆	or	◆	or	◆)	and	(◆	or	◆)	271	269
2	(◆	or	◆	or	◆)	and			◆	146	146
3	(◆	or	◆)			and	(◆	or	◆)	244	242
4	(◆	or	◆)			and			◆	139	139
5	◆					and	(◆	or	◆)	112	111
6	◆					and			◆	50	50
7			◆			and	(◆	or	◆)	132	131
8			◆			and			◆	89	89

Table A-1. Strong-Motion Database

Earthquake Yr.Mo.Dy	Earthquake Location	Mw	Fault Type	Station Desig.	Station Location	Structure Code	Station Location Latitude	Station Location Longitude	Site Class	Alluvial Depth	Geologic Reference	Closest Approach Distance [km]	PGA [g] H1	PGA [g] H2	PGA [g] V	Strong-Motion Data Source	Database Subsets
33.03.11	Long Beach	6.4	S	131	Long Beach, Utility Bldg	3/1	33.770 °N	118.190 °W	B	3.0	(7),(13),(39)	5.0	0.20	0.16	0.29	(10),(6)	1, 2, 3, 4, 5, 6
33.03.11	Long Beach	6.4	S	288	Vernon, Cmd Terminal	6/1	33.999 °N	118.196 °W	C	6.4	(7),(10),(4),(39)	19.5	0.13	0.15	0.15	(10),(5)	1, 2, 3, 4, 7, 8
40.05.19	Imperial Valley	7.0	S	117	El Centro, Imperial. Val. Irrig. Dist.	2/0	32.790 °N	115.550 °W	C	6.1	(36),(38),(7),(26),(27),(31)	10.0	0.35	0.21	0.21	(10),(5)	1, 2, 3, 4, 7, 8
52.07.21	Kern County	7.4	R	1094	Taft, Lincoln School Tunnel	2/0	35.150 °N	119.460 °W	B	NA	(38),(7),(28),(11),(31)	42.0	0.16	0.18	0.10	(10),(5)	1, 3, 5
52.07.21	Kern County	7.4	R	283	Santa Barbara Courthouse	2/1	34.420 °N	119.700 °W	B	0.5	(38),(7),(28),(12),(31),(3)	85.0	0.09	0.13	0.04	(10),(5)	1, 2, 3, 4, 5, 6
52.07.21	Kern County	7.4	R	135	Los Angeles, Hollywood Storage PE Lot		34.090 °N	118.339 °W	C	2.3	(7),(10),(30),(31),(39)	107.0	0.06	0.04	0.02	(10),(5)	1, 2, 3, 4, 7, 8
52.07.21	Kern County	7.4	R	475	Pasadena, CIT Athenaeum	2/1	34.139 °N	118.121 °W	B	0.9	(7),(12),(39)	109.0	0.05	0.05	0.03	(10),(5)	1, 2, 3, 4, 5, 6
66.06.28	Central California	6.1	S	1013	Parkfield, Cholame 2WA		35.733 °N	120.290 °W	C	3.0	(34),(27),(31),(13),(3)	0.1	0.49	NA	0.21	(10),(5)	1, 2, 3, 4, 7, 8
66.06.28	Central California	6.1	S	1014	Parkfield, Cholame 5W		35.697 °N	120.328 °W	C	1.1	(34),(13),(3)	5.0	0.35	0.43	0.12	(10),(5)	1, 2, 3, 4, 7, 8
66.06.28	Central California	6.1	S	1015	Parkfield, Cholame 8W	1/0	35.671 °N	120.359 °W	C	1.9	(34),(11),(13),(3)	9.5	0.24	0.27	0.08	(10),(5)	1, 2, 3, 4, 7, 8
66.06.28	Central California	6.1	S	1097	Parkfield, Cholame (Shandon Temblor)		35.710 °N	120.170 °W	B	NA	(11)	11.3	0.27	0.35	0.13	(10),(5)	1, 3, 5
66.06.28	Central California	6.1	S	1016	Parkfield, Cholame 12W		35.639 °N	120.404 °W	B	2.6	(34),(11),(13),(3)	15.0	0.05	0.06	0.05	(10),(5)	1, 2, 3, 4, 5, 6
66.06.28	Central California	6.1	S	1094	Taft, Lincoln School Tunnel	2/0	35.150 °N	119.460 °W	B	NA	(38),(7),(28),(11),(31)	131.0	0.01	0.01	0.01	(10),(5),(6)	1, 3, 5
66.06.07	Baja	6.3	S	117	El Centro, Imperial. Val. Irrig. Dist.	2/0	32.790 °N	115.550 °W	C	6.1	(36),(38),(7),(26),(27),(31)	148.0	0.01	0.02	0.005	(10),(5),(6)	1, 2, 3, 4, 7, 8
68.04.09	Borrego Mountain	6.6	S	117	El Centro, Imperial. Val. Irrig. Dist.	2/0	32.790 °N	115.550 °W	C	6.1	(36),(38),(7),(26),(27),(31)	45.0	0.13	0.06	0.03	(10),(5)	1, 2, 3, 4, 7, 8
68.04.09	Borrego Mountain	6.6	S	280	San Onofre, SCE Power Plant	1/0	33.370 °N	117.560 °W	B	NA	(32)	122.0	0.04	0.05	0.06	(10),(5)	1, 3, 5
68.04.09	Borrego Mountain	6.6	S	113	Colton, SCE	1/0	34.060 °N	117.320 °W	C	0.2	(7),(12),(3)	130.0	0.02	0.03	0.02	(10),(5)	1, 2, 3, 4, 7, 8
68.04.09	Borrego Mountain	6.6	S	130	Long Beach, Terminal Island	1/1	33.770 °N	118.230 °W	C	2.1	(7),(17),(39)	187.0	0.01	0.01	0.01	(10),(5)	1, 2, 3, 4, 7, 8
68.04.09	Borrego Mountain	6.6	S	475	Pasadena, CIT Athenaeum	2/1	34.139 °N	118.121 °W	B	0.9	(7),(12),(39)	196.0	0.01	0.01	0.004	(10),(5)	1, 2, 3, 4, 5, 6
68.04.09	Borrego Mountain	6.6	S	288	Vernon, Cmd Terminal	6/1	33.999 °N	118.196 °W	C	6.4	(7),(10),(4),(39)	196.0	0.02	0.02	0.01	(10),(5)	1, 2, 3, 4, 7, 8
68.04.09	Borrego Mountain	6.6	S	135	Los Angeles, Hollywood Storage PE Lot		34.090 °N	118.339 °W	C	2.3	(7),(10),(30),(31),(39)	211.0	0.01	0.01	0.005	(10),(5)	1, 2, 3, 4, 7, 8
70.09.12	Lytle Creek	5.2	R	290	Wrightwood, 6074 Park Dr.	2/0	34.360 °N	117.630 °W	B	0.1	(12),(3)	15.0	0.14	0.20	0.05	(10)	1, 2, 3, 4, 5, 6
70.09.12	Lytle Creek	5.2	R	274	San Bernardino, Hall of Records	6/1	34.110 °N	117.290 °W	C	1.1	(4),(3)	28.0	0.12	0.06	0.05	(10)	1, 2, 3, 4, 7, 8
70.09.12	Lytle Creek	5.2	R	113	Colton, SCE	1/0	34.060 °N	117.320 °W	C	0.2	(7),(12),(3)	29.0	0.04	0.04	0.03	(10)	1, 2, 3, 4, 7, 8
71.02.09	San Fernando	6.6	R	122	Glendale, 633 E Broadway	3/1	34.150 °N	118.250 °W	B	NA	(32),(33),(31)	18.0	0.27	0.21	0.13	(10),(5)	1, 3, 5
71.02.09	San Fernando	6.6	R	128	Lake Hughes, Array Station 12	1/0	34.570 °N	118.560 °W	B	NA	(32),(4)	21.0	0.35	0.28	0.11	(10),(5)	1, 3, 5
71.02.09	San Fernando	6.6	R	135	Los Angeles, Hollywood Storage PE Lot		34.090 °N	118.339 °W	C	2.3	(7),(10),(30),(31),(39)	23.0	0.17	0.21	0.09	(10),(5)	1, 2, 3, 4, 7, 8
71.02.09	San Fernando	6.6	R	262	Palmdale Fire Station	1/0	34.580 °N	118.110 °W	B	0.2	(10),(3)	24.0	0.11	0.14	0.09	(10),(5)	1, 2, 3, 4, 5, 6
71.02.09	San Fernando	6.6	R	475	Pasadena, CIT Athenaeum	2/1	34.139 °N	118.121 °W	B	0.9	(7),(12),(39)	24.0	0.10	0.11	0.09	(10),(5)	1, 2, 3, 4, 5, 6
71.02.09	San Fernando	6.6	R	125	Lake Hughes, Array Station 1	1/0	34.680 °N	118.440 °W	B	3.0	(10),(29),(31),(3)	25.0	0.15	0.11	0.09	(10),(5)	1, 2, 3, 4, 5, 6
71.02.09	San Fernando	6.6	R	110	Castaic, Old Ridge Route	1/	34.560 °N	118.660 °W	B	10.0	(12),(32),(31),(3)	26.0	0.32	0.27	0.16	(10),(5)	1, 2, 3, 4, 5, 6
71.02.09	San Fernando	6.6	R	288	Vernon, Cmd Terminal	6/1	33.999 °N	118.196 °W	C	6.4	(7),(10),(4),(39)	33.5	0.11	0.08	0.04	(10),(5)	1, 2, 3, 4, 7, 8
71.02.09	San Fernando	6.6	R	585	Pearblossom Pump Plant	1/0	34.510 °N	117.920 °W	B	NA	(10)	36.0	0.09	0.12	0.05	(10),(5)	1, 3, 5
71.02.09	San Fernando	6.6	R	289	Whittier Narrows Dam (Upstream)		34.030 °N	118.050 °W	C	2.4	(4),(39)	38.0	0.10	0.10	0.06	(10),(5)	1, 2, 3, 4, 7, 8
71.02.09	San Fernando	6.6	R	411	Palos Verdes Estates, 2516 Via Tejon	2/	33.800 °N	118.380 °W	B	0.0	(12),(32),(31),(39)	52.0	0.03	0.04	0.02	(10),(5)	1, 2, 3, 4, 5, 6
71.02.09	San Fernando	6.6	R	130	Long Beach, Terminal Island	1/1	33.770 °N	118.230 °W	C	2.1	(7),(17),(39)	58.0	0.03	0.03	0.02	(10),(5)	1, 2, 3, 4, 7, 8
71.02.09	San Fernando	6.6	R	131	Long Beach, Utility Bldg	3/1	33.770 °N	118.190 °W	B	3.0	(7),(13),(39)	58.0	0.03	0.02	0.01	(10),(5)	1, 2, 3, 4, 5, 6
71.02.09	San Fernando	6.6	R	290	Wrightwood, 6074 Park Dr.	2/0	34.360 °N	117.630 °W	B	0.1	(12),(3)	59.0	0.04	0.06	0.02	(10),(5)	1, 2, 3, 4, 5, 6
71.02.09	San Fernando	6.6	R	281	Santa Ana, Engineering Bldg	3/1	33.750 °N	117.870 °W	C	2.9	(4),(39)	71.5	0.03	0.03	0.02	(10),(5)	1, 2, 3, 4, 7, 8
71.02.09	San Fernando	6.6	R	1102	Wheeler Ridge, Ground Station		35.030 °N	119.010 °W	B	NA	(12)	80.0	0.03	0.03	0.01	(10),(5)	1, 3, 5
71.02.09	San Fernando	6.6	R	274	San Bernardino, Hall of Records	6/1	34.110 °N	117.290 °W	C	1.1	(4),(3)	100.0	0.04	0.04	0.02	(10),(5)	1, 2, 3, 4, 7, 8
71.02.09	San Fernando	6.6	R	465	San Juan Capistrano, City Hall	1/	33.490 °N	117.670 °W	C	NA	(4)	104.0	0.04	0.03	0.02	(10),(5)	1, 3, 7
71.02.09	San Fernando	6.6	R	282	Goleta, UCSB Fluid Mech. Lab.	1/	34.410 °N	119.850 °W	B	NA	(32),(31)	120.0	0.02	0.02	0.01	(10),(5)	1, 3, 5
71.02.09	San Fernando	6.6	R	280	San Onofre, SCE Power Plant	1/0	33.370 °N	117.560 °W	B	NA	(32)	121.0	0.01	0.02	0.01	(10),(5)	1, 3, 5
71.02.09	San Fernando	6.6	R	123	Hemet, Stetson Av Fire Station	1/	33.729 °N	116.979 °W	C	NA	(13),(4)	134.0	0.04	0.04	0.03	(10),(5)	1, 3, 7
74.11.28	Central California	5.2	S	1377	San Juan Bautista, 24 Polk Street	1/	36.846 °N	121.536 °W	B	NA	(2)	8.9	0.04	0.11	0.05	(10)	1, 3, 5
74.11.28	Central California	5.2	S	1250	Gilroy, Gavilan College	1/	36.973 °N	121.568 °W	B	NA	(8),(31)	10.8	0.10	0.13	0.03	(10)	1, 3, 5
74.11.28	Central California	5.2	S	1028	Hollister Public Library	2/1	36.850 °N	121.400 °W	C	1.7	(38),(8),(30),(31),(1)	10.8	0.09	0.16	0.07	(10)	1, 2, 3, 4, 7, 8
78.08.13	Santa Barbara	5.8	R	283	Santa Barbara Courthouse	2/1	34.420 °N	119.700 °W	B	0.5	(38),(7),(28),(12),(31),(3)	5.0	0.10	0.20	0.08	(10)	1, 2, 3, 4, 5, 6
78.08.13	Santa Barbara	5.8	R	91	Goleta, UCSB Free Field		34.422 °N	119.851 °W	B	NA	(2)	8.0	0.35	0.29	0.14	(2)	1, 3, 5
78.09.12	Tabas, Iran	7.4	R	NA	Tabas, Iran		33.600 °N	56.920 °E	B/C	NA	(20)	3.0	0.88	0.93	0.75	(1)	1
78.09.12	Tabas, Iran	7.4	R	NA	Dayhook, Iran		33.300 °N	57.520 °E	B/C	NA	(20)	14.0	0.37	0.40	0.19	(1)	1
78.09.12	Tabas, Iran	7.4	R	NA	Boshrooyeh, Iran		33.880 °N	57.430 °E	B/C	NA	(20)	24.0	0.11	0.09	0.08	(1)	1
78.09.12	Tabas, Iran	7.4	R	NA	Ferdows, Iran		34.030 °N	58.173 °E	B/C	NA	(20)	83.0	0.10	0.11	0.05	(1)	1
78.09.12	Tabas, Iran	7.4	R	NA	Bajestan, Iran		34.510 °N	58.180 °E	B/C	NA	(20)	108.0	0.09	0.07	0.03	(1)	1
78.09.12	Tabas, Iran	7.4	R	NA	Sedeh, Iran		33.330 °N	59.230 °E	B/C	NA	(20)	138.0	0.03	0.03	0.01	(1)	1
78.09.12	Tabas, Iran	7.4	R	NA	Kashmar, Iran		35.300 °N	58.450 °E	B/C	NA	(20)	186.0	0.03	0.04	0.03	(1)	1
79.08.06	Coyote Lake	5.8	S	57383	Gilroy #6, San Ysidro Microwave Site		37.026 °N	121.484 °W	B	0.5	(8),(11),(3)	1.0	0.42	0.32	0.15	(2)	1, 2, 3, 4, 5, 6
79.08.06	Coyote Lake	5.8	S	47381	Gilroy #3, Gilroy Sewage Treat. Plant		36.987 °N	121.536 °W	C	0.8	(8),(11),(23)	5.0	0.25	0.26	0.14	(2)	1, 2, 3, 4, 7, 8
79.08.06	Coyote Lake	5.8	S	47380	Gilroy #2, Hwy 101/Bolsa Road Motel		36.982 °N	121.556 °W	C	0.3	(8),(11),(14),(23)	7.0	0.25	0.19	0.17	(2)	1, 2, 3, 4, 7, 8
79.08.06	Coyote Lake	5.8	S	47126	San Juan Bautista Fire Station	1/0	36.848 °N	121.536 °W	B	0.4	(2),(3)	16.0	0.10	0.11	0.12	(2)	1, 2, 3, 4, 5, 6
79.08.06	Coyote Lake	5.8	S	57191	Halls Valley, Grant Ranch Park, Old HQ		37.338 °N	121.714 °W	B	0.0	(2),(3)	30.0	0.05	0.04	0.02	(2)	1, 2, 3, 4, 5, 6
79.10.15	Imperial Valley	6.5	S	1336	El Centro, Rt 8 / Meloland Rd.		32.773 °N	115.448 °W	C	6.1	(5),(38)	0.5	0.30	0.32	0.23	(2)	1, 2, 3, 4, 7, 8

Table A-1. Strong-Motion Database

Earthquake Yr.Mo.Dy	Earthquake Location	Mw	Fault Type	Station Desig.	Station Location	Structure Code	Station Location Latitude	Station Location Longitude	Site Class	Alluvial Depth	Geologic Reference	Closest Approach Distance [km]	PGA [g] H1	PGA [g] H2	PGA [g] V	Strong-Motion Data Source	Database Subsets
79.10.15	Imperial Valley	6.5	S	5158	El Centro #6, 551 Huston Road		32.839 °N	115.487 °W	C	6.1	(26),(38)	1.0	0.44	0.38	1.70	(10),(6)	1, 2, 3, 4, 7, 8
79.10.15	Imperial Valley	6.5	S	5028	El Centro #7, Imperial Valley College	1/	32.829 °N	115.504 °W	C	6.1	(36),(26),(38)	1.0	0.46	0.33	0.51	(10),(6)	1, 2, 3, 4, 7, 8
79.10.15	Imperial Valley	6.5	S	6616	Aeropuerto		32.650 °N	115.330 °W	C	6.1	(2),(38)	1.4	0.26	0.33	0.16	(10),(7)	1, 2, 3, 4, 7, 8
79.10.15	Imperial Valley	6.5	S	5054	Bonds Corner	1/	32.693 °N	115.338 °W	C	6.1	(26),(38)	3.0	0.79	0.59	0.35	(10),(6)	1, 2, 3, 4, 7, 8
79.10.15	Imperial Valley	6.5	S	952	El Centro #5, James Road	1/	32.855 °N	115.466 °W	C	6.1	(26),(38)	4.0	0.37	0.53	0.44	(10),(6)	1, 2, 3, 4, 7, 8
79.10.15	Imperial Valley	6.5	S	5159	El Centro #8, Cruickshank Road	1/	32.811 °N	115.532 °W	C	6.1	(26),(38)	4.0	0.47	0.61	0.41	(10)	1, 2, 3, 4, 7, 8
79.10.15	Imperial Valley	6.5	S	5165	El Centro, Dogwood Road	1/	32.800 °N	115.540 °W	C	6.1	(35),(26),(38)	5.0	0.49	0.35	0.66	(10),(6)	1, 2, 3, 4, 7, 8
79.10.15	Imperial Valley	6.5	S	5060	Brawley Municipal Airport	1/	32.988 °N	115.509 °W	C	6.1	(26),(38)	7.0	0.22	0.17	0.15	(10),(6)	1, 2, 3, 4, 7, 8
79.10.15	Imperial Valley	6.5	S	955	El Centro #4, Anderson Road	1/	32.860 °N	115.430 °W	C	6.1	(26),(38)	7.0	0.36	0.49	0.20	(10),(6)	1, 2, 3, 4, 7, 8
79.10.15	Imperial Valley	6.5	S	5055	Holtville Post Office	1/	32.810 °N	115.380 °W	C	6.1	(26),(38)	8.0	0.22	0.25	0.23	(10),(6)	1, 2, 3, 4, 7, 8
79.10.15	Imperial Valley	6.5	S	412	El Centro #10, Community Hospital		32.780 °N	115.567 °W	C	6.1	(36),(26),(38)	9.0	0.17	0.23	0.10	(10),(6)	1, 2, 3, 4, 7, 8
79.10.15	Imperial Valley	6.5	S	5053	Calexico Fire Station		32.699 °N	115.492 °W	C	6.1	(26),(38)	11.0	0.20	0.27	0.18	(10),(6)	1, 2, 3, 4, 7, 8
79.10.15	Imperial Valley	6.5	S	6617	Cucupah		32.550 °N	115.230 °W	C	6.1	(2),(38)	11.0	0.31	NA	0.14	(10),(7)	1, 2, 3, 4, 7, 8
79.10.15	Imperial Valley	6.5	S	5057	El Centro #3, Pine Union School	1/	32.894 °N	115.380 °W	C	4.6	(26),(38)	12.7	0.22	0.27	0.13	(10),(7)	1, 2, 3, 4, 7, 8
79.10.15	Imperial Valley	6.5	S	5058	El Centro #11, McCabe Union School	1/	32.752 °N	115.594 °W	C	6.1	(26),(38)	13.0	0.38	0.36	0.14	(10),(6)	1, 2, 3, 4, 7, 8
79.10.15	Imperial Valley	6.5	S	5051	El Centro, Parachute Test Facility	1/	32.930 °N	115.700 °W	B	4.0	(26),(38)	15.0	0.20	0.11	0.16	(10),(6)	1, 2, 3, 4, 5, 6
79.10.15	Imperial Valley	6.5	S	931	El Centro #12, 907 Brockman Road	1/	32.710 °N	115.630 °W	C	4.6	(26),(38)	18.0	0.12	0.14	0.07	(10),(6)	1, 2, 3, 4, 7, 8
79.10.15	Imperial Valley	6.5	S	6622	Compuertas		32.573 °N	115.083 °W	C	6.1	(2),(38)	22.0	0.19	0.07	0.15	(10),(7)	1, 2, 3, 4, 7, 8
79.10.15	Imperial Valley	6.5	S	5059	El Centro #13, Strobel Residence	1/	32.709 °N	115.683 °W	C	2.1	(26),(38)	22.0	0.14	0.12	0.04	(10),(7)	1, 2, 3, 4, 7, 8
79.10.15	Imperial Valley	6.5	S	5056	El Centro #1, Borchard Ranch	1/	32.960 °N	115.319 °W	C	5.2	(2),(38)	22.0	0.14	0.14	0.04	(10),(6)	1, 2, 3, 4, 7, 8
79.10.15	Imperial Valley	6.5	S	5052	Plaster City Storehouse	1/	32.790 °N	115.850 °W	C	1.5	(2),(38)	31.0	0.06	0.04	0.03	(10),(6)	1, 2, 3, 4, 7, 8
79.10.15	Imperial Valley	6.5	S	11023	Niland Fire Station	1/	33.239 °N	115.512 °W	C	2.4	(2),(38)	34.0	0.11	0.07	0.03	(2)	1, 2, 3, 4, 7, 8
79.10.15	Imperial Valley	6.5	S	5066	Coachella Canal #4	1/	33.360 °N	115.590 °W	C	NA	(2)	49.0	0.13	0.12	0.04	(10),(7)	1, 3, 7
80.01.24	Livermore	5.8	S	57187	San Ramon, Eastman Kodak		37.729 °N	121.928 °W	C	NA	(2)	17.0	0.15	0.06	0.03	(2)	1, 3, 7
80.01.24	Livermore	5.8	S	57134	San Ramon		37.780 °N	121.980 °W	C	NA	(2)	18.0	0.05	0.04	0.02	(2)	1, 3, 7
80.01.24	Livermore	5.8	S	67070	Antioch		38.015 °N	121.813 °W	B	NA	(2)	21.0	0.04	0.02	0.01	(2)	1, 3, 5
80.01.24	Livermore	5.8	S	57063	Tracy		37.766 °N	121.421 °W	C	NA	(2)	29.0	0.05	0.06	0.02	(2)	1, 3, 7
80.01.24	Livermore	5.8	S	58219	Hayward, CSUH Stadium Grounds		37.657 °N	122.061 °W	B	NA	(8),(15)	31.0	0.06	0.06	0.02	(2)	1, 3, 5
80.01.24	Livermore	5.8	S	57064	Fremont, Mission San Jose	1/	37.530 °N	121.919 °W	B	2.3	(8),(13),(37),(3)	32.0	0.05	0.05	0.03	(2)	1, 2, 3, 4, 5, 6
81.04.26	Westmorland	5.9	S	5060	Brawley, Municipal Airport	1/	32.988 °N	115.509 °W	C	6.1	(26),(38)	19.0	0.18	0.16	0.11	(2)	1, 2, 3, 4, 7, 8
81.04.26	Westmorland	5.9	S	5051	El Centro, Parachute Test Facility	1/	32.930 °N	115.700 °W	B	4.0	(26),(38)	19.0	0.23	0.16	0.16	(2)	1, 2, 3, 4, 5, 6
81.04.26	Westmorland	5.9	S	11023	Niland Fire Station	1/	33.239 °N	115.512 °W	C	2.4	(2),(38)	21.0	0.19	0.11	0.13	(10)	1, 2, 3, 4, 7, 8
83.05.02	Coalinga	6.4	R	1162	Pleasant Valley Pump Plant, Switchyard	NA	36.308 °N	120.249 °W	B/C	NA	(13),(4)	12.0	0.52	0.45	0.38	(10)	1
83.05.02	Coalinga	6.4	R	36453	Parkfield, Fault Zone 11		35.896 °N	120.398 °W	B	NA	(13)	33.1	0.09	0.08	0.04	(2)	1, 3, 5
83.05.02	Coalinga	6.4	R	36439	Parkfield, Gold Hill 3E		35.870 °N	120.334 °W	B	NA	(13)	34.1	0.07	0.10	0.06	(2)	1, 3, 5
83.05.02	Coalinga	6.4	R	36138	Parkfield, Fault Zone 12		35.899 °N	120.433 °W	C	NA	(13)	34.2	0.11	0.11	0.07	(2)	1, 3, 7
83.05.02	Coalinga	6.4	R	36438	Parkfield, Stone Corral 4E		35.855 °N	120.281 °W	B	NA	(13)	35.1	0.07	0.07	0.03	(2)	1, 3, 5
83.05.02	Coalinga	6.4	R	36454	Parkfield, Fault Zone 6		35.859 °N	120.420 °W	B	NA	(13)	37.6	0.06	0.06	0.03	(2)	1, 3, 5
83.05.02	Coalinga	6.4	R	36414	Parkfield, Fault Zone 4		35.836 °N	120.395 °W	B	NA	(13)	39.2	0.12	0.07	0.05	(2)	1, 3, 5
83.05.02	Coalinga	6.4	R	36416	Parkfield, Gold Hill 2W		35.812 °N	120.391 °W	B	NA	(13)	41.6	0.08	0.08	0.04	(2)	1, 3, 5
83.05.02	Coalinga	6.4	R	36413	Parkfield, Fault Zone 2		35.787 °N	120.334 °W	C	NA	(13)	43.1	0.14	0.12	0.04	(2)	1, 3, 7
83.05.02	Coalinga	6.4	R	36420	Parkfield, Gold Hill 3W		35.796 °N	120.411 °W	B	NA	(13)	43.8	0.12	0.14	0.07	(2)	1, 3, 5
83.05.02	Coalinga	6.4	R	36450	Parkfield, Cholame 3E		35.770 °N	120.247 °W	B	NA	(13)	44.4	0.05	0.04	0.03	(2)	1, 3, 5
83.05.02	Coalinga	6.4	R	36433	Parkfield, Gold Hill 4W		35.785 °N	120.444 °W	B	NA	(13)	46.0	0.10	0.06	0.03	(2)	1, 3, 5
83.05.02	Coalinga	6.4	R	36441	Parkfield, Vineyard Canyon 6W		35.861 °N	120.600 °W	B	NA	(13)	46.3	0.08	0.05	0.04	(2)	1, 3, 5
83.05.02	Coalinga	6.4	R	36230	Parkfield, Cholame 2E (Temblor II)		35.752 °N	120.264 °W	B	NA	(13)	46.4	0.04	0.03	0.02	(2)	1, 3, 5
83.05.02	Coalinga	6.4	R	36452	Parkfield, Cholame 1E		35.743 °N	120.277 °W	C	NA	(13)	47.4	0.09	0.09	0.06	(2)	1, 3, 7
83.05.02	Coalinga	6.4	R	36228	Parkfield, Cholame 2WA		35.733 °N	120.290 °W	C	3.0	(34),(27),(31),(13),(3)	48.6	0.11	0.11	0.04	(2)	1, 2, 3, 4, 7, 8
83.05.02	Coalinga	6.4	R	36411	Parkfield, Cholame 4W		35.718 °N	120.304 °W	B	NA	(13)	50.3	0.13	0.13	0.04	(2)	1, 3, 5
83.05.02	Coalinga	6.4	R	36227	Parkfield, Cholame 5W		35.697 °N	120.328 °W	C	1.1	(34),(13),(3)	52.9	0.14	0.14	0.03	(2)	1, 2, 3, 4, 7, 8
83.05.02	Coalinga	6.4	R	36226	Parkfield, Cholame 8W	1/	35.671 °N	120.359 °W	C	1.9	(34),(11),(13),(3)	56.1	0.10	0.10	0.03	(2)	1, 2, 3, 4, 7, 8
83.05.02	Coalinga	6.4	R	36229	Parkfield, Cholame 12W		35.639 °N	120.404 °W	B	2.6	(34),(11),(13),(3)	60.4	0.05	0.02	0.04	(2)	1, 2, 3, 4, 5, 6
84.04.24	Morgan Hill	6.3	S	1652	Anderson Dam, Downstream		37.166 °N	121.628 °W	B	0.0	(8),(13),(3)	3.9	0.29	0.42	0.21	(10),(3)	1, 2, 3, 4, 5, 6
84.04.24	Morgan Hill	6.3	S	57383	Gilroy #6, San Ysidro Microwave Site		37.026 °N	121.484 °W	B	0.5	(8),(11),(3)	11.5	0.29	0.23	0.43	(2),(3)	1, 2, 3, 4, 5, 6
84.04.24	Morgan Hill	6.3	S	57425	Gilroy #7, Mantelli Ranch, Jamison Rd		37.033 °N	121.434 °W	C	0.5	(13),(16),(3)	13.7	0.11	0.19	0.45	(2),(3)	1, 2, 3, 4, 7, 8
84.04.24	Morgan Hill	6.3	S	47381	Gilroy #3, Gilroy Sewage Treat. Plant		36.987 °N	121.536 °W	C	0.6	(8),(11),(23)	14.4	0.20	0.20	0.39	(2),(3)	1, 2, 3, 4, 7, 8
84.04.24	Morgan Hill	6.3	S	47380	Gilroy #2, Hwy 101/Bolsa Road Motel		36.982 °N	121.556 °W	C	0.3	(8),(11),(14),(23)	14.9	0.22	0.17	0.60	(2),(3)	1, 2, 3, 4, 7, 8
84.04.24	Morgan Hill	6.3	S	47006	Gilroy, Gavilan College Phys. Sci. Bldg.	1/	36.973 °N	121.568 °W	B	NA	(8),(31)	16.0	0.12	0.10	0.12	(2)	1, 3, 5
84.04.24	Morgan Hill	6.3	S	57007	Corralitos, Eureka Canyon Road		37.046 °N	121.803 °W	B	3.8	(8),(13),(16),(3)	23.5	0.11	0.08	0.05	(2),(3)	1, 2, 3, 4, 5, 6
84.04.24	Morgan Hill	6.3	S	57066	Agnews, Agnews State Hospital	1/	37.397 °N	121.952 °W	C	0.4	(8),(13),(37),(3)	25.5	0.03	0.03	0.02	(2),(3)	1, 2, 3, 4, 7, 8
84.04.24	Morgan Hill	6.3	S	1656	Hollister Airport Differential Array		36.888 °N	121.413 °W	C	1.8	(8),(1)	28.0	0.10	0.09	0.23	(10),(3)	1, 2, 3, 4, 7, 8
84.04.24	Morgan Hill	6.3	S	57064	Fremont, Mission San Jose	1/	37.530 °N	121.919 °W	B	2.3	(8),(13),(37),(3)	31.6	0.03	0.02	0.02	(2),(3)	1, 2, 3, 4, 5, 6
84.04.24	Morgan Hill	6.3	S	1575	Hollister City Hall Annex		36.851 °N	121.402 °W	C	1.7	(38),(8),(30),(31),(1)	32.3	0.07	0.07	0.54	(10)	1, 2, 3, 4, 7, 8

Table A-1. Strong-Motion Database

Earthquake Yr.Mo.Dy	Earthquake Location	Mw	Fault Type	Station Desig.	Station Location	Structure Code	Station Location Latitude	Station Location Longitude	Site Class	Alluvial Depth	Geologic Reference	Closest Approach Distance [km]	PGA [g] H1	PGA [g] H2	PGA [g] V	Strong-Motion Data Source	Database Subsets
84.04.24	Morgan Hill	6.3	S	47125	Capitola Fire Station	1/	36.974 °N	121.952 °W	B	NA	(13),(37)	38.9	0.14	0.10	0.04	(2)	1, 3, 5
84.04.24	Morgan Hill	6.3	S	58135	Santa Cruz, UCSC Lick Lab.	1/	37.001 °N	122.060 °W	B	NA	(8)	46.0	0.04	0.08	0.03	(2)	1, 3, 5
86.01.26	Hollister	5.4	S	47391	Hollister, Glorietta Warehouse		36.851 °N	121.398 °W	C	1.7	(38),(8),(30),(31),(4),(1)	13.4	0.14	0.11	0.26	(2)	1, 2, 3, 4, 7, 8
86.07.08	Palm Springs	6.1	S	12025	Palm Springs Airport		33.829 °N	116.501 °W	C	0.7	(13),(4),(3)	11.2	0.20	0.17	0.19	(2),(3)	1, 2, 3, 4, 7, 8
86.07.08	Palm Springs	6.1	S	12331	Hemet, Stetson Av Fire Station	1/	33.729 °N	116.979 °W	C	NA	(13),(4)	29.2	0.14	0.15	0.10	(2)	1, 3, 7
86.07.08	Palm Springs	6.1	S	22170	Joshua Tree Fire Station	1/	34.131 °N	116.314 °W	B	0.2	(2),(3)	31.1	0.07	0.05	0.04	(2),(3)	1, 2, 3, 4, 5, 6
86.07.08	Palm Springs	6.1	S	12168	Puerta La Cruz, USFS Storage Bldg	1/	33.324 °N	116.683 °W	B	NA	(2)	67.9	0.06	0.08	0.04	(2)	1, 3, 5
86.07.08	Palm Springs	6.1	S	13172	Temecula, CDF Fire Station		33.496 °N	117.149 °W	C	NA	(2)	69.9	0.10	0.11	0.03	(2)	1, 3, 7
86.07.08	Palm Springs	6.1	S	13123	Riverside Airport	1/	33.951 °N	117.446 °W	B	NA	(4)	75.7	0.04	0.05	0.03	(2)	1, 3, 5
86.07.08	Palm Springs	6.1	S	23497	Rancho Cucamonga, Law & Just. Cntr.		34.104 °N	117.574 °W	C	NA	(13),(4)	89.1	0.02	0.02	NA	(2)	1, 3, 7
87.10.01	Whittier	6.0	R	289	Whittier Narrows Dam (Upstream)		34.030 °N	118.050 °W	C	2.4	(4),(39)	11.1	0.30	0.23	0.53	(10)	1, 2, 3, 4, 7, 8
87.10.01	Whittier	6.0	R	709	Garvey Reservoir Abutment Bldg	1/	34.050 °N	118.110 °W	B	2.7	(13),(4),(39)	11.3	0.37	0.48	0.38	(10)	1, 2, 3, 4, 5, 6
87.10.01	Whittier	6.0	R	5129	Bell, Los Angeles Bulk Mail Center		33.990 °N	118.160 °W	C	5.5	(13),(4),(39)	12.2	0.33	0.45	0.53	(10)	1, 2, 3, 4, 7, 8
87.10.01	Whittier	6.0	R	24461	Alhambra, Fremont School	1/	34.070 °N	118.150 °W	B	1.5	(13),(4),(39)	12.3	0.40	0.29	0.20	(2),(3)	1, 2, 3, 4, 5, 6
87.10.01	Whittier	6.0	R	288	Vernon, Cmd Terminal	6/1	33.999 °N	118.196 °W	C	6.4	(7),(10),(4),(39)	13.2	0.27	0.24	0.14	(10)	1, 2, 3, 4, 7, 8
87.10.01	Whittier	6.0	R	5244	Los Angeles, 4407 Jasper Street		34.061 °N	118.188 °W	B	0.9	(13),(4),(39)	14.0	0.33	0.22	0.12	(10)	1, 2, 3, 4, 5, 6
87.10.01	Whittier	6.0	R	24401	San Marino, Southwestern Academy	1/	34.115 °N	118.130 °W	B	1.4	(13),(4),(39)	14.9	0.19	0.14	0.14	(2),(3)	1, 2, 3, 4, 5, 6
87.10.01	Whittier	6.0	R	80053	Pasadena, CIT Athenaeum	2/1	34.139 °N	118.121 °W	B	0.9	(7),(12),(39)	16.0	0.11	0.18	0.15	(2)	1, 2, 3, 4, 5, 6
87.10.01	Whittier	6.0	R	14368	Downey, County Maintenance Bldg	1/	33.924 °N	118.167 °W	C	9.1	(13),(4),(39)	16.2	0.16	0.21	0.16	(2),(3)	1, 2, 3, 4, 7, 8
87.10.01	Whittier	6.0	R	24400	Los Angeles, Obregon park	1/	34.037 °N	118.178 °W	B/C	4.3	(13),(4),(39)	17.1	0.43	0.45	0.14	(2)	1, 2
87.10.01	Whittier	6.0	R	14196	Inglewood, Union Oil Yard		33.905 °N	118.279 °W	B	4.3	(13),(4),(39)	22.5	0.23	0.26	0.07	(2),(3)	1, 2, 3, 4, 5, 6
87.10.01	Whittier	6.0	R	24303	Los Angeles, Hollywood Storage PE Lot		34.090 °N	118.339 °W	C	2.3	(7),(10),(30),(31),(39)	23.8	0.12	0.21	0.08	(2),(3)	1, 2, 3, 4, 7, 8
87.10.01	Whittier	6.0	R	14403	Los Angeles, 116th St School	1/	33.929 °N	118.260 °W	C	6.7	(13),(4),(39)	26.7	0.40	0.28	0.11	(2)	1, 2, 3, 4, 7, 8
87.10.01	Whittier	6.0	R	24390	Century City, LA Country Club South		34.062 °N	118.416 °W	C	4.0	(13),(25),(4),(39)	29.6	0.07	0.06	0.03	(2),(3)	1, 2, 3, 4, 7, 8
87.10.01	Whittier	6.0	R	14241	Long Beach Recreation park		33.778 °N	118.133 °W	B	4.6	(13),(4),(39)	29.6	0.06	0.06	0.04	(2),(3)	1, 2, 3, 4, 5, 6
87.10.01	Whittier	6.0	R	23525	Pomona, 4th and Locust FF		34.056 °N	117.748 °W	C	0.0	(13),(4),(39)	29.9	0.06	0.07	0.06	(2)	1, 2, 3, 4, 7, 8
87.10.01	Whittier	6.0	R	24157	Los Angeles, Baldwin Hills		34.009 °N	118.361 °W	B/C	4.9	(13),(4),(39)	30.3	0.16	0.15	0.11	(2)	1, 2
87.10.01	Whittier	6.0	R	14395	Long Beach, Harbor Admin. Bldg		33.754 °N	118.200 °W	C	2.4	(13),(4),(39)	32.8	0.07	0.05	0.03	(2)	1, 2, 3, 4, 7, 8
87.10.01	Whittier	6.0	R	13197	Huntington Beach, Lake St Fire Sta.	1/	33.662 °N	117.997 °W	B	2.7	(13),(4),(39)	42.8	0.04	0.05	0.03	(2)	1, 2, 3, 4, 5, 6
87.10.01	Whittier	6.0	R	13122	Featherly Park, Park Maint. Bldg.	NA	33.869 °N	117.709 °W	B/C	NA	(13),(4)	42.9	0.08	0.08	0.05	(2)	1
87.10.01	Whittier	6.0	R	23497	Rancho Cucamonga, Law & Just. Cntr.		34.104 °N	117.574 °W	C	NA	(13),(4)	45.5	0.06	0.05	0.04	(2)	1, 3, 7
87.10.01	Whittier	6.0	R	24087	Arleta, Nordhoff Ave. Fire Station	1/	34.236 °N	118.439 °W	C	4.3	(13),(21)	45.7	0.09	0.09	0.09	(2)	1, 2, 3, 4, 7, 8
87.10.01	Whittier	6.0	R	24514	Sylmar, Olive View Medical Center	1/	34.326 °N	118.444 °W	B	NA	(13)	45.9	0.05	0.06	0.04	(2)	1, 3, 5
87.10.01	Whittier	6.0	R	24279	Newhall, LA County Fire Station	1/	34.390 °N	118.530 °W	B/C	NA	(4)	56.7	0.06	0.05	0.03	(2)	1
87.10.01	Whittier	6.0	R	13123	Riverside Airport	1/	33.951 °N	117.446 °W	B	NA	(4)	57.8	0.06	0.05	0.05	(2)	1, 3, 5
87.10.01	Whittier	6.0	R	24396	Malibu, Point Dume School	1/	34.013 °N	118.800 °W	B	NA	(4)	63.6	0.05	0.05	0.03	(2)	1, 3, 5
87.10.01	Whittier	6.0	R	23516	San Bernardino, Sunwest Office Bldg	3/0	34.065 °N	117.289 °W	C	NA	(4)	70.9	0.03	0.03	0.02	(2)	1, 3, 7
87.10.01	Whittier	6.0	R	24526	Lancaster, Medical Office Bldg FF		34.688 °N	118.156 °W	B	NA	(4)	72.2	0.06	0.06	0.03	(2)	1, 3, 5
87.10.01	Whittier	6.0	R	24283	Moorpark, Ventura Co. Fire Dept. Garage	1/	34.228 °N	118.881 °W	B/C	NA	(4)	77.3	0.05	0.02	0.05	(2)	1
87.10.01	Whittier	6.0	R	24278	Castaic, Old Ridge Route	1/	34.564 °N	118.642 °W	B	10.0	(12),(32),(31),(3)	77.3	0.07	0.07	0.03	(2)	1, 2, 3, 4, 5, 6
87.10.01	Whittier	6.0	R	24271	Lake Hughes, #1-Fire Station #78	1/	34.674 °N	118.430 °W	B	NA	(10),(29),(31)	78.2	0.03	0.04	NA	(2)	1, 3, 5
87.10.01	Whittier	6.0	R	24274	Rosamond, Goode Ranch		34.827 °N	118.265 °W	C	NA	(4)	89.0	0.05	0.08	0.02	(2)	1, 3, 7
87.10.01	Whittier	6.0	R	12331	Hemet, Stetson Av Fire Station	1/	33.729 °N	116.979 °W	C	NA	(13),(4)	106.0	0.04	0.03	0.03	(2)	1, 3, 7
89.10.17	Loma Prieta	7.0	S	57007	Corralitos, Eureka Canyon Road		37.046 °N	121.803 °W	B	3.8	(8),(13),(16),(3)	2.2	0.49	0.64	0.46	(2)	1, 2, 3, 4, 5, 6
89.10.17	Loma Prieta	7.0	S	47459	Watsonville, 4-story commercial bldg	4/0	36.909 °N	121.756 °W	C	0.9	(4),(24)	6.3	0.28	0.39	0.66	(2),(4)	1, 2, 3, 4, 7, 8
89.10.17	Loma Prieta	7.0	S	47006	Gilroy, Gavilan College Phys. Sci. Bldg.	1/	36.973 °N	121.568 °W	B	NA	(8),(31)	11.2	0.37	0.33	0.20	(2)	1, 3, 5
89.10.17	Loma Prieta	7.0	S	58065	Saratoga, Aloha Ave	1/	37.255 °N	122.031 °W	B	NA	(8),(13)	12.4	0.33	0.53	0.41	(2),(4)	1, 3, 5
89.10.17	Loma Prieta	7.0	S	47380	Gilroy #2, Hwy 101/Bolsa Road Motel		36.982 °N	121.556 °W	C	0.3	(8),(11),(14),(23)	12.6	0.33	0.37	0.30	(2),(4)	1, 2, 3, 4, 7, 8
89.10.17	Loma Prieta	7.0	S	47381	Gilroy #3, Gilroy Sewage Treat. Plant		36.987 °N	121.536 °W	C	0.6	(8),(11),(23)	14.4	0.37	0.55	0.37	(2),(4)	1, 2, 3, 4, 7, 8
89.10.17	Loma Prieta	7.0	S	58135	Santa Cruz, UCSC Lick Lab.	1/	37.001 °N	122.060 °W	B	NA	(8)	16.8	0.43	0.46	0.39	(2)	1, 3, 5
89.10.17	Loma Prieta	7.0	S	57383	Gilroy #6, San Ysidro Microwave Site		37.026 °N	121.484 °W	B	0.5	(8),(11),(3)	20.5	0.17	0.13	0.10	(2)	1, 2, 3, 4, 5, 6
89.10.17	Loma Prieta	7.0	S	1652	Anderson Dam, Downstream		37.166 °N	121.628 °W	B	0.0	(8),(13),(3)	22.4	0.26	0.25	0.17	(10),(4)	1, 2, 3, 4, 5, 6
89.10.17	Loma Prieta	7.0	S	57504	Coyote Lake Dam, Downstream		37.118 °N	121.550 °W	B	NA	(8),(13)	23.1	0.18	0.16	0.10	(2),(4)	1, 3, 5
89.10.17	Loma Prieta	7.0	S	1656	Hollister Airport Differential Array		36.888 °N	121.413 °W	C	1.8	(8),(1)	24.5	0.29	0.27	0.16	(10),(4)	1, 2, 3, 4, 7, 8
89.10.17	Loma Prieta	7.0	S	57425	Gilroy #7, Mantelli Ranch, Jamison Rd		37.033 °N	121.434 °W	C	0.5	(13),(16),(3)	24.7	0.33	0.23	0.12	(2),(4)	1, 2, 3, 4, 7, 8
89.10.17	Loma Prieta	7.0	S	1575	Hollister City Hall Annex		36.851 °N	121.402 °W	C	1.7	(38),(8),(30),(31),(1)	26.6	0.25	0.23	0.22	(10),(4)	1, 2, 3, 4, 7, 8
89.10.17	Loma Prieta	7.0	S	57066	Agnews, Agnews State Hospital	1/	37.397 °N	121.952 °W	C	0.4	(8),(13),(37),(3)	27.6	0.16	0.17	0.10	(2),(4)	1, 2, 3, 4, 7, 8
89.10.17	Loma Prieta	7.0	S	1695	Sunnyvale, Colton Avenue		37.340 °N	121.756 °W	C	NA	(8),(13)	29.1	0.19	0.22	0.10	(10),(4)	1, 3, 7
89.10.17	Loma Prieta	7.0	S	47179	Salinas, John and Work St.	1/	36.671 °N	121.642 °W	C	NA	(8),(13)	29.3	0.12	0.09	0.11	(2),(4)	1, 3, 7
89.10.17	Loma Prieta	7.0	S	1227	Palo Alto, VA Hospital, Bldg 1		37.400 °N	122.140 °W	B	NA	(14),(37)	31.0	0.38	0.34	0.20	(10),(4)	1, 3, 5
89.10.17	Loma Prieta	7.0	S	1601	Stanford University, SLAC Test Lab		37.419 °N	122.205 °W	C	NA	(8),(13)	35.7	0.19	0.29	0.10	(10),(4)	1, 3, 7
89.10.17	Loma Prieta	7.0	S	1687	Calaveras Array, Calaveras Reservoir		37.452 °N	121.807 °W	B	NA	(8),(13)	36.9	0.13	0.08	0.07	(10),(4)	1, 3, 5
89.10.17	Loma Prieta	7.0	S	1230	Menlo Park VA Hospital, Bldg 137		37.468 °N	122.157 °W	C	0.2	(13),(37),(19),(18)	38.5	0.12	0.27	0.10	(10),(4)	1, 2, 3, 4, 7, 8

Table A-1. Strong-Motion Database

Earthquake Yr.Mo.Dy	Earthquake Location	Mw	Fault Type	Station Desig.	Station Location	Structure Code	Station Location Latitude	Station Location Longitude	Site Class	Alluvial Depth	Geologic Reference	Closest Approach Distance [km]	PGA [g] H1	PGA [g] H2	PGA [g] V	Strong-Motion Data Source	Database Subsets
89.10.17	Loma Prieta	7.0	S	58127	Woodside Fire Station	1/	37.429 'N	122.258 'W	B	NA	(8),(13),(16)	39.4	0.08	0.08	0.05	(2)	1, 3, 5
89.10.17	Loma Prieta	7.0	S	57064	Fremont, Mission San Jose	1/	37.530 'N	121.919 'W	B	2.3	(8),(13),(37),(3)	42.6	0.11	0.13	0.09	(2),(4)	1, 2, 3, 4, 5, 6
89.10.17	Loma Prieta	7.0	S	1686	Fremont, Calaveras Array, Emerson Crt.		37.535 'N	121.929 'W	C	NA	(8),(13)	43.0	0.15	0.20	0.07	(10),(4)	1, 3, 7
89.10.17	Loma Prieta	7.0	S	1161	Crystal Springs Reservoir		37.470 'N	122.320 'W	B	NA	(38),(8),(13)	46.3	0.11	0.12	0.06	(10)	1, 3, 5
89.10.17	Loma Prieta	7.0	S	1481	Bear Valley Stn #12, Williams Ranch		36.658 'N	121.249 'W	C	NA	(8)	49.2	0.17	0.16	0.10	(10),(4)	1, 3, 7
89.10.17	Loma Prieta	7.0	S	1688	Calaveras Array, Sunol Fire Station		37.597 'N	121.880 'W	B	NA	(8),(13)	50.4	0.07	0.10	0.03	(10)	1, 3, 5
89.10.17	Loma Prieta	7.0	S	1474	Bear Valley Stn #5, Callens Ranch		36.673 'N	121.195 'W	B	NA	(8)	52.1	0.07	0.07	0.04	(10),(4)	1, 3, 5
89.10.17	Loma Prieta	7.0	S	58219	Hayward, CSUH Stadium Grounds		37.657 'N	122.061 'W	B	NA	(8),(15)	58.7	0.08	0.08	0.05	(2)	1, 3, 5
89.10.17	Loma Prieta	7.0	S	58393	Hayward, John Muir School	1/	37.657 'N	122.081 'W	C	NA	(8)	56.9	0.14	0.18	0.10	(2),(4)	1, 3, 7
89.10.17	Loma Prieta	7.0	S	1689	Calaveras Array, Dublin Fire Station		37.709 'N	121.932 'W	C	NA	(8)	62.2	0.08	0.09	0.03	(10),(4)	1, 3, 7
89.10.17	Loma Prieta	7.0	S	1479	Bear Valley Stn #10, Webb Residence		36.532 'N	121.143 'W	C	NA	(8)	65.5	0.10	0.13	0.05	(10),(4)	1, 3, 7
89.10.17	Loma Prieta	7.0	S	58224	Oakland 2 story	2/	37.806 'N	122.267 'W	C	NA	(8),(37)	77.0	0.25	0.20	0.15	(2),(4)	1, 3, 7
89.10.17	Loma Prieta	7.0	S	58163	Yerba Buena Island		37.807 'N	122.361 'W	B	NA	(14)	80.2	0.07	0.03	0.03	(2)	1, 3, 5
89.10.17	Loma Prieta	7.0	S	1005	UC Berkeley, Strawberry Canyon		37.870 'N	122.240 'W	B	NA	(8)	83.1	0.04	0.08	0.02	(10)	1, 3, 5
89.10.17	Loma Prieta	7.0	S	58471	Berkeley, Lawrence Berkeley Lab.		37.876 'N	122.249 'W	B	NA	(8)	83.9	0.12	0.05	0.04	(2)	1, 3, 5
89.10.17	Loma Prieta	7.0	S	1678	San Francisco, Golden Gate Bridge		37.806 'N	122.472 'W	B	NA	(8)	84.6	0.24	0.12	0.06	(10),(4)	1, 3, 5
89.10.17	Loma Prieta	7.0	S	58505	Richmond City Hall Parking Lot		37.935 'N	122.342 'W	C	NA	(8),(37)	92.7	0.11	0.13	0.04	(2),(4)	1, 3, 7
89.10.17	Loma Prieta	7.0	S	1448	Martinez VA Hospital		37.993 'N	122.115 'W	B	NA	(37)	94.3	0.07	0.05	0.03	(10)	1, 3, 5
90.02.28	Upland	5.6	S	23525	Pomona, 4th and Locust FF		34.056 'N	117.748 'W	C	0.0	(13),(4),(39)	11.5	0.19	0.21	0.10	(2)	1, 2, 3, 4, 7, 8
90.02.28	Upland	5.6	S	23497	Rancho Cucamonga, Law & Just. Cntr.		34.104 'N	117.574 'W	C	NA	(13),(4)	13.2	0.23	0.24	0.16	(2)	1, 3, 7
91.06.28	Sierra Madre	5.6	R	24402	Altadena, Eaton Canyon Park	1/	34.177 'N	118.076 'W	C	0.9	(4),(39)	16.0	0.45	0.18	0.15	(2)	1, 2, 3, 4, 7, 8
91.06.28	Sierra Madre	5.6	R	24401	San Marino, Southwestern Academy	1/	34.115 'N	118.130 'W	B	1.4	(13),(4),(39)	22.9	0.17	0.14	0.13	(2)	1, 2, 3, 4, 5, 6
91.06.28	Sierra Madre	5.6	R	24400	Los Angeles, Obregon park	1/	34.037 'N	118.178 'W	B/C	4.3	(13),(4),(39)	31.7	0.23	0.22	0.07	(2)	1, 2
92.06.28	Landers	7.3	S	22170	Joshua Tree Fire Station	1/	34.131 'N	116.314 'W	B	0.2	(2),(3)	7.1	0.29	0.28	0.19	(2)	1, 2, 3, 4, 5, 6
92.06.28	Landers	7.3	S	MVH	Morongo valley		34.053 'N	116.572 'W	B	NA	(4)	18.0	0.19	0.14	0.16	(11)	1, 3, 5
92.06.28	Landers	7.3	S	NA	Coolwater SCE		34.852 'N	116.858 'W	C	NA	(4)	18.6	0.28	0.42	0.18	(8)	1, 3, 7
92.06.28	Landers	7.3	S	22074	Yermo Fire Station	1/	34.903 'N	116.823 'W	C	NA	(4)	22.4	0.15	0.25	0.16	(2)	1, 3, 7
92.06.28	Landers	7.3	S	12025	Palm Springs Airport		33.829 'N	116.501 'W	C	0.7	(13),(4),(3)	28.2	0.09	0.09	0.11	(2)	1, 2, 3, 4, 7, 8
92.06.28	Landers	7.3	S	12149	Desert Hot Springs, Pierson Blvd Fire Sta.	1/0	33.962 'N	116.509 'W	B/C	NA	(13),(4)	30.6	0.15	0.17	0.18	(2)	1
92.06.28	Landers	7.3	S	12026	Indio, Coachella Canal	NA	33.717 'N	116.156 'W	B/C	NA	(13),(4)	61.8	0.10	0.12	0.05	(2)	1
92.06.28	Landers	7.3	S	24577	Fort Irwin		35.268 'N	116.684 'W	C	NA	(4)	62.2	0.12	0.11	0.06	(2)	1, 3, 7
92.06.28	Landers	7.3	S	12331	Hemet, Stetson Av Fire Station	1/	33.729 'N	116.979 'W	C	NA	(13),(4)	66.8	0.10	0.09	0.08	(2)	1, 3, 7
92.06.28	Landers	7.3	S	12168	Puerta La Cruz, USFS Storage Bldg	1/	33.324 'N	116.683 'W	B	NA	(2)	86.5	0.05	0.05	0.04	(2)	1, 3, 5
92.06.28	Landers	7.3	S	32075	Baker Fire Station	1/	35.272 'N	116.066 'W	C	NA	(4)	88.1	0.11	0.11	0.06	(2)	1, 3, 7
92.06.28	Landers	7.3	S	33083	Boron, Fire Station	1/	35.002 'N	117.650 'W	C	NA	(4)	88.2	0.09	0.13	0.05	(2)	1, 3, 7
92.06.28	Landers	7.3	S	23559	Barstow, Vineyard & H St	NA	34.887 'N	117.047 'W	B/C	NA	(13),(4)	93.8	0.15	0.14	0.07	(2)	1
92.06.28	Landers	7.3	S	13123	Riverside Airport	1/	33.951 'N	117.446 'W	B	NA	(4)	98.1	0.04	0.05	0.05	(2)	1, 3, 5
92.06.28	Landers	7.3	S	23525	Pomona, 4th and Locust FF		34.056 'N	117.748 'W	C	0.0	(13),(4),(39)	117.0	0.05	0.07	0.04	(2)	1, 2, 3, 4, 7, 8
92.06.28	Landers	7.3	S	13122	Featherly Park, Park Maint. Bldg.	NA	33.869 'N	117.709 'W	B/C	NA	(13),(4)	124.1	0.05	0.05	0.03	(2)	1
92.06.28	Landers	7.3	S	24541	Pasadena, 6-story office bldg	6/1	34.146 'N	118.147 'W	B	0.6	(4),(39)	142.4	0.03	0.04	0.02	(2)	1, 2, 3, 4, 5, 6
92.06.28	Landers	7.3	S	14368	Downey, County Maintennance Bldg	1/	33.924 'N	118.167 'W	C	9.1	(13),(4),(39)	156.0	0.04	0.06	0.02	(2)	1, 2, 3, 4, 7, 8
92.06.28	Landers	7.3	S	24400	Los Angeles, Obregon Park	1/	34.037 'N	118.178 'W	B/C	4.3	(13),(4),(39)	162.1	0.07	0.05	0.02	(2)	1, 2
92.06.28	Landers	7.3	S	14196	Inglewood, Union Oil Yard		33.905 'N	118.279 'W	B	4.3	(13),(4),(39)	166.0	0.03	0.05	0.01	(2)	1, 2, 3, 4, 5, 6
92.06.28	Landers	7.3	S	14403	Los Angeles, 116th St School	1/	33.929 'N	118.260 'W	C	6.7	(13),(4),(39)	171.5	0.04	0.05	0.02	(2)	1, 2, 3, 4, 7, 8
92.06.28	Landers	7.3	S	24436	Tarzana, Cedar Hills Nursery		34.160 'N	118.534 'W	B	0.3	(9),(39)	174.0	0.04	0.06	0.03	(2)	1, 2, 3, 4, 5, 6
94.01.17	Northridge	6.7	R	24514	Sylmar, Olive View Medical Center	1/	34.326 'N	118.444 'W	B	NA	(13)	6.7	0.60	0.84	0.54	(2)	1, 3, 5
94.01.17	Northridge	6.7	R	24279	Newhall, LA County Fire Station	1/	34.390 'N	118.530 'W	B/C	NA	(4)	7.5	0.58	0.59	0.55	(2)	1
94.01.17	Northridge	6.7	R	24087	Arleta, Nordhoff Ave. Fire Station	1/	34.236 'N	118.439 'W	C	4.3	(13),(21)	10.2	0.34	0.31	0.55	(2)	1, 2, 3, 4, 7, 8
94.01.17	Northridge	6.7	R	USC006	Sun Valley, 13248 Roscoe Blvd.		34.221 'N	118.421 'W	B	3.7	(22),(21)	11.7	0.44	0.27	0.28	(9)	1, 2, 3, 4, 5, 6
94.01.17	Northridge	6.7	R	USC003	Northridge, 17645 Saticoy		34.209 'N	118.517 'W	C	3.2	(22),(21)	13.2	0.45	0.33	0.80	(9)	1, 2, 3, 4, 7, 8
94.01.17	Northridge	6.7	R	USC053	Canoga Park, 7769 Topanga Canyon Rd.		34.212 'N	118.606 'W	C	1.2	(22),(21)	15.9	0.39	0.35	0.42	(9)	1, 2, 3, 4, 7, 8
94.01.17	Northridge	6.7	R	24278	Castaic, Old Ridge Route	1/	34.564 'N	118.642 'W	B	10.0	(12),(32),(31),(3)	22.8	0.57	0.51	0.22	(2)	1, 2, 3, 4, 5, 6
94.01.17	Northridge	6.7	R	24607	Lake Hughes, Array Station 12A		34.571 'N	118.560 'W	B	NA	(4)	22.9	0.17	0.26	0.12	(2)	1, 3, 5
94.01.17	Northridge	6.7	R	24688	Los Angeles, UCLA Grounds		34.068 'N	118.439 'W	B/C	0.6	(7),(4),(39)	24.5	0.28	0.47	0.27	(2)	1, 2
94.01.17	Northridge	6.7	R	24389	Century City, LA Country Club North		34.063 'N	118.418 'W	C	4.0	(13),(25),(4),(39)	25.5	0.26	0.22	0.12	(2)	1, 2, 3, 4, 7, 8
94.01.17	Northridge	6.7	R	24303	Los Angeles, Hollywood Storage PE Lot		34.090 'N	118.339 'W	C	2.3	(7),(10),(30),(31),(39)	26.0	0.23	0.39	0.14	(2)	1, 2, 3, 4, 7, 8
94.01.17	Northridge	6.7	R	24283	Moorpark, Ventura Co. Fire Dept. Garage	1/	34.228 'N	118.881 'W	B/C	NA	(4)	28.3	0.29	0.19	0.15	(2)	1
94.01.17	Northridge	6.7	R	24538	Santa Monica, City Hall Grounds		34.011 'N	118.490 'W	B	2.1	(4),(39)	28.6	0.88	0.37	0.23	(2)	1, 2, 3, 4, 5, 6
94.01.17	Northridge	6.7	R	24157	Los Angeles, Baldwin Hills		34.009 'N	118.361 'W	B/C	4.9	(13),(4),(39)	32.0	0.24	0.17	0.09	(2)	1, 2
94.01.17	Northridge	6.7	R	24612	Los Angeles, Pico & Sentous		34.043 'N	118.271 'W	C	NA	(4)	33.3	0.10	0.19	0.07	(2)	1, 3, 7
94.01.17	Northridge	6.7	R	24611	Los Angeles, Temple & Hope		34.059 'N	118.246 'W	B	NA	(4)	33.4	0.13	0.18	0.10	(2)	1, 3, 5
94.01.17	Northridge	6.7	R	24396	Malibu, Point Dume School	1/	34.013 'N	118.800 'W	B	NA	(4)	36.0	0.13	0.09	0.09	(2)	1, 3, 5
94.01.17	Northridge	6.7	R	24605	Los Angeles, Univ. Hospital Grounds		34.062 'N	118.198 'W	B	NA	(4)	36.0	0.49	0.21	0.12	(2)	1, 3, 5

Table A-1. Strong-Motion Database

Earthquake Yr.Mo.Dy	Earthquake Location	Mw	Fault Type	Station Desig.	Station Location	Structure Code	Station Location Latitude	Station Location Longitude	Site Class	Alluvial Depth	Geologic Reference	Closest Approach Distance [km]	PGA [g] H1	PGA [g] H2	PGA [g] V	Strong-Motion Data Source	Database Subsets
94.01.17	Northridge	6.7	R	24401	San Marino, Southwestern Academy	1/	34.115 °N	118.130 °W	B	1.4	(13),(4),(39)	36.8	0.12	0.15	0.09	(2)	1, 2, 3, 4, 5, 6
94.01.17	Northridge	6.7	R	24592	Los Angeles, City Terrace		34.053 °N	118.171 °W	B	NA	(4)	38.4	0.26	0.32	0.13	(2)	1, 3, 5
94.01.17	Northridge	6.7	R	24461	Alhambra, Fremont School	1/	34.070 °N	118.150 °W	B	1.5	(13),(4),(39)	38.5	0.10	0.08	0.05	(2)	1, 2, 3, 4, 5, 6
94.01.17	Northridge	6.7	R	24400	Los Angeles, Obregon Park	1/	34.037 °N	118.178 °W	B/C	4.3	(13),(4),(39)	39.2	0.35	0.41	0.11	(2)	1, 2
94.01.17	Northridge	6.7	R	14403	Los Angeles, 116th St School	1/	33.929 °N	118.260 °W	C	6.7	(13),(4),(39)	43.3	0.20	0.14	0.06	(2)	1, 2, 3, 4, 7, 8
94.01.17	Northridge	6.7	R	25282	Camarillo	1/	34.208 °N	119.079 °W	C	NA	(4)	43.5	0.12	0.12	0.05	(2)	1, 3, 7
94.01.17	Northridge	6.7	R	14368	Downey, County Maintennance Bldg	1/	33.924 °N	118.167 °W	C	9.1	(13),(4),(39)	48.7	0.18	0.22	0.13	(2)	1, 2, 3, 4, 7, 8
94.01.17	Northridge	6.7	R	25147	Point Mugu, Naval Air Station		34.113 °N	119.119 °W	C	NA	(17),(4)	49.3	0.14	0.18	0.06	(2)	1, 3, 7
94.01.17	Northridge	6.7	R	24475	Lancaster, Fox Airfield Grounds		34.739 °N	118.214 °W	C	NA	(4)	52.5	0.06	0.08	0.05	(2)	1, 3, 7
94.01.17	Northridge	6.7	R	24586	Neenach, Sacatara Creek		34.848 °N	118.536 °W	C	NA	(4)	53.2	0.06	0.07	0.05	(2)	1, 3, 7
94.01.17	Northridge	6.7	R	14560	Long Beach, City Hall Grounds		33.768 °N	118.196 °W	B	3.0	(4),(39)	60.0	0.04	0.05	0.02	(2)	1, 2, 3, 4, 5, 6
94.01.17	Northridge	6.7	R	25340	Ventura, Harbor and California		34.276 °N	119.293 °W	C	NA	(4)	61.3	0.05	0.08	0.03	(2)	1, 3, 7
94.01.17	Northridge	6.7	R	14578	Seal Beach, Parking Lot		33.757 °N	118.084 °W	C	NA	(6)	66.8	0.06	0.08	0.04	(2)	1, 3, 7
94.01.17	Northridge	6.7	R	13610	Newport Beach, Newport & Coast Hwy		33.623 °N	117.931 °W	B/C	NA	(4)	86.7	0.11	0.08	0.02	(2)	1
94.01.17	Northridge	6.7	R	23597	Phelan, Wilson Ranch Road		34.467 °N	117.520 °W	B/C	NA	(4)	87.2	0.05	0.06	0.04	(2)	1
94.01.17	Northridge	6.7	R	23672	San Bernardino, CSUSB Grounds		34.183 °N	117.321 °W	B/C	NA	(4)	104.7	0.03	0.07	0.02	(2)	1
94.01.17	Northridge	6.7	R	23542	San Bernardino, E & Hospitality		34.065 °N	117.292 °W	C	NA	(2)	109.9	0.08	0.10	0.04	(2)	1, 3, 7
94.01.17	Northridge	6.7	R	13660	Hemet, Ryan Airfield		33.731 °N	117.023 °W	C	NA	(2),(4)	146.3	0.06	0.05	0.03	(2)	1, 3, 7
94.01.17	Northridge	6.7	R	12673	San Jacinto, CDF Fire Station		33.787 °N	116.958 °W	C	NA	(4)	149.2	0.08	0.10	0.02	(2)	1, 3, 7

Geologic References

1. Blümling, P., W.D. Mooney, and W.H.K. Lee (1985). "Crustal Structure of the Southern Calaveras Fault Zone, Central California, from Seismic Refraction Investigations," *Bulletin of the Seismological Society of America*, vol. 75, no. 1, February, pp. 193–209.

2. Boore, D.M., W.B. Joyner, and T.E. Fumal, (1993). "Estimation of Response Spectra and Peak Accelerations from Western North American Earthquakes: An Interim Report," *U.S. Geological Survey Open-File Report 93-509*, 72 pages.

3. Campbell, K.W. (1990). "Empirical Prediction of Near-Source Soil and Soft-Rock Ground Motion for the Diablo Canyon Power Plant Site, San Luis Obisbo County, California," *Dames and Moore Report*, prepared for Lawrence Livermore Laboratory, September, 110 pages.

4. California Division of Mines and Geology, *1:250,000 Scale Local Geologic Map Series.*

5. Dames and Moore. *Dames and Moore Report*, used to classify site of El Centro, Route 8, Meloland Overcrossing station, recording the 1979 Imperial Valley earthquake.

6. Dames and Moore (1988). proprietary *Dames and Moore Geotechnical Report*, on Rockwell site, used to classify Seal Beach, Parking Lot station, recording the 1994 Northridge earthquake.

7. Duke, C.M. and D.J. Leeds, (1962). "Site Characteristics of Southern California Strong-Motion Earthquake Stations," School of Engineering and Applied Science, University of California, Los Angeles, *UCLA-ENG Report No. 62-55.*

8. Fumal, T.E. (1991). "A Compilation of the Geology and Measured and Estimated Shear-Wave Velocity Profiles at Strong-Motion Stations that Recorded the Loma Prieta, California, Earthquake," *U.S. Geological Survey Open-File Report 91-311.*

9. Fumal, T.E., J.F. Gibbs, and E.F. Roth, (1981). "In-Situ Measurements of Seismic Velocities at 19 Locations in the Los Angeles, California, Region," *U.S. Geological Survey Open-File Report 81-399.*

10. Fumal, T.E., J.F. Gibbs, and E.F. Roth, (1982). "In-Situ Measurements of Seismic Velocities at 22 Locations in the Los Angeles, California, Region," *U.S. Geological Survey Open-File Report 82-833.*

11. Fumal, T.E., J.F. Gibbs, and E.F. Roth, (1982). "In-Situ Measurements of Seismic Velocities at 10 Strong-Motion Accelerograph Stations in Central California," *U.S. Geological Survey Open-File Report 82-407.*

12. Fumal, T.E., J.F. Gibbs, and E.F. Roth, (1984). "In-Situ Measurements of Seismic Velocities at 16 Locations in the Los Angeles, California, Region," *U.S. Geological Survey Open-File Report 84-681.*

13. Geomatrix Consultants (1993). "Compilation of Geotechnical Data for Strong-Ground Motion Stations in the Western United States," *Geomatrix Consultants Report*, prepared for Lawrence Livermore National Laboratory, December, Project No. 2256.

14. Gibbs, J.F., T.E. Fumal, D.M. Boore, and W.B. Joyner, (1992). "Seismic Velocities and Geologic Logs from Borehole Measurements at Seven Strong-Motion Stations that Recorded the 1989 Loma Prieta Earthquake," *U.S. Geological Survey Open-File Report 92-287.*

15. Gibbs, J.F., T.E. Fumal, and R.D. Borcherdt, (1976). "In-Situ Measurements of Seismic Velocities in the San Francisco Bay Region–Part II," *U.S. Geological Survey Open-File Report 76-731.*

16. Gibbs, J.F., T.E. Fumal, and T.J. Powers, (1993). "Seismic Velocities and Geologic Logs from Borehole Measurements at Eight Strong-Motion Stations that Recorded the 1989 Loma Prieta, California, Earthquake," *U.S. Geological Survey Open-File Report 93-376.*

17. Gibbs, J.F., T.E. Fumal, and E.F. Roth, (1980). "In-Situ Measurements of Seismic Velocities at 27 Locations in the Los Angeles, California Region," *U.S. Geological Survey Open-File Report 80-378.*

18. Hazlewood, (1976). "Contour Map and Interpretive Cross Sections Showing Depth and Configuration of Bedrock Surface, South San Francisco Bay Region, California," *U.S. Geological Survey Map MF-796.*

19. Hensolt, W.H., and E.E. Brabb (1990). "Maps Showing Elevation of Bedrock and Implications for Design of Engineered Structures to Withstand Earthquake Shaking in San Mateo County, California," *U.S. Geological Survey Open-File Report 90-496.*

20. Jafar, S.T., and J.G. Anderson (1988). "The 1978 Tabs, Iran, Earthquake: An Interpretation of the Strong Motion Records," *Bulletin of the Seismological Society of America*, vol. 78, no. 2, February, pp. 142–145.

21. Magistrate, H. (1995). Personal communication.

22. Martin, G.R. (1994). Personal communication, USC.

23. Mooney, W.D., and J.H. Luetgert (1982). "A Seismic Refraction Study of the Santa Clara Valley and Southern Santa Cruz Mountains, West-Central California," *Bulletin of the Seismological Society of America*, vol. 72, no. 3, June, pp. 901–909.

24. Mooney, W.D., and R.H. Colburn (1985). "A Seismic-Refraction Profile Across the San Andreas, Sargent, and Calaveras Faults, West-Central California," *Bulletin of the Seismological Society of America*, vol. 75, no. 1, February, pp. 175–191.

25. Shannon & Wilson, Inc., and Agbabian Associates (1978). "Data from Selected Accelerograph Stations at Wilshire Boulevard, Century City, and Ventura Boulevard, Los Angeles, California," prepared for U.S. Nuclear Regulatory Commission, *NUREG/CR-0074.*

26. Porcella, R. (1984). "Geological Investigations at Strong-Motion Stations in the Imperial Valley, California," *U.S. Geological Survey Open-File Report 84-562.*

27. Shannon & Wilson, Inc., and Agbabian Associates (1976). "Geotechnical and Strong-Motion Earthquake Data from U.S. Accelerograph Stations," prepared for U.S. Nuclear Regulatory Commission, *NUREG/CR-0029, Vol. 1.*

28. Shannon & Wilson, Inc., and Agbabian Associates (1978). "Geotechnical and Strong-Motion Earthquake Data from U.S. Accelerograph Stations," prepared for U.S. Nuclear Regulatory Commission, *NUREG/CR-0029, Vol. 2.*

29. Shannon & Wilson, Inc., and Agbabian Associates (1978). "Verification of Subsurface Conditions at Selected 'Rock' Accelerograph Stations in California," prepared for U.S. Nuclear Regulatory Commission, *NUREG/CR-0055, Vol. 1.*

30. Shannon & Wilson, Inc., and Agbabian Associates (1980). "Geotechnical and Strong-Motion Earthquake Data from U.S. Accelerograph Stations," prepared for U.S. Nuclear Regulatory Commission, *NUREG/CR-0985, Vol. 5.*

31. Shannon & Wilson, Inc., and Agbabian Associates (1980). "Geotechnical Data from Accelerograph Stations Investigated During the Period 1975–1979, Summary Report," prepared for U.S. Nuclear Regulatory Commission, *NUREG/CR-1643.*

32. Shannon & Wilson, Inc., and Agbabian Associates (1980). "Verification of Subsurface Conditions at Selected 'Rock' Accelerograph Stations in California," report prepared for U.S. Nuclear Regulatory Commission, *NUREG/CR-0055, Vol. 2.*

33. Shannon & Wilson, Inc. (1980). "Verification of Subsurface Conditions at Selected 'Rock' Accelerograph Stations in California," prepared for U.S. Nuclear Regulatory Commission, *NUREG/CR-0055, Vol. 3.*

34. Silverstein, B.L. (1979). "Geologic Description of Selected Strong-Motion Accelerograph Sites, Part II," *U.S. Geologic Survey Open-File Report 79-428.*

35. Silverstein, B.L. (1979). "Geologic Description of Selected Strong-Motion Accelerograph Sites, Part III," *U.S. Geologic Survey Open-File Report 79-1619.*

36. Silverstein, B.L. (1980). "Geologic Description of Selected Strong-Motion Accelerograph Sites, Part IV," *U.S. Geologic Survey Open-File Report 80-473.*

37. Thiel, C.C. and J.F. Schneider, (1993). "Investigations of Thirty-Three Loma Prieta Earthquake Strong-Motion Recording Sites," *CUREe Report*, California Universities for Research in Earthquake Engineering, July 1993.

38. Woodward-Lundgren Associates (1973). "Geotechnical Data Compilation for Selected Strong-Motion Seismograph Sites in California," *Woodward-Lundgren Report* prepared for NOAA, December.

39. Yerkes, R.F., T.H. McCulloh, J.E. Schoellhamer, and J.G. Vedder (1965). *Geology of the Los Angeles Basin, California—and Introduction*, U.S. Geological Survey, Professional Paper 420-A.

Strong-Motion Data Sources

1. Anderson, J. (1994). Personal Communication, University of Nevada at Reno.

2. California Division of Mines and Geology.

3. Campbell, K.W. (1990). "Empirical Prediction of Near-Source Soil and Soft-Rock Ground Motion for the Diablo Canyon Power Plant Site, San Luis Obisbo, California," *Dames & Moore Report*, prepared for Lawrence Livermore National Laboratory, September, 110 p.

4. Campbell, K.W. (1991). "An Empirical Analysis of Peak Horizontal Acceleration for the Loma Prieta, California, Earthquake of 18 October 1989," *Bulletin of the Seismological Society of America*, vol. 81, p. 1838-1858.

5. Crouse, C.B., J.A. Hileman, B.E. Turner, and G.R. Martin, G.R. (1980). "Compilation, Assessment, and Expansion of the Strong Earthquake Ground Motion Data Base," prepared for U.S. Nuclear Regulatory Commission, *NUREG/CR-1660, UCRL-15227.*

6. Crouse, C.B. (1988). Unpublished data used in development of Crouse attenuation equations published in: Joyner, W.B., and D.M. Boore, (1988). "Measurement, Characterization, and Prediction of Strong Ground Motion," *Earthquake Engineering and Soil Dynamics II—Recent Advances in Ground Motion Evaluation*, ASCE Geotech, Special Publication No. 20, pp. 43-102.

7. Joyner, W.B. and D.M. Boore, (1981). "Peak Horizontal Acceleration and Velocity from Strong-Motion Records, Including Records from the 1979 Imperial Valley, California, Earthquake," *Bulletin of the Seismological Society of America*, vol. 71, p. 2011-2038.

8. Southern California Edison (1993).

9. Structural and Earthquake Engineering Consultants, Arcadia, California (1994).

10. U.S. Geological Survey.

11. U.S. Geological Survey, GEOS Program.

Appendix B. Ground-Motion Equation Sets

The general form of the ground-motion model, as given in equation (2), is as follows.

$$\ln Y \;=\; p_1 + p_2 M + p_3 \ln\left(R + p_4 \exp\{p_5 M\}\right) + p_6 S + p_7 F + p_8 D \qquad (2)$$

where
- $Y \equiv$ ground-motion parameter—either peak ground acceleration (PGA), or peak 5 percent-damped psuedo-spectral velocity (PSV)
- $M \equiv$ moment magnitude, M_w
- $R \equiv$ closest distance from the site to the fault rupture surface
- $S \equiv$ site classification code: $S = 0$ for site class B, $S = 1$ for site class C
- $F \equiv$ fault-type code: $F = 0$ for strike-slip, $F = 1$ for reverse
- $D \equiv$ alluvial depth
- $p_i \equiv$ regression parameters, $i = 1$ to 8

Different sceismic hazard analysis scenarios may arise depending upon which, if any, of the proper values of the variables *S*, *F*, and *D* are known. To provide ground-motion equations appropriate for the different scenarios, 16 variations of equation (2) were developed. Table 3 is repeated here; it indicates the database subset which was utilized to develop each equation set, the hazard analysis secenarios for which it is applicable, and which (if any) of the terms of the general regression model are not present.

Table 3. Ground-Motion Equation Sets

Regression Equation Set No.	Database Subset No.	Applicable Ground-Motion Modeling Scenario: Site Class (within B–C range) Unknown	Class B		Class C		Fault-Type Unknown	Known		Alluvial Depth Unknown	Known	Term Present, Eqn. (2): p_6S n	y	p_7F n	y	p_8D n	y
1	1	◆				and	◆		and	◆		◆		◆		◆	
2	2	◆				and	◆		and		◆	◆		◆			◆
3	1	◆				and		◆	and	◆		◆			◆	◆	
4	2	◆				and		◆	and		◆	◆			◆		◆
5	3		(◆	or	◆)	and	◆		and	◆			◆	◆		◆	
6	4		(◆	or	◆)	and	◆		and		◆		◆	◆			◆
7	3		(◆	or	◆)	and		◆	and	◆			◆		◆	◆	
8	4		(◆	or	◆)	and		◆	and		◆		◆		◆		◆
9	5		◆			and	◆		and	◆		◆		◆		◆	
10	6		◆			and	◆		and		◆	◆		◆			◆
11	5		◆			and		◆	and	◆		◆			◆	◆	
12	6		◆			and		◆	and		◆	◆			◆		◆
13	7				◆	and	◆		and	◆		◆		◆		◆	
14	8				◆	and	◆		and		◆	◆		◆			◆
15	7				◆	and		◆	and	◆		◆			◆	◆	
16	8				◆	and		◆	and		◆	◆			◆		◆

Note: Database Subset No. *refers to designation assigned in Table 2*

Each equation set provides horizontal- and vertical-component ground-motion equations for PGA and for PSV at fourteen periods *T* in the band $0.04 \le T \le 4.00$ sec. The values of the parameters p_i in the general equation (2) to be used with each equation set are provided in the following pages, along with the standard errors of the regression.

Equation Set (1)

$$\ln Y^{c,T} = p_1^{c,T} + p_2^{c,T} M + p_3^{c,T} \ln\left(R + p_4^{c,T} \exp\{p_5^{c,T} M\}\right) + p_6^{c,T} S + p_7^{c,T} F + p_8^{c,T} D$$

- Y ≡ ground-motion parameter—either peak ground acceleration (PGA), or peak 5 percent-damped pseudo-spectral velocity (PSV); units of PGA: [PGA] = g; units of PSV: [PSV] = cm/sec
- M ≡ moment magnitude, M_w
- R ≡ closest distance from site to fault rupture surface in km
- S ≡ site classification code: $S = 0$ for site class B, $S = 1$ for site class C
- F ≡ fault-type code: $F = 0$ for strike-slip, $F = 1$ for reverse
- D ≡ depth to basement in km

Horizontal Component

Ground-Motion	Period				Attenuation Equation Coefficients					
Parameter, $Y^{H,T}$	T [sec]	$p_1^{H,T}$	$p_2^{H,T}$	$p_3^{H,T}$	$p_4^{H,T}$	$p_5^{H,T}$	$p_6^{H,T}$	$p_7^{H,T}$	$p_8^{H,T}$	$\sigma_{\ln Y}^{H,T}$
PGA	...	−1.826494	0.898703	−1.528388	1.805913	0.384652	...	...	...	0.500496
PSV(T, ξ=5%)	0.04	0.415852	0.828727	−1.529806	2.275710	0.335225	...	...	...	0.491588
⋮	0.10	3.889594	0.811368	−1.928031	3.947718	0.319103	...	...	...	0.576350
⋮	0.15	5.237534	0.762958	−1.992922	10.201714	0.188202	...	...	...	0.554117
⋮	0.20	5.841993	0.726846	−1.962920	15.877590	0.134864	...	...	...	0.535507
⋮	0.30	3.074889	0.889607	−1.566408	2.812896	0.327707	...	...	...	0.532991
⋮	0.40	1.458764	0.966950	−1.311823	0.762335	0.456588	...	...	...	0.529098
⋮	0.50	0.212295	1.102586	−1.220250	0.163758	0.649799	...	...	...	0.530063
⋮	0.60	−0.418378	1.128076	−1.110254	0.092720	0.695204	...	...	...	0.545546
⋮	0.80	−0.951663	1.189240	−1.068707	0.045227	0.795371	...	...	...	0.579128
⋮	1.00	−1.246766	1.237005	−1.051439	0.033744	0.865451	...	...	...	0.574562
⋮	1.50	−2.474145	1.329566	−0.938841	0.011997	0.954221	...	...	...	0.631785
⋮	2.00	−4.376082	1.617826	−0.986933	0.003486	1.140356	...	...	...	0.660365
⋮	3.00	−6.300801	1.822044	−0.905630	0.002038	1.172921	...	...	...	0.731170
PSV(T, ξ=5%)	4.00	−7.049439	1.860690	−0.825680	0.002028	1.138160	...	...	...	0.755865

Vertical Component

Ground-Motion	Period				Attenuation Equation Coefficients					
Parameter, $Y^{V,T}$	T [sec]	$p_1^{V,T}$	$p_2^{V,T}$	$p_3^{V,T}$	$p_4^{V,T}$	$p_5^{V,T}$	$p_6^{V,T}$	$p_7^{V,T}$	$p_8^{V,T}$	$\sigma_{\ln Y}^{V,T}$
PGA	...	−0.420255	0.567468	−1.523217	64.413473	−0.230552	...	...	...	0.608076
PSV(T, ξ=5%)	0.04	1.086234	0.655359	−1.563409	29.353282	−0.135606	...	...	...	0.686514
⋮	0.10	3.476641	0.800828	−1.958642	12.147261	0.072498	...	...	...	0.701957
⋮	0.15	3.856017	0.579190	−1.601048	51.714540	−0.172180	...	...	...	0.675994
⋮	0.20	3.516854	0.523822	−1.390493	103.403636	−0.295485	...	...	...	0.646573
⋮	0.30	2.570071	0.579469	−1.182356	33.776868	−0.110130	...	...	...	0.642234
⋮	0.40	0.944152	0.748781	−1.044290	8.006099	0.068917	...	...	...	0.625417
⋮	0.50	−0.214903	0.884953	−0.970706	3.010809	0.209564	...	...	...	0.594918
⋮	0.60	−1.731805	1.046352	−0.847555	0.041267	0.819865	...	...	...	0.631281
⋮	0.80	−1.403330	0.899436	−0.701899	0.024722	0.754776	...	...	...	0.636414
⋮	1.00	−2.181922	1.055373	−0.743692	0.014854	0.868208	...	...	...	0.622854
⋮	1.50	−4.355019	1.487144	−0.896605	0.007058	1.108591	...	...	...	0.609350
⋮	2.00	−4.333284	1.423001	−0.844245	0.010587	0.983350	...	...	...	0.651698
⋮	3.00	−6.271883	1.698933	−0.831494	0.014414	0.954196	...	...	...	0.765945
PSV(T, ξ=5%)	4.00	−7.202396	1.776405	−0.771832	0.012625	0.921229	...	...	...	0.826970

Equation Set (2)

$$\ln Y^{c,T} = p_1^{c,T} + p_2^{c,T} M + p_3^{c,T} \ln\left(R + p_4^{c,T} \exp\{p_5^{c,T} M\}\right) + p_6^{c,T} S + p_7^{c,T} F + p_8^{c,T} D$$

$Y \equiv$ ground-motion parameter—either peak ground acceleration (PGA), or peak 5 percent-damped pseudo-spectral velocity (PSV); units of PGA: [PGA] = g; units of PSV: [PSV] = cm/sec
$M \equiv$ moment magnitude, M_w
$R \equiv$ closest distance from site to fault rupture surface in km
$S \equiv$ site classification code: $S = 0$ for site class B, $S = 1$ for site class C
$F \equiv$ fault-type code: $F = 0$ for strike-slip, $F = 1$ for reverse
$D \equiv$ depth to basement in km

Horizontal Component

Ground-Motion Parameter, $Y^{H,T}$	Period T [sec]	Attenuation Equation Coefficients $p_1^{H,T}$	$p_2^{H,T}$	$p_3^{H,T}$	$p_4^{H,T}$	$p_5^{H,T}$	$p_6^{H,T}$	$p_7^{H,T}$	$p_8^{H,T}$	$\sigma_{\ln Y}^{H,T}$
PGA	...	−0.925593	1.116971	−2.011655	1.877203	0.457525	...	...	0.047708	0.458657
PSV(T, ξ=5%)	0.04	1.082789	1.092776	−2.016675	1.931618	0.449201	...	...	0.050021	0.452815
⋮	0.10	5.004488	1.323057	−2.789442	2.926544	0.456240	...	...	0.046876	0.517700
⋮	0.15	7.228633	1.088598	−2.769144	6.941401	0.332718	...	...	0.042427	0.521840
⋮	0.20	9.184486	1.268612	−3.214297	10.879958	0.312801	...	...	0.047817	0.508698
⋮	0.30	4.763761	1.052274	−2.095003	3.981025	0.363815	...	...	0.033463	0.477981
⋮	0.40	2.588286	0.980640	−1.560662	1.371389	0.446447	...	...	0.045827	0.485773
⋮	0.50	1.409793	1.119591	−1.485708	1.019778	0.474518	...	...	0.062125	0.456288
⋮	0.60	0.606499	1.125760	−1.332519	0.887478	0.453334	...	...	0.067838	0.468326
⋮	0.80	−0.205291	1.183967	−1.230206	0.349114	0.565715	...	...	0.059224	0.471848
⋮	1.00	−1.857786	1.452333	−1.221642	0.049229	0.894565	...	...	0.050016	0.417780
⋮	1.50	−3.252566	1.455728	−0.944487	0.006746	1.087308	...	...	0.050871	0.475660
⋮	2.00	−4.236469	1.536262	−0.877410	0.003793	1.128387	...	...	0.061122	0.525022
⋮	3.00	−6.112303	1.750267	−0.828712	0.002839	1.140328	...	...	0.065419	0.594884
PSV(T, ξ=5%)	4.00	−6.669831	1.707610	−0.660340	0.002664	1.068951	...	...	0.073473	0.635562

Vertical Component

Ground-Motion Parameter, $Y^{V,T}$	Period T [sec]	Attenuation Equation Coefficients $p_1^{V,T}$	$p_2^{V,T}$	$p_3^{V,T}$	$p_4^{V,T}$	$p_5^{V,T}$	$p_6^{V,T}$	$p_7^{V,T}$	$p_8^{V,T}$	$\sigma_{\ln Y}^{V,T}$
PGA	...	1.152136	0.895727	−2.283947	10.810002	0.166843	...	...	0.014882	0.571390
PSV(T, ξ=5%)	0.04	2.634447	0.895512	−2.250953	8.341168	0.159267	...	...	0.022771	0.619068
⋮	0.10	5.399237	1.438647	−3.157725	4.493495	0.355489	...	...	0.024786	0.641381
⋮	0.15	6.078216	1.071609	−2.681960	8.804304	0.251388	...	...	0.041648	0.586767
⋮	0.20	6.514754	1.072366	−2.679984	11.127699	0.239038	...	...	0.023149	0.572392
⋮	0.30	4.829629	0.605686	−1.706696	12.907796	0.129995	...	...	0.011077	0.512384
⋮	0.40	2.772716	0.880077	−1.599645	5.265655	0.268893	...	...	−0.007752	0.533358
⋮	0.50	1.251533	0.818546	−1.186216	6.443529	0.161247	...	...	−0.014986	0.503701
⋮	0.60	0.464308	0.869439	−1.087370	1.182470	0.396176	...	...	−0.013204	0.509657
⋮	0.80	−1.149074	1.101089	−1.059543	0.039830	0.891801	...	...	−0.032011	0.483399
⋮	1.00	−1.906826	1.105279	−0.853945	0.017349	0.946270	...	...	−0.045880	0.481034
⋮	1.50	−2.869474	1.120952	−0.672083	0.002232	1.095861	...	...	−0.025317	0.507517
⋮	2.00	−3.825313	1.269568	−0.729762	0.008178	0.962295	...	...	0.014824	0.551933
⋮	3.00	−5.403820	1.475101	−0.678949	0.016319	0.901165	...	...	0.036935	0.680365
PSV(T, ξ=5%)	4.00	−7.045648	1.654034	−0.611025	0.005226	0.992985	...	...	0.044167	0.775762

Equation Set (3)

$$\ln Y^{c,T} = p_1^{c,T} + p_2^{c,T}M + p_3^{c,T}\ln\left(R + p_4^{c,T}\exp\left(p_5^{c,T}M\right)\right) + p_6^{c,T}S + p_7^{c,T}F + p_8^{c,T}D$$

Y ≡ ground-motion parameter—either peak ground acceleration (PGA), or peak 5 percent-damped pseudo-spectral velocity (PSV); units of PGA: [PGA] = g; units of PSV: [PSV] = cm/sec
M ≡ moment magnitude, M_w
R ≡ closest distance from site to fault rupture surface in km
S ≡ site classification code: $S = 0$ for site class B, $S = 1$ for site class C
F ≡ fault-type code: $F = 0$ for strike-slip, $F = 1$ for reverse
D ≡ depth to basement in km

Horizontal Component

Ground-Motion Parameter, $Y^{H,T}$	Period T [sec]	Attenuation Equation Coefficients								
		$p_1^{H,T}$	$p_2^{H,T}$	$p_3^{H,T}$	$p_4^{H,T}$	$p_5^{H,T}$	$p_6^{H,T}$	$p_7^{H,T}$	$p_8^{H,T}$	$\sigma_{\ln Y}^{H,T}$
PGA	...	−2.973118	0.958510	−1.418787	0.553905	0.517553	...	0.315526	...	0.478714
PSV(T, ξ=5%)	0.04	−0.635901	0.895135	−1.442779	0.782726	0.458198	...	0.285575	...	0.473636
⋮	0.10	2.353312	0.866985	−1.746517	1.494712	0.418542	...	0.330451	...	0.555963
⋮	0.15	3.537834	0.832342	−1.796019	4.376252	0.269973	...	0.297057	...	0.537258
⋮	0.20	4.468647	0.879321	−1.933220	7.654564	0.227807	...	0.293602	...	0.517855
⋮	0.30	1.819319	0.948682	−1.434008	0.868946	0.455707	...	0.300989	...	0.514802
⋮	0.40	0.578677	1.030081	−1.252742	0.195845	0.622161	...	0.295721	...	0.511218
⋮	0.50	0.166936	1.020238	−1.126046	0.137744	0.613623	...	0.296822	...	0.511627
⋮	0.60	−0.441868	1.037171	−1.008007	0.031536	0.771329	...	0.301932	...	0.528284
⋮	0.80	−0.689891	1.064474	−0.978399	0.041903	0.723009	...	0.290644	...	0.563296
⋮	1.00	−1.371869	1.244671	−1.054250	0.033576	0.854741	...	0.154686	...	0.570128
⋮	1.50	−2.501831	1.333911	−0.941424	0.012339	0.949305	...	0.022116	...	0.632752
⋮	2.00	−4.290447	1.608647	−0.989652	0.004231	1.115607	...	−0.035913	...	0.663050
⋮	3.00	−6.047354	1.813332	−0.936756	0.003538	1.119950	...	−0.125432	...	0.730024
PSV(T, ξ=5%)	4.00	−6.874815	1.837996	−0.815348	0.002453	1.115448	...	−0.141722	...	0.754417

Vertical Component

Ground-Motion Parameter, $Y^{V,T}$	Period T [sec]	Attenuation Equation Coefficients								
		$p_1^{V,T}$	$p_2^{V,T}$	$p_3^{V,T}$	$p_4^{V,T}$	$p_5^{V,T}$	$p_6^{V,T}$	$p_7^{V,T}$	$p_8^{V,T}$	$\sigma_{\ln Y}^{V,T}$
PGA	...	−1.466121	0.689488	−1.506439	24.802573	−0.104816	...	0.258775	...	0.596982
PSV(T, ξ=5%)	0.04	−0.046408	0.799312	−1.561229	8.240786	0.041384	...	0.289366	...	0.674300
⋮	0.10	1.760928	0.968362	−1.886887	3.569343	0.225988	...	0.393451	...	0.678612
⋮	0.15	2.060786	0.772517	−1.549102	11.621561	0.017530	...	0.421300	...	0.647763
⋮	0.20	1.974263	0.693616	−1.354106	26.300197	−0.124369	...	0.396846	...	0.620281
⋮	0.30	0.834308	0.744055	−1.106999	4.989823	0.114100	...	0.451235	...	0.607422
⋮	0.40	−0.211548	0.876085	−1.027099	1.304037	0.302065	...	0.390883	...	0.598705
⋮	0.50	−1.426904	1.032462	−0.967958	0.225565	0.565802	...	0.386362	...	0.567428
⋮	0.60	−1.691264	0.959589	−0.780651	0.020540	0.820167	...	0.413754	...	0.599416
⋮	0.80	−1.838584	0.963794	−0.750940	0.023557	0.748164	...	0.428735	...	0.599963
⋮	1.00	−2.498612	1.101946	−0.778979	0.014676	0.858907	...	0.311232	...	0.604093
⋮	1.50	−4.632581	1.518225	−0.896530	0.003976	1.180458	...	0.132974	...	0.605124
⋮	2.00	−4.381900	1.431232	−0.849722	0.011116	0.975125	...	0.037943	...	0.652444
⋮	3.00	−6.245191	1.696495	−0.828662	0.015736	0.942859	...	−0.037438	...	0.767560
PSV(T, ξ=5%)	4.00	−7.147568	1.769768	−0.764497	0.013939	0.909260	...	−0.074572	...	0.828362

Equation Set (4)

$$\ln Y^{c,T} = p_1^{c,T} + p_2^{c,T} M + p_3^{c,T} \ln\left(R + p_4^{c,T} \exp\{p_5^{c,T} M\}\right) + p_6^{c,T} S + p_7^{c,T} F + p_8^{c,T} D$$

Y ≡ ground-motion parameter—either peak ground acceleration (PGA), or peak 5 percent-damped pseudo-spectral velocity (PSV); units of PGA: [PGA] = g; units of PSV: [PSV] = cm/sec
M ≡ moment magnitude, M_w
R ≡ closest distance from site to fault rupture surface in km
S ≡ site classification code: $S = 0$ for site class B, $S = 1$ for site class C
F ≡ fault-type code: $F = 0$ for strike-slip, $F = 1$ for reverse
D ≡ depth to basement in km

Horizontal Component

Ground-Motion Parameter, $Y^{H,T}$	Period T [sec]	Attenuation Equation Coefficients $p_1^{H,T}$	$p_2^{H,T}$	$p_3^{H,T}$	$p_4^{H,T}$	$p_5^{H,T}$	$p_6^{H,T}$	$p_7^{H,T}$	$p_8^{H,T}$	$\sigma_{\ln Y}^{H,T}$
PGA	...	−1.960277	1.021393	−1.731595	1.227342	0.458359	...	0.238326	0.043569	0.448174
PSV(T, ξ=5%)	0.04	−0.031636	0.997907	−1.723962	1.216450	0.451377	...	0.259392	0.045536	0.439811
⋮	0.10	3.297923	1.139206	−2.303488	1.880561	0.457264	...	0.263310	0.042407	0.506628
⋮	0.15	5.283693	0.970835	−2.315736	4.694957	0.332737	...	0.211927	0.038933	0.515572
⋮	0.20	6.239964	1.069607	−2.513069	7.157238	0.304225	...	0.212421	0.044055	0.504250
⋮	0.30	3.311867	0.951260	−1.734332	2.482151	0.361226	...	0.230472	0.029180	0.469199
⋮	0.40	1.783361	0.940439	−1.381161	0.790918	0.465951	...	0.222735	0.042029	0.477410
⋮	0.50	0.624709	1.086751	−1.320682	0.552067	0.499784	...	0.253467	0.057972	0.443688
⋮	0.60	−0.143094	1.113835	−1.200014	0.456611	0.480093	...	0.281853	0.063294	0.452547
⋮	0.80	−0.656123	1.166387	−1.145141	0.247885	0.557262	...	0.254024	0.055221	0.459254
⋮	1.00	−2.004512	1.421215	−1.166965	0.036341	0.909203	...	0.124965	0.048009	0.415449
⋮	1.50	−3.131335	1.474613	−0.983956	0.008569	1.087556	...	−0.109444	0.052898	0.474631
⋮	2.00	−3.878540	1.500693	−0.869760	0.005468	1.108444	...	−0.300950	0.064036	0.508515
⋮	3.00	−5.550138	1.681191	−0.812373	0.007749	1.026301	...	−0.343696	0.068632	0.578424
PSV(T, ξ=5%)	4.00	−6.323197	1.679342	−0.651413	0.004152	1.086283	...	−0.359481	0.077406	0.616248

Vertical Component

Ground-Motion Parameter, $Y^{V,T}$	Period T [sec]	Attenuation Equation Coefficients $p_1^{V,T}$	$p_2^{V,T}$	$p_3^{V,T}$	$p_4^{V,T}$	$p_5^{V,T}$	$p_6^{V,T}$	$p_7^{V,T}$	$p_8^{V,T}$	$\sigma_{\ln Y}^{V,T}$
PGA	...	0.436427	0.870379	−2.135827	10.347691	0.143971	...	0.138384	0.012434	0.570163
PSV(T, ξ=5%)	0.04	2.265602	0.888983	−2.183771	8.185176	0.146035	...	0.097932	0.021190	0.619735
⋮	0.10	4.477458	1.358108	−2.913281	3.927480	0.346932	...	0.138209	0.022259	0.640882
⋮	0.15	4.461552	0.978435	−2.303463	7.213977	0.224701	...	0.219484	0.037446	0.581157
⋮	0.20	4.247641	0.744983	−1.892818	13.385628	0.093196	...	0.205382	0.014260	0.570750
⋮	0.30	3.634259	0.568296	−1.461322	12.825104	0.056164	...	0.241970	0.006301	0.503001
⋮	0.40	2.264642	0.845202	−1.473512	4.850673	0.245067	...	0.104319	−0.009831	0.533337
⋮	0.50	0.498748	0.800597	−1.041802	7.411392	0.052896	...	0.251045	−0.019889	0.492800
⋮	0.60	−0.368418	0.848713	−0.929327	0.605519	0.373632	...	0.339558	−0.019471	0.488047
⋮	0.80	−1.413291	1.010911	−0.921639	0.018309	0.889328	...	0.332785	−0.038584	0.461304
⋮	1.00	−2.096829	1.103633	−0.824906	0.011375	0.968928	...	0.140340	−0.048150	0.476676
⋮	1.50	−2.692949	1.098252	−0.664876	0.004207	1.023370	...	−0.109709	−0.024254	0.507001
⋮	2.00	−3.702465	1.257321	−0.709443	0.003725	1.110361	...	−0.218134	0.016386	0.541946
⋮	3.00	−5.780729	1.609142	−0.750101	0.012615	1.045014	...	−0.407816	0.043784	0.649770
PSV(T, ξ=5%)	4.00	−6.638539	1.611389	−0.608355	0.008560	0.980659	...	−0.294329	0.047485	0.766518

Equation Set (5)

$$\ln Y^{c,T} = p_1^{c,T} + p_2^{c,T} M + p_3^{c,T} \ln\left(R + p_4^{c,T} \exp\left(p_5^{c,T} M\right)\right) + p_6^{c,T} S + p_7^{c,T} F + p_8^{c,T} D$$

Y ≡ ground-motion parameter—either peak ground acceleration (PGA), or peak 5 percent-damped pseudo-spectral velocity (PSV); units of PGA: [PGA] = g; units of PSV: [PSV] = cm/sec
M ≡ moment magnitude, M_w
R ≡ closest distance from site to fault rupture surface in km
S ≡ site classification code: $S = 0$ for site class B, $S = 1$ for site class C
F ≡ fault-type code: $F = 0$ for strike-slip, $F = 1$ for reverse
D ≡ depth to basement in km

Horizontal Component

Ground-Motion Parameter, $Y^{H,T}$	Period T [sec]	Attenuation Equation Coefficients $p_1^{H,T}$	$p_2^{H,T}$	$p_3^{H,T}$	$p_4^{H,T}$	$p_5^{H,T}$	$p_6^{H,T}$	$p_7^{H,T}$	$p_8^{H,T}$	$\sigma_{\ln Y}^{H,T}$
PGA	...	−2.787721	1.032112	−1.534951	0.717696	0.530994	0.210306	...	...	0.476146
PSV(T, ξ=5%)	0.04	−0.599470	0.961561	−1.521269	0.837291	0.491723	0.197585	...	...	0.467455
⋮	0.10	2.849412	1.004369	−1.994636	1.729899	0.462844	0.274861	...	...	0.547736
⋮	0.15	4.748527	0.938137	−2.138764	5.774321	0.302408	0.259702	...	...	0.525700
⋮	0.20	6.254352	1.042144	−2.428963	9.798588	0.274104	0.233821	...	...	0.507596
⋮	0.30	1.988346	1.012084	−1.536163	1.343317	0.434903	0.214532	...	...	0.500580
⋮	0.40	0.665723	1.066675	−1.311833	0.309477	0.596545	0.228421	...	...	0.516513
⋮	0.50	0.108715	1.044495	−1.144128	0.164764	0.623111	0.255154	...	...	0.526697
⋮	0.60	−1.093715	1.218170	−1.118899	0.050525	0.797242	0.228446	...	...	0.536233
⋮	0.80	−0.867446	1.093852	−0.975996	0.048238	0.741039	0.244843	...	...	0.573700
⋮	1.00	−1.820460	1.313539	−1.058491	0.036297	0.868850	0.237031	...	...	0.565670
⋮	1.50	−3.096112	1.417525	−0.951799	0.012963	0.965539	0.237982	...	...	0.620702
⋮	2.00	−5.284766	1.834076	−1.127883	0.005414	1.169954	0.365500	...	...	0.635486
⋮	3.00	−6.647735	1.918545	−1.015715	0.005007	1.110406	0.383238	...	...	0.712264
PSV(T, ξ=5%)	4.00	−7.471061	1.948893	−0.899025	0.005526	1.070108	0.362112	...	...	0.738777

Vertical Component

Ground-Motion Parameter, $Y^{V,T}$	Period T [sec]	Attenuation Equation Coefficients $p_1^{V,T}$	$p_2^{V,T}$	$p_3^{V,T}$	$p_4^{V,T}$	$p_5^{V,T}$	$p_6^{V,T}$	$p_7^{V,T}$	$p_8^{V,T}$	$\sigma_{\ln Y}^{V,T}$
PGA	...	−1.017423	0.663159	−1.563180	35.980089	−0.131541	0.268116	...	...	0.598805
PSV(T, ξ=5%)	0.04	0.883645	0.699459	−1.635801	31.454772	−0.135981	0.387184	...	...	0.665080
⋮	0.10	3.405820	0.801140	−1.991944	14.419155	0.047112	0.330342	...	...	0.689820
⋮	0.15	3.427922	0.638985	−1.639597	34.311269	−0.103102	0.331214	...	...	0.656969
⋮	0.20	3.178900	0.599475	−1.458262	62.640531	−0.205290	0.227204	...	...	0.629254
⋮	0.30	1.886921	0.688969	−1.210684	12.637607	0.047933	0.127228	...	...	0.632620
⋮	0.40	0.309031	0.878118	−1.097943	2.098725	0.300157	0.061585	...	...	0.615605
⋮	0.50	−0.755943	0.968205	−0.978550	1.265573	0.343607	0.024359	...	...	0.599089
⋮	0.60	−1.986970	1.087306	−0.860841	0.017564	0.954548	0.038759	...	...	0.637193
⋮	0.80	−1.341437	0.916909	−0.745289	0.025140	0.794821	−0.035566	...	...	0.641046
⋮	1.00	−2.120266	1.077798	−0.788798	0.014581	0.922117	−0.047609	...	...	0.621221
⋮	1.50	−3.313020	1.265139	−0.824610	0.011732	0.965734	0.081809	...	...	0.620567
⋮	2.00	−4.545243	1.497095	−0.921039	0.011247	1.026582	0.124268	...	...	0.653182
⋮	3.00	−6.552699	1.783845	−0.906212	0.015430	0.999277	0.144260	...	...	0.766232
PSV(T, ξ=5%)	4.00	−7.392247	1.799476	−0.778070	0.013515	0.931120	0.147589	...	...	0.834813

Equation Set (6)

$$\ln Y^{c,T} = p_1^{c,T} + p_2^{c,T}M + p_3^{c,T}\ln\left(R + p_4^{c,T}\exp\{p_5^{c,T}M\}\right) + p_6^{c,T}S + p_7^{c,T}F + p_8^{c,T}D$$

Y ≡ ground-motion parameter—either peak ground acceleration (PGA), or peak 5 percent-damped pseudo-spectral velocity (PSV); units of PGA: [PGA] = g; units of PSV: [PSV] = cm/sec
M ≡ moment magnitude, M_w
R ≡ closest distance from site to fault rupture surface in km
S ≡ site classification code: $S = 0$ for site class B, $S = 1$ for site class C
F ≡ fault-type code: $F = 0$ for strike-slip, $F = 1$ for reverse
D ≡ depth to basement in km

Horizontal Component

Ground-Motion Parameter, $Y^{H,T}$	Period T [sec]	Attenuation Equation Coefficients $p_1^{H,T}$	$p_2^{H,T}$	$p_3^{H,T}$	$p_4^{H,T}$	$p_5^{H,T}$	$p_6^{H,T}$	$p_7^{H,T}$	$p_8^{H,T}$	$\sigma_{\ln Y}^{H,T}$
PGA	...	−1.895854	1.159895	−1.906878	1.184828	0.508597	0.158566	...	0.039787	0.437772
PSV(T, ξ=5%)	0.04	0.117335	1.133274	−1.908447	1.210491	0.500865	0.151692	...	0.042350	0.433445
⋮	0.10	3.749339	1.408525	−2.698676	1.968552	0.506723	0.252957	...	0.037649	0.493222
⋮	0.15	6.275421	1.161677	−2.720033	5.498722	0.362696	0.287764	...	0.030977	0.491920
⋮	0.20	8.110289	1.338022	−3.137898	8.920299	0.336644	0.241695	...	0.038122	0.486423
⋮	0.30	3.551440	1.096635	−1.948918	2.421452	0.415324	0.157746	...	0.024862	0.458351
⋮	0.40	1.927179	1.014568	−1.500978	0.898598	0.495706	0.195379	...	0.037162	0.472384
⋮	0.50	0.978224	1.132263	−1.433145	0.746797	0.506893	0.099792	...	0.058614	0.461113
⋮	0.60	0.123009	1.147509	−1.272629	0.532229	0.509609	0.040735	...	0.065428	0.474686
⋮	0.80	−0.559846	1.207822	−1.199266	0.234712	0.612466	0.048375	...	0.057421	0.478584
⋮	1.00	−2.263159	1.494407	−1.208334	0.031866	0.955805	0.088997	...	0.048097	0.421450
⋮	1.50	−3.327187	1.466315	−0.966685	0.012328	1.005897	0.129478	...	0.048211	0.476798
⋮	2.00	−4.564634	1.544654	−0.861043	0.003402	1.132342	0.328478	...	0.053100	0.503742
⋮	3.00	−6.271920	1.706041	−0.788675	0.005418	1.003499	0.452452	...	0.056882	0.564915
PSV(T, ξ=5%)	4.00	−6.817475	1.690330	−0.659633	0.004659	0.984982	0.426588	...	0.066450	0.610257

Vertical Component

Ground-Motion Parameter, $Y^{V,T}$	Period T [sec]	Attenuation Equation Coefficients $p_1^{V,T}$	$p_2^{V,T}$	$p_3^{V,T}$	$p_4^{V,T}$	$p_5^{V,T}$	$p_6^{V,T}$	$p_7^{V,T}$	$p_8^{V,T}$	$\sigma_{\ln Y}^{V,T}$
PGA	...	0.478575	0.962048	−2.261099	8.275468	0.203742	0.170791	...	0.009990	0.576233
PSV(T, ξ=5%)	0.04	2.021977	0.975973	−2.269520	6.212511	0.207487	0.291655	...	0.016067	0.614969
⋮	0.10	4.800225	1.550978	−3.214835	3.711393	0.390121	0.290267	...	0.017959	0.638745
⋮	0.15	5.552711	1.095756	−2.631953	7.660410	0.267173	0.140272	...	0.036343	0.595166
⋮	0.20	5.715579	1.018200	−2.479719	10.431655	0.225780	0.026048	...	0.017690	0.568293
⋮	0.30	4.352338	0.577076	−1.570616	13.100457	0.094328	−0.133538	...	0.008807	0.504904
⋮	0.40	2.250287	0.855143	−1.459349	4.427120	0.259042	−0.136423	...	−0.008975	0.530693
⋮	0.50	1.023721	0.799708	−1.094297	6.406105	0.120518	−0.231852	...	−0.013138	0.494612
⋮	0.60	0.478709	0.813131	−0.991258	1.158308	0.350032	−0.234438	...	−0.012007	0.499304
⋮	0.80	−0.987655	1.041056	−0.991241	0.032814	0.879558	−0.218572	...	−0.030796	0.473957
⋮	1.00	−1.837322	1.093054	−0.839372	0.016433	0.934871	−0.132996	...	−0.045043	0.479322
⋮	1.50	−2.930992	1.112075	−0.669749	0.004734	0.965576	0.151251	...	−0.029185	0.504181
⋮	2.00	−3.726446	1.230340	−0.708449	0.003878	1.059438	0.155064	...	0.010191	0.549557
⋮	3.00	−5.614011	1.484269	−0.682160	0.017123	0.897857	0.259376	...	0.034858	0.673793
PSV(T, ξ=5%)	4.00	−7.182161	1.657145	−0.627111	0.006338	0.984802	0.279164	...	0.041492	0.773138

Equation Set (7)

$$ln\, Y^{c,T} = p_1^{c,T} + p_2^{c,T} M + p_3^{c,T} ln\left(R + p_4^{c,T} exp\{p_5^{c,T} M\}\right) + p_6^{c,T} S + p_7^{c,T} F + p_8^{c,T} D$$

Y ≡ ground-motion parameter—either peak ground acceleration (PGA), or peak 5 percent-damped pseudo-spectral velocity (PSV); units of PGA: [PGA] = g; units of PSV: [PSV] = cm/sec
M ≡ moment magnitude, M_w
R ≡ closest distance from site to fault rupture surface in km
S ≡ site classification code: $S = 0$ for site class B, $S = 1$ for site class C
F ≡ fault-type code: $F = 0$ for strike-slip, $F = 1$ for reverse
D ≡ depth to basement in km

Horizontal Component

Ground-Motion	Period				Attenuation Equation Coefficients					
Parameter, $Y^{H,T}$	T [sec]	$p_1^{H,T}$	$p_2^{H,T}$	$p_3^{H,T}$	$p_4^{H,T}$	$p_5^{H,T}$	$p_6^{H,T}$	$p_7^{H,T}$	$p_8^{H,T}$	$\sigma_{ln\,Y}^{H,T}$
PGA	...	−3.682981	1.048296	−1.419542	0.342687	0.593107	0.231204	0.307178	...	0.456027
PSV(T, ξ=5%)	0.04	−1.444034	0.989498	−1.427005	0.420028	0.552299	0.217216	0.286451	...	0.449758
⋮	0.10	1.452624	1.006257	−1.776129	0.789506	0.527877	0.296161	0.321017	...	0.529116
⋮	0.15	2.947740	0.967142	−1.876925	2.674755	0.365764	0.277498	0.273850	...	0.512118
⋮	0.20	3.797223	1.036507	−2.018345	4.578807	0.326014	0.250514	0.263253	...	0.494792
⋮	0.30	0.969349	1.034973	−1.405230	0.624128	0.496075	0.235313	0.308876	...	0.481481
⋮	0.40	−0.020076	1.097554	−1.252242	0.150858	0.660515	0.249941	0.307720	...	0.497955
⋮	0.50	−0.959503	1.217197	−1.206966	0.055196	0.784470	0.281880	0.339516	...	0.502022
⋮	0.60	−1.595945	1.246869	−1.095264	0.030839	0.825545	0.253590	0.344335	...	0.513415
⋮	0.80	−1.302631	1.137974	−0.981676	0.031521	0.772832	0.268046	0.311102	...	0.554858
⋮	1.00	−2.181092	1.351909	−1.057922	0.021732	0.928495	0.250440	0.184402	...	0.558472
⋮	1.50	−4.344454	1.670077	−1.051580	0.007951	1.086046	0.247649	0.069048	...	0.615469
⋮	2.00	−5.304621	1.747688	−1.000325	0.002976	1.197313	0.362098	−0.004484	...	0.636919
⋮	3.00	−6.622133	1.925991	−1.019458	0.006357	1.090327	0.377962	−0.074118	...	0.713194
PSV(T, ξ=5%)	4.00	−6.439521	1.742149	−0.803943	0.005855	1.006544	0.347583	−0.128097	...	0.744734

Vertical Component

Ground-Motion	Period				Attenuation Equation Coefficients					
Parameter, $Y^{V,T}$	T [sec]	$p_1^{V,T}$	$p_2^{V,T}$	$p_3^{V,T}$	$p_4^{V,T}$	$p_5^{V,T}$	$p_6^{V,T}$	$p_7^{V,T}$	$p_8^{V,T}$	$\sigma_{ln\,Y}^{V,T}$
PGA	...	−2.219481	0.787144	−1.522146	16.800628	−0.046877	0.283754	0.289824	...	0.585491
PSV(T, ξ=5%)	0.04	−0.396054	0.844219	−1.611074	12.837068	−0.028035	0.405532	0.334279	...	0.648936
⋮	0.10	1.612459	0.957945	−1.894247	5.860012	0.141872	0.351950	0.413471	...	0.665353
⋮	0.15	1.533558	0.822602	−1.558951	11.272702	0.015681	0.354912	0.444947	...	0.626649
⋮	0.20	1.542334	0.752164	−1.380485	26.551342	−0.128634	0.247691	0.387630	...	0.605605
⋮	0.30	0.265437	0.814392	−1.106173	3.793672	0.147029	0.149662	0.441099	...	0.601444
⋮	0.40	−0.640059	0.955510	−1.052736	0.862049	0.380680	0.080000	0.348630	...	0.595937
⋮	0.50	−1.648846	1.046999	−0.948643	0.488990	0.427148	0.044578	0.379218	...	0.574644
⋮	0.60	−2.521400	1.135271	−0.869586	0.017417	0.903728	0.063751	0.433557	...	0.605228
⋮	0.80	−2.559682	1.127003	−0.834868	0.015204	0.883060	−0.005826	0.448799	...	0.606628
⋮	1.00	−2.545782	1.127890	−0.806318	0.014951	0.882006	−0.029397	0.310008	...	0.604193
⋮	1.50	−4.515074	1.543483	−0.990903	0.005865	1.148640	0.096328	0.155889	...	0.611949
⋮	2.00	−4.591737	1.501827	−0.921105	0.012261	1.009155	0.126165	0.028280	...	0.654355
⋮	3.00	−6.507521	1.780567	−0.904163	0.017762	0.981797	0.141697	−0.050790	...	0.768139
PSV(T, ξ=5%)	4.00	−8.402034	2.009070	−0.867110	0.008660	1.050751	0.151746	−0.025302	...	0.829157

Equation Set (8)

$$\ln Y^{c,T} = p_1^{c,T} + p_2^{c,T} M + p_3^{c,T} \ln\left(R + p_4^{c,T} \exp\{p_5^{c,T} M\}\right) + p_6^{c,T} S + p_7^{c,T} F + p_8^{c,T} D$$

Y ≡ ground-motion parameter—either peak ground acceleration (PGA), or peak 5 percent-damped pseudo-spectral velocity (PSV); units of PGA: [PGA] = g; units of PSV: [PSV] = cm/sec
M ≡ moment magnitude, M_w
R ≡ closest distance from site to fault rupture surface in km
S ≡ site classification code: $S = 0$ for site class B, $S = 1$ for site class C
F ≡ fault-type code: $F = 0$ for strike-slip, $F = 1$ for reverse
D ≡ depth to basement in km

Horizontal Component

Ground-Motion Parameter, $Y^{H,T}$	Period T [sec]	Attenuation Equation Coefficients								
		$p_1^{H,T}$	$p_2^{H,T}$	$p_3^{H,T}$	$p_4^{H,T}$	$p_5^{H,T}$	$p_6^{H,T}$	$p_7^{H,T}$	$p_8^{H,T}$	$\sigma_{\ln Y}^{H,T}$
PGA	...	−2.744812	1.077356	−1.678289	0.775010	0.514537	0.192870	0.245794	0.035211	0.425829
PSV(T, ξ=5%)	0.04	−0.791941	1.051772	−1.671470	0.766266	0.508120	0.189106	0.266159	0.037408	0.418894
⋮	0.10	2.212340	1.221897	−2.242692	1.209446	0.514127	0.290996	0.290450	0.032296	0.478475
⋮	0.15	4.269983	1.034441	−2.249298	3.429838	0.369431	0.319532	0.248123	0.026500	0.481907
⋮	0.20	5.209203	1.134796	−2.440668	5.495904	0.334676	0.269727	0.237064	0.033619	0.477636
⋮	0.30	2.436908	1.011586	−1.668167	1.532734	0.418415	0.188880	0.233305	0.020243	0.448711
⋮	0.40	1.204089	0.974111	−1.340593	0.512187	0.517249	0.230928	0.241411	0.032603	0.461953
⋮	0.50	0.251978	1.104080	−1.290327	0.409234	0.532254	0.141385	0.273709	0.053708	0.446437
⋮	0.60	−0.516174	1.139763	−1.171566	0.292395	0.533667	0.086702	0.288917	0.060356	0.458439
⋮	0.80	−0.973020	1.193942	−1.130911	0.172925	0.603576	0.089939	0.258804	0.052997	0.465927
⋮	1.00	−2.395634	1.464671	−1.160501	0.023992	0.969556	0.108630	0.128380	0.045880	0.419081
⋮	1.50	−3.304606	1.471783	−0.961716	0.010443	1.042147	0.112105	−0.107861	0.049239	0.477426
⋮	2.00	−4.184121	1.501460	−0.847053	0.008202	1.022173	0.285184	−0.256523	0.056028	0.494719
⋮	3.00	−6.030547	1.705080	−0.804609	0.005309	1.068762	0.408600	−0.259210	0.060866	0.551307
PSV(T, ξ=5%)	4.00	−6.568532	1.674798	−0.652718	0.003166	1.104478	0.378852	−0.281094	0.070104	0.598142

Vertical Component

Ground-Motion Parameter, $Y^{V,T}$	Period T [sec]	Attenuation Equation Coefficients								
		$p_1^{V,T}$	$p_2^{V,T}$	$p_3^{V,T}$	$p_4^{V,T}$	$p_5^{V,T}$	$p_6^{V,T}$	$p_7^{V,T}$	$p_8^{V,T}$	$\sigma_{\ln Y}^{V,T}$
PGA	...	−0.265110	0.930956	−2.105163	7.844418	0.179499	0.193771	0.163279	0.006873	0.573918
PSV(T, ξ=5%)	0.04	1.505604	0.960918	−2.171684	6.040860	0.188147	0.314012	0.150697	0.013347	0.613640
⋮	0.10	3.625903	1.435420	−2.892284	3.071738	0.380715	0.314431	0.190954	0.014179	0.635812
⋮	0.15	3.956292	0.999208	−2.257056	6.209988	0.239944	0.171634	0.244273	0.031345	0.587972
⋮	0.20	4.468856	0.913391	−2.149757	10.028279	0.179664	0.045220	0.164865	0.013609	0.566144
⋮	0.30	3.573333	0.568035	−1.434275	12.893824	0.047586	−0.105310	0.190456	0.005107	0.499734
⋮	0.40	2.040653	0.845497	−1.414469	4.250864	0.249483	−0.128537	0.055110	−0.010047	0.532161
⋮	0.50	0.532146	0.804787	−1.027427	6.789834	0.059363	−0.200567	0.194075	−0.016713	0.488746
⋮	0.60	−0.161128	0.826508	−0.915606	0.709383	0.342336	−0.186441	0.290147	−0.017125	0.483774
⋮	0.80	−1.284679	1.005764	−0.919576	0.019391	0.876831	−0.171387	0.291246	−0.036236	0.455442
⋮	1.00	−2.018028	1.097218	−0.818204	0.011350	0.961438	−0.115265	0.105115	−0.047030	0.478718
⋮	1.50	−2.819066	1.116179	−0.686540	0.003078	1.087299	0.132352	−0.107085	−0.027010	0.500927
⋮	2.00	−3.950598	1.290066	−0.718690	0.002947	1.131886	0.119099	−0.214437	0.013467	0.539929
⋮	3.00	−6.027019	1.632305	−0.762058	0.013231	1.037168	0.197880	−0.375626	0.041843	0.647313
PSV(T, ξ=5%)	4.00	−6.836353	1.615381	−0.607479	0.009157	0.961684	0.236317	−0.252200	0.044164	0.764499

Equation Set (9)

$$\ln Y^{c,T} \;=\; p_1^{c,T} + p_2^{c,T} M + p_3^{c,T} \ln\left(R + p_4^{c,T} \exp\{p_5^{c,T} M\}\right) + p_6^{c,T} S + p_7^{c,T} F + p_8^{c,T} D$$

Y ≡ ground-motion parameter—either peak ground acceleration (PGA), or peak 5 percent-damped pseudo-spectral velocity (PSV); units of PGA: [PGA] = g; units of PSV: [PSV] = cm/sec
M ≡ moment magnitude, M_w
R ≡ closest distance from site to fault rupture surface in km
S ≡ site classification code: $S = 0$ for site class B, $S = 1$ for site class C
F ≡ fault-type code: $F = 0$ for strike-slip, $F = 1$ for reverse
D ≡ depth to basement in km

Horizontal Component

Ground-Motion Parameter, $Y^{H,T}$	Period T [sec]	Attenuation Equation Coefficients $p_1^{H,T}$	$p_2^{H,T}$	$p_3^{H,T}$	$p_4^{H,T}$	$p_5^{H,T}$	$p_6^{H,T}$	$p_7^{H,T}$	$p_8^{H,T}$	$\sigma_{\ln Y}^{H,T}$
PGA	...	−2.788816	1.083898	−1.664933	0.707328	0.495853	...	...	...	0.512829
PSV(T, ξ=5%)	0.04	−1.131621	1.064646	−1.603504	0.482076	0.534007	...	...	...	0.500078
⋮	0.10	1.922701	1.280780	−2.219585	0.750588	0.577036	...	...	...	0.573296
⋮	0.15	4.038685	1.273050	−2.472638	4.053933	0.358246	...	...	...	0.557202
⋮	0.20	4.769454	1.042985	−2.229934	8.803985	0.226976	...	...	...	0.536325
⋮	0.30	0.379647	1.203289	−1.508531	0.394318	0.563735	...	...	...	0.544030
⋮	0.40	1.267698	0.992687	−1.387504	1.238820	0.333826	...	...	...	0.560330
⋮	0.50	−0.260832	1.193668	−1.335564	0.091568	0.684649	...	...	...	0.594013
⋮	0.60	0.322824	1.013788	−1.171220	10.250271	−0.063997	...	...	...	0.620264
⋮	0.80	0.778887	0.805584	−0.944971	441.348158	−0.891756	...	...	...	0.706759
⋮	1.00	−2.180062	1.368885	−1.085105	0.026836	0.864184	...	...	...	0.635404
⋮	1.50	−2.906396	1.349051	−0.904186	0.023762	0.802783	...	...	...	0.684178
⋮	2.00	−3.915624	1.484747	−0.925547	0.021264	0.825384	...	...	...	0.702187
⋮	3.00	−5.599219	1.649287	−0.813291	0.022213	0.810870	...	...	...	0.770092
PSV(T, ξ=5%)	4.00	−6.504493	1.721184	−0.728078	0.054943	0.696101	...	...	...	0.743540

Vertical Component

Ground-Motion Parameter, $Y^{V,T}$	Period T [sec]	Attenuation Equation Coefficients $p_1^{V,T}$	$p_2^{V,T}$	$p_3^{V,T}$	$p_4^{V,T}$	$p_5^{V,T}$	$p_6^{V,T}$	$p_7^{V,T}$	$p_8^{V,T}$	$\sigma_{\ln Y}^{V,T}$
PGA	...	−1.908120	0.784642	−1.578886	60.541179	−0.254580	...	...	...	0.561273
PSV(T, ξ=5%)	0.04	−0.993340	1.011749	−1.698632	2.940387	0.210184	...	...	...	0.605406
⋮	0.10	3.696014	0.902516	−2.207327	24.862105	−0.021694	...	...	...	0.646358
⋮	0.15	2.769831	0.946909	−1.963181	15.230470	0.037613	...	...	...	0.600471
⋮	0.20	3.144321	0.488987	−1.339467	1020.727462	−0.736072	...	...	...	0.562656
⋮	0.30	2.906451	0.856123	−1.686463	26.650402	−0.006950	...	...	...	0.648353
⋮	0.40	0.187352	1.003687	−1.305215	1.941374	0.289952	...	...	...	0.617719
⋮	0.50	0.782077	0.813542	−1.142128	108.207463	−0.363402	...	...	...	0.646774
⋮	0.60	−2.096018	1.266625	−1.128617	0.072995	0.767891	...	...	...	0.675332
⋮	0.80	−2.218989	1.271748	−1.101685	0.058953	0.767712	...	...	...	0.672424
⋮	1.00	−3.531512	1.503780	−1.095060	0.025170	0.954013	...	...	...	0.665477
⋮	1.50	−3.388237	1.435326	−1.070858	0.030044	0.896974	...	...	...	0.586906
⋮	2.00	−4.196881	1.463912	−0.969876	0.021912	0.882104	...	...	...	0.587994
⋮	3.00	−6.661736	1.798592	−0.900619	0.024747	0.873355	...	...	...	0.740270
PSV(T, ξ=5%)	4.00	−7.572208	1.841813	−0.776934	0.057415	0.715533	...	...	...	0.774544

Equation Set (10)

$$\ln Y^{c,T} = p_1^{c,T} + p_2^{c,T}M + p_3^{c,T}\ln\left(R + p_4^{c,T}\exp\{p_5^{c,T}M\}\right) + p_6^{c,T}S + p_7^{c,T}F + p_8^{c,T}D$$

Y ≡ ground-motion parameter—either peak ground acceleration (PGA), or peak 5 percent-damped pseudo-spectral velocity (PSV); units of PGA: [PGA] = g; units of PSV: [PSV] = cm/sec
M ≡ moment magnitude, M_w
R ≡ closest distance from site to fault rupture surface in km
S ≡ site classification code: $S = 0$ for site class B, $S = 1$ for site class C
F ≡ fault-type code: $F = 0$ for strike-slip, $F = 1$ for reverse
D ≡ depth to basement in km

Horizontal Component

Ground-Motion Parameter, $Y^{H,T}$	Period T [sec]	Attenuation Equation Coefficients $p_1^{H,T}$	$p_2^{H,T}$	$p_3^{H,T}$	$p_4^{H,T}$	$p_5^{H,T}$	$p_6^{H,T}$	$p_7^{H,T}$	$p_8^{H,T}$	$\sigma_{\ln Y}^{H,T}$
PGA	...	−2.975972	1.227410	−1.826005	0.380017	0.653480	...	...	0.088530	0.521704
PSV(T, ξ=5%)	0.04	−1.186804	1.206466	−1.789849	0.330341	0.664250	...	...	0.089930	0.514579
⋮	0.10	3.558792	1.440038	−2.707265	1.728860	0.531916	...	...	0.083526	0.579104
⋮	0.15	3.318964	1.731238	−2.910269	1.228889	0.594872	...	...	0.097973	0.553521
⋮	0.20	3.515965	1.832299	−2.975927	1.318012	0.597221	...	...	0.105846	0.538029
⋮	0.30	2.322878	1.250004	−1.965869	0.610081	0.608388	...	...	0.075645	0.538924
⋮	0.40	1.113333	1.111242	−1.515351	0.282792	0.649108	...	...	0.077654	0.508098
⋮	0.50	−0.485406	1.345685	−1.491065	0.091843	0.801033	...	...	0.123208	0.479628
⋮	0.60	−0.562702	1.165825	−1.194658	0.110654	0.702911	...	...	0.101819	0.543346
⋮	0.80	−0.083439	0.984456	−1.009230	0.239936	0.518725	...	...	0.080042	0.578846
⋮	1.00	−2.282153	1.491504	−1.220639	0.034404	0.935634	...	...	0.071760	0.460305
⋮	1.50	−2.725069	1.424097	−1.007494	0.027306	0.939001	...	...	0.039470	0.483458
⋮	2.00	−3.815055	1.515648	−0.952742	0.015385	0.999464	...	...	0.045058	0.508216
⋮	3.00	−5.105444	1.576954	−0.808169	0.046226	0.789838	...	...	0.041625	0.634938
PSV(T, ξ=5%)	4.00	−6.354649	1.832419	−0.922558	0.030480	0.939452	...	...	0.041799	0.697312

Vertical Component

Ground-Motion Parameter, $Y^{V,T}$	Period T [sec]	Attenuation Equation Coefficients $p_1^{V,T}$	$p_2^{V,T}$	$p_3^{V,T}$	$p_4^{V,T}$	$p_5^{V,T}$	$p_6^{V,T}$	$p_7^{V,T}$	$p_8^{V,T}$	$\sigma_{\ln Y}^{V,T}$
PGA	...	−1.745624	1.258930	−2.238205	1.681324	0.445083	...	...	0.073718	0.524466
PSV(T, ξ=5%)	0.04	−0.074963	1.247277	−2.206172	1.080728	0.479615	...	...	0.062950	0.607714
⋮	0.10	3.037641	1.576617	−2.920754	1.319271	0.533158	...	...	0.078502	0.579639
⋮	0.15	1.159517	2.263270	−3.303948	0.911895	0.628358	...	...	0.101764	0.479091
⋮	0.20	1.685676	1.628569	−2.552692	1.430087	0.513860	...	...	0.098227	0.465015
⋮	0.30	3.954387	1.038534	−2.095539	2.979234	0.406017	...	...	0.055404	0.548947
⋮	0.40	1.651880	1.087724	−1.687173	1.703544	0.429518	...	...	0.032979	0.667411
⋮	0.50	0.783063	1.191835	−1.634659	1.410876	0.446215	...	...	0.037507	0.638982
⋮	0.60	−0.437303	1.573796	−1.861511	0.474193	0.663463	...	...	0.031699	0.527261
⋮	0.80	−1.696306	1.388415	−1.364766	0.111526	0.776249	...	...	−0.000778	0.515933
⋮	1.00	−3.597728	1.876025	−1.603209	0.042114	0.989815	...	...	0.018430	0.528956
⋮	1.50	−2.515605	1.323412	−1.098184	0.033257	0.901461	...	...	0.009161	0.461807
⋮	2.00	−3.957006	1.484074	−1.034928	0.021273	0.943302	...	...	0.009717	0.534376
⋮	3.00	−6.225355	1.803000	−1.015070	0.050851	0.824879	...	...	0.007102	0.746333
PSV(T, ξ=5%)	4.00	−8.035118	2.206232	−1.214621	0.066910	0.865049	...	...	0.021768	0.858834

Equation Set (11)

$$\ln Y^{c,T} = p_1^{c,T} + p_2^{c,T} M + p_3^{c,T} \ln\left(R + p_4^{c,T} \exp\left(p_5^{c,T} M\right)\right) + p_6^{c,T} S + p_7^{c,T} F + p_8^{c,T} D$$

$Y \equiv$ ground-motion parameter—either peak ground acceleration (PGA), or peak 5 percent-damped pseudo-spectral velocity (PSV); units of PGA: [PGA] = g; units of PSV: [PSV] = cm/sec
$M \equiv$ moment magnitude, M_w
$R \equiv$ closest distance from site to fault rupture surface in km
$S \equiv$ site classification code: $S = 0$ for site class B, $S = 1$ for site class C
$F \equiv$ fault-type code: $F = 0$ for strike-slip, $F = 1$ for reverse
$D \equiv$ depth to basement in km

Horizontal Component

Ground-Motion Parameter, $Y^{H,T}$	Period T [sec]	Attenuation Equation Coefficients $p_1^{H,T}$	$p_2^{H,T}$	$p_3^{H,T}$	$p_4^{H,T}$	$p_5^{H,T}$	$p_6^{H,T}$	$p_7^{H,T}$	$p_8^{H,T}$	$\sigma_{\ln Y}^{H,T}$
PGA	...	−3.229398	1.058631	−1.569282	0.555772	0.502083	...	0.246531	...	0.500355
PSV(T, ξ = 5%)	0.04	−1.493416	1.039559	−1.522169	0.395433	0.535196	...	0.240741	...	0.487849
⋮	0.10	1.308554	1.183205	−2.013513	0.585070	0.577923	...	0.291273	...	0.560151
⋮	0.15	2.795351	1.245220	−2.233571	2.664349	0.388011	...	0.236726	...	0.547434
⋮	0.20	3.517292	1.053323	−2.030828	5.764815	0.258966	...	0.205956	...	0.529178
⋮	0.30	−0.159937	1.157771	−1.370789	0.229350	0.592318	...	0.309128	...	0.524558
⋮	0.40	0.763372	1.009554	−1.329585	0.758015	0.378668	...	0.226178	...	0.551544
⋮	0.50	−0.484874	1.173649	−1.288407	0.088343	0.659828	...	0.267115	...	0.581656
⋮	0.60	−0.730714	1.119583	−1.128444	1.370645	0.202240	...	0.315513	...	0.603128
⋮	0.80	−0.412443	0.946502	−0.937018	325.351657	−0.916925	...	0.418869	...	0.668120
⋮	1.00	−2.389088	1.344771	−1.038823	0.022485	0.850346	...	0.294596	...	0.619869
⋮	1.50	−3.148562	1.351275	−0.883364	0.018389	0.805251	...	0.267464	...	0.672821
⋮	2.00	−4.114766	1.475830	−0.900053	0.025749	0.755808	...	0.282090	...	0.690049
⋮	3.00	−6.043688	1.685735	−0.801787	0.013854	0.844482	...	0.291622	...	0.756917
PSV(T, ξ = 5%)	4.00	−6.785239	1.745056	−0.719497	0.040240	0.719221	...	0.157421	...	0.740978

Vertical Component

Ground-Motion Parameter, $Y^{V,T}$	Period T [sec]	Attenuation Equation Coefficients $p_1^{V,T}$	$p_2^{V,T}$	$p_3^{V,T}$	$p_4^{V,T}$	$p_5^{V,T}$	$p_6^{V,T}$	$p_7^{V,T}$	$p_8^{V,T}$	$\sigma_{\ln Y}^{V,T}$
PGA	...	−2.777517	0.873859	−1.542786	29.313166	−0.160838	...	0.208319	...	0.554450
PSV(T, ξ = 5%)	0.04	−1.543074	1.047073	−1.653648	1.889054	0.259351	...	0.197220	...	0.600268
⋮	0.10	2.011563	1.014549	−2.058034	12.213589	0.053198	...	0.359792	...	0.624498
⋮	0.15	1.144293	1.054101	−1.819363	6.278832	0.133932	...	0.378567	...	0.573359
⋮	0.20	1.776488	0.666243	−1.332980	178.868558	−0.480565	...	0.329434	...	0.541644
⋮	0.30	0.813255	0.998376	−1.499581	7.421244	0.134084	...	0.383800	...	0.623120
⋮	0.40	−0.235440	1.020187	−1.258865	1.323526	0.325556	...	0.174487	...	0.614509
⋮	0.50	0.028004	0.905740	−1.131307	36.888452	−0.209692	...	0.185911	...	0.643288
⋮	0.60	−2.291067	1.237300	−1.074666	0.062961	0.756007	...	0.248750	...	0.666156
⋮	0.80	−2.460049	1.244583	−1.045379	0.047929	0.756300	...	0.300661	...	0.657639
⋮	1.00	−3.690274	1.449928	−1.022106	0.019590	0.947230	...	0.301460	...	0.649932
⋮	1.50	−3.477299	1.413406	−1.038323	0.027333	0.889701	...	0.147568	...	0.584247
⋮	2.00	−4.321775	1.451576	−0.944296	0.019156	0.877036	...	0.170777	...	0.583487
⋮	3.00	−6.930307	1.785811	−0.861179	0.018352	0.872870	...	0.333657	...	0.722341
PSV(T, ξ = 5%)	4.00	−7.999473	1.873483	−0.758510	0.035303	0.751569	...	0.248938	...	0.764899

Equation Set (12)

$$\ln Y^{c,T} = p_1^{c,T} + p_2^{c,T} M + p_3^{c,T} \ln\left(R + p_4^{c,T} \exp\{p_5^{c,T} M\}\right) + p_6^{c,T} S + p_7^{c,T} F + p_8^{c,T} D$$

- Y ≡ ground-motion parameter—either peak ground acceleration (PGA), or peak 5 percent-damped pseudo-spectral velocity (PSV); units of PGA: [PGA] = g; units of PSV: [PSV] = cm/sec
- M ≡ moment magnitude, M_w
- R ≡ closest distance from site to fault rupture surface in km
- S ≡ site classification code: $S = 0$ for site class B, $S = 1$ for site class C
- F ≡ fault-type code: $F = 0$ for strike-slip, $F = 1$ for reverse
- D ≡ depth to basement in km

Horizontal Component

Ground-Motion Parameter, $Y^{H,T}$	Period T [sec]	$p_1^{H,T}$	$p_2^{H,T}$	$p_3^{H,T}$	$p_4^{H,T}$	$p_5^{H,T}$	$p_6^{H,T}$	$p_7^{H,T}$	$p_8^{H,T}$	$\sigma_{\ln Y}^{H,T}$
PGA	...	−3.438716	1.064905	−1.561987	0.321121	0.609753	...	0.280577	0.079106	0.510114
PSV(T, ξ=5%)	0.04	−1.647263	1.047523	−1.530232	0.273347	0.620739	...	0.293666	0.080130	0.500896
⋮	0.10	1.621750	1.149988	−2.059471	0.826683	0.553212	...	0.416721	0.071282	0.556546
⋮	0.15	1.921374	1.421424	−2.334328	0.794180	0.591839	...	0.325302	0.087794	0.543871
⋮	0.20	2.310864	1.464855	−2.366754	1.014116	0.567785	...	0.270557	0.096824	0.528672
⋮	0.30	1.650729	0.987419	−1.538759	0.445397	0.555187	...	0.278617	0.066522	0.529563
⋮	0.40	0.905411	1.033991	−1.388657	0.244439	0.629116	...	0.128276	0.073497	0.510368
⋮	0.50	−0.648045	1.257772	−1.361937	0.070190	0.788589	...	0.164481	0.117822	0.479357
⋮	0.60	−0.853291	1.116790	−1.092971	0.089299	0.670684	...	0.224815	0.094713	0.538663
⋮	0.80	−0.527344	0.970331	−0.929313	0.292487	0.398540	...	0.305814	0.070271	0.565890
⋮	1.00	−2.407397	1.411386	−1.109214	0.023552	0.937149	...	0.176104	0.065991	0.457812
⋮	1.50	−2.724998	1.436501	−1.019332	0.026961	0.948828	...	−0.038394	0.040855	0.488773
⋮	2.00	−3.778425	1.535854	−0.976907	0.016162	1.010442	...	−0.085977	0.048010	0.513143
⋮	3.00	−4.949367	1.585589	−0.835488	0.054454	0.795634	...	−0.140836	0.046186	0.639955
PSV(T, ξ=5%)	4.00	−6.271135	1.990673	−1.104244	0.040989	0.985296	...	−0.317117	0.052907	0.691268

Vertical Component

Ground-Motion Parameter, $Y^{V,T}$	Period T [sec]	$p_1^{V,T}$	$p_2^{V,T}$	$p_3^{V,T}$	$p_4^{V,T}$	$p_5^{V,T}$	$p_6^{V,T}$	$p_7^{V,T}$	$p_8^{V,T}$	$\sigma_{\ln Y}^{V,T}$
PGA	...	−2.137768	1.166247	−2.066330	1.758670	0.406429	...	0.155372	0.068244	0.525213
PSV(T, ξ=5%)	0.04	−0.319928	1.189360	−2.100133	1.122773	0.452080	...	0.128142	0.058463	0.611568
⋮	0.10	2.209228	1.337061	−2.511478	1.278082	0.484613	...	0.292905	0.068251	0.569062
⋮	0.15	0.665751	2.064686	−3.001224	0.836162	0.611992	...	0.151046	0.096520	0.479159
⋮	0.20	1.632934	1.607519	−2.519910	1.432867	0.509265	...	0.017748	0.097571	0.470315
⋮	0.30	2.941213	0.815381	−1.661896	3.218954	0.309727	...	0.238623	0.047027	0.544001
⋮	0.40	1.798776	1.120817	−1.750044	1.702403	0.443681	...	−0.049630	0.034686	0.674710
⋮	0.50	0.804862	1.198130	−1.645614	1.405009	0.449549	...	−0.009391	0.037842	0.646354
⋮	0.60	−0.363992	1.606969	−1.911277	0.489891	0.667659	...	−0.032574	0.032815	0.533128
⋮	0.80	−1.897051	1.308849	−1.241638	0.092559	0.753703	...	0.187640	−0.006993	0.513911
⋮	1.00	−3.631091	1.850152	−1.568477	0.038388	0.995507	...	0.034305	0.017309	0.534805
⋮	1.50	−2.334508	1.401436	−1.208727	0.044850	0.913271	...	−0.235660	0.017041	0.454505
⋮	2.00	−3.838157	1.539424	−1.108019	0.024409	0.968853	...	−0.207828	0.016777	0.533039
⋮	3.00	−6.322026	1.932611	−1.130873	0.027935	0.982444	...	−0.294537	0.018324	0.741991
PSV(T, ξ=5%)	4.00	−8.707985	2.576310	−1.509543	0.035019	1.054745	...	−0.310699	0.034863	0.857161

Equation Set (13)

$$\ln Y^{c,T} = p_1^{c,T} + p_2^{c,T}M + p_3^{c,T}\ln\left(R + p_4^{c,T}\exp\left(p_5^{c,T}M\right)\right) + p_6^{c,T}S + p_7^{c,T}F + p_8^{c,T}D$$

Y ≡ ground-motion parameter—either peak ground acceleration (PGA), or peak 5 percent-damped pseudo-spectral velocity (PSV); units of PGA: [PGA] = g; units of PSV: [PSV] = cm/sec

M ≡ moment magnitude, M_w

R ≡ closest distance from site to fault rupture surface in km

S ≡ site classification code: $S = 0$ for site class B, $S = 1$ for site class C

F ≡ fault-type code: $F = 0$ for strike-slip, $F = 1$ for reverse

D ≡ depth to basement in km

Horizontal Component

Ground-Motion Parameter, $Y^{H,T}$	Period T [sec]	Attenuation Equation Coefficients $p_1^{H,T}$	$p_2^{H,T}$	$p_3^{H,T}$	$p_4^{H,T}$	$p_5^{H,T}$	$p_6^{H,T}$	$p_7^{H,T}$	$p_8^{H,T}$	$\sigma_{\ln Y}^{H,T}$
PGA	...	−3.171847	1.105604	−1.495235	0.315897	0.670390	...	...	...	0.432386
PSV(T, ξ=5%)	0.04	−0.631375	1.014424	−1.529255	0.504387	0.591804	...	...	...	0.428633
⋮	0.10	2.469940	0.990540	−1.851245	0.975031	0.535067	...	...	...	0.499553
⋮	0.15	3.585989	0.851706	−1.763100	2.015547	0.409572	...	...	...	0.466280
⋮	0.20	5.910391	1.174911	−2.463648	5.807310	0.368350	...	...	...	0.464664
⋮	0.30	2.581938	0.913354	−1.471862	2.134150	0.362448	...	...	...	0.466536
⋮	0.40	0.347917	1.079412	−1.205913	0.109990	0.739537	...	...	...	0.457061
⋮	0.50	−0.432626	1.167464	−1.141107	0.113232	0.707330	...	...	...	0.457979
⋮	0.60	−1.361394	1.234138	−1.017782	0.016784	0.933752	...	...	...	0.473798
⋮	0.80	−1.339666	1.237347	−1.017965	0.029211	0.857198	...	...	...	0.496888
⋮	1.00	−1.795883	1.345774	−1.049509	0.021121	0.960719	...	...	...	0.532648
⋮	1.50	−4.119871	1.625452	−0.969601	0.008157	1.060542	...	...	...	0.567066
⋮	2.00	−4.682409	1.615584	−0.872844	0.002119	1.139593	...	...	...	0.598645
⋮	3.00	−6.364540	1.838184	−0.883308	0.001993	1.120150	...	...	...	0.667339
PSV(T, ξ=5%)	4.00	−7.006554	1.825652	−0.744807	0.001555	1.063866	...	...	...	0.710394

Vertical Component

Ground-Motion Parameter, $Y^{V,T}$	Period T [sec]	Attenuation Equation Coefficients $p_1^{V,T}$	$p_2^{V,T}$	$p_3^{V,T}$	$p_4^{V,T}$	$p_5^{V,T}$	$p_6^{V,T}$	$p_7^{V,T}$	$p_8^{V,T}$	$\sigma_{\ln Y}^{V,T}$
PGA	...	−0.559472	0.620993	−1.558580	42.672176	−0.170980	...	...	...	0.621805
PSV(T, ξ=5%)	0.04	1.961399	0.561932	−1.619466	266.066139	−0.508069	...	...	...	0.692416
⋮	0.10	2.914728	0.713356	−1.742818	39.399670	−0.203078	...	...	...	0.719386
⋮	0.15	3.177836	0.537737	−1.395497	73.871073	−0.304972	...	...	...	0.674064
⋮	0.20	2.786204	0.635713	−1.392705	93.213717	−0.305204	...	...	...	0.679197
⋮	0.30	1.189784	0.641793	−0.974013	35.770574	−0.194924	...	...	...	0.589851
⋮	0.40	0.046961	0.817867	−0.943034	4.276434	0.143474	...	...	...	0.575021
⋮	0.50	−1.406940	1.039507	−0.916857	0.489645	0.508104	...	...	...	0.535768
⋮	0.60	−1.797061	0.931776	−0.669255	0.119863	0.492423	...	...	...	0.600575
⋮	0.80	−1.753020	0.959881	−0.716849	0.017301	0.885265	...	...	...	0.592254
⋮	1.00	−2.221688	1.049198	−0.733990	0.011650	0.946231	...	...	...	0.557499
⋮	1.50	−3.894661	1.272470	−0.675605	0.002920	1.123433	...	...	...	0.601683
⋮	2.00	−4.260013	1.381443	−0.775603	0.010486	1.019084	...	...	...	0.661584
⋮	3.00	−7.246310	1.863324	−0.831041	0.008931	1.089968	...	...	...	0.765604
PSV(T, ξ=5%)	4.00	−7.794594	1.814333	−0.675976	0.005623	1.038565	...	...	...	0.841187

Equation Set (14)

$$\ln Y^{c,T} = p_1^{c,T} + p_2^{c,T} M + p_3^{c,T} \ln\left(R + p_4^{c,T} \exp\left(p_5^{c,T} M\right)\right) + p_6^{c,T} S + p_7^{c,T} F + p_8^{c,T} D$$

Y ≡ ground-motion parameter—either peak ground acceleration (PGA), or peak 5 percent-damped pseudo-spectral velocity (PSV); units of PGA: [PGA] = g; units of PSV: [PSV] = cm/sec
M ≡ moment magnitude, M_w
R ≡ closest distance from site to fault rupture surface in km
S ≡ site classification code: $S = 0$ for site class B, $S = 1$ for site class C
F ≡ fault-type code: $F = 0$ for strike-slip, $F = 1$ for reverse
D ≡ depth to basement in km

Horizontal Component

Ground-Motion Parameter, $Y^{H,T}$	Period T [sec]				Attenuation Equation Coefficients				
		$p_1^{H,T}$	$p_2^{H,T}$	$p_3^{H,T}$	$p_4^{H,T}$	$p_5^{H,T}$	$p_6^{H,T}$	$p_7^{H,T}$	$p_8^{H,T}$	$\sigma_{\ln Y}^{H,T}$
PGA	...	−2.015820	1.153071	−1.852876	0.750521	0.563234	...	...	0.025951	0.406245
PSV(T, ξ=5%)	0.04	0.364718	1.093490	−1.885195	0.974180	0.524345	...	...	0.029432	0.406711
⋮	0.10	3.731035	1.201834	−2.431032	1.633315	0.494372	...	...	0.028169	0.456326
⋮	0.15	5.472566	0.950331	−2.287954	3.752345	0.360953	...	...	0.003618	0.450936
⋮	0.20	6.686006	1.264552	−2.776806	5.703215	0.370405	...	...	0.017663	0.460511
⋮	0.30	3.049698	1.125886	−1.864507	1.542490	0.462788	...	...	0.001928	0.421470
⋮	0.40	1.454307	1.086857	−1.469933	0.343272	0.622287	...	...	0.017469	0.475111
⋮	0.50	0.927555	1.125258	−1.398409	0.647430	0.507691	...	...	0.035606	0.458459
⋮	0.60	0.325510	1.095849	−1.251366	0.955739	0.384565	...	...	0.049201	0.457015
⋮	0.80	−1.842585	1.447201	−1.256686	0.026909	0.944773	...	...	0.048728	0.454654
⋮	1.00	−2.568056	1.535995	−1.207010	0.013423	1.057494	...	...	0.047540	0.441020
⋮	1.50	−3.387277	1.447946	−0.929657	0.014107	0.931298	...	...	0.062390	0.475158
⋮	2.00	−4.139228	1.471404	−0.804379	0.004391	0.981605	...	...	0.066278	0.493842
⋮	3.00	−6.042967	1.698842	−0.752102	0.003704	0.938893	...	...	0.070925	0.517036
PSV(T, ξ=5%)	4.00	−6.393076	1.621853	−0.567337	0.001769	0.905683	...	...	0.085956	0.562746

Vertical Component

Ground-Motion Parameter, $Y^{V,T}$	Period T [sec]				Attenuation Equation Coefficients				
		$p_1^{V,T}$	$p_2^{V,T}$	$p_3^{V,T}$	$p_4^{V,T}$	$p_5^{V,T}$	$p_6^{V,T}$	$p_7^{V,T}$	$p_8^{V,T}$	$\sigma_{\ln Y}^{V,T}$
PGA	...	1.077007	0.636199	−1.944540	31.146485	−0.072968	...	...	−0.016066	0.621109
PSV(T, ξ=5%)	0.04	3.761469	0.504742	−1.965056	130.081121	−0.352853	...	...	−0.014180	0.649008
⋮	0.10	4.781791	0.923477	−2.420698	12.082899	0.091979	...	...	−0.013047	0.695227
⋮	0.15	5.699239	0.539835	−1.950878	28.089125	−0.048326	...	...	−0.001192	0.661795
⋮	0.20	4.022075	0.413019	−1.376288	97.287931	−0.374042	...	...	−0.033745	0.658784
⋮	0.30	4.026279	0.442460	−1.366140	46.966826	−0.190756	...	...	−0.013939	0.497968
⋮	0.40	1.773771	0.697511	−1.195841	12.669448	−0.006028	...	...	−0.026550	0.481226
⋮	0.50	0.132259	0.787930	−0.936336	11.781855	−0.063293	...	...	−0.032734	0.447273
⋮	0.60	−0.029126	0.689685	−0.746210	1.652385	0.032242	...	...	−0.045091	0.467070
⋮	0.80	−0.613553	0.829203	−0.813486	0.016326	0.866179	...	...	−0.043985	0.442880
⋮	1.00	−1.709742	0.956814	−0.692547	0.006802	0.917881	...	...	−0.068927	0.435347
⋮	1.50	−3.374020	1.149316	−0.592391	0.001597	1.055927	...	...	−0.032309	0.515452
⋮	2.00	−4.314197	1.327705	−0.709110	0.009266	0.965933	...	...	0.024308	0.557013
⋮	3.00	−5.874392	1.477967	−0.583182	1.231425	0.176819	...	...	0.060847	0.635854
PSV(T, ξ=5%)	4.00	−5.907418	1.407442	−0.489391	25.479222	−0.382398	...	...	0.068681	0.746116

Equation Set (15)

$$\ln Y^{c,T} = p_1^{c,T} + p_2^{c,T} M + p_3^{c,T} \ln\left(R + p_4^{c,T} \exp\{p_5^{c,T} M\}\right) + p_6^{c,T} S + p_7^{c,T} F + p_8^{c,T} D$$

Y ≡ ground-motion parameter—either peak ground acceleration (PGA), or peak 5 percent-damped pseudo-spectral velocity (PSV); units of PGA: [PGA] = g; units of PSV: [PSV] = cm/sec
M ≡ moment magnitude, M_w
R ≡ closest distance from site to fault rupture surface in km
S ≡ site classification code: $S = 0$ for site class B, $S = 1$ for site class C
F ≡ fault-type code: $F = 0$ for strike-slip, $F = 1$ for reverse
D ≡ depth to basement in km

Horizontal Component

Ground-Motion	Period				Attenuation Equation Coefficients					
Parameter, $Y^{H,T}$	T [sec]	$p_1^{H,T}$	$p_2^{H,T}$	$p_3^{H,T}$	$p_4^{H,T}$	$p_5^{H,T}$	$p_6^{H,T}$	$p_7^{H,T}$	$p_8^{H,T}$	$\sigma_{\ln Y}^{H,T}$
PGA	...	−3.936006	1.131331	−1.407338	0.132766	0.762349	...	0.222134	...	0.423165
PSV(T, ξ=5%)	0.04	−1.357995	1.047913	−1.454411	0.238403	0.672454	...	0.191981	...	0.422150
⋮	0.10	1.583506	1.007164	−1.732633	0.566841	0.581291	...	0.222755	...	0.492162
⋮	0.15	2.655102	0.891582	−1.658653	1.057827	0.474372	...	0.182737	...	0.461422
⋮	0.20	3.797246	1.150935	−2.090457	2.707418	0.429144	...	0.197572	...	0.458925
⋮	0.30	1.757966	0.964154	−1.399615	1.068671	0.433155	...	0.191845	...	0.460916
⋮	0.40	−0.341344	1.143885	−1.184304	0.040152	0.855455	...	0.283950	...	0.441457
⋮	0.50	−1.250108	1.262700	−1.132481	0.023059	0.904682	...	0.322455	...	0.439150
⋮	0.60	−1.308109	1.174087	−0.985260	0.021467	0.826603	...	0.291465	...	0.453652
⋮	0.80	−1.678807	1.291551	−1.039450	0.019647	0.909185	...	0.172694	...	0.490725
⋮	1.00	−1.862627	1.355410	−1.053069	0.023326	0.942043	...	0.038112	...	0.534120
⋮	1.50	−4.012763	1.608815	−0.962336	0.008855	1.051218	...	−0.060261	...	0.568799
⋮	2.00	−4.228495	1.526558	−0.822749	0.003465	1.038725	...	−0.213967	...	0.597052
⋮	3.00	−5.897752	1.747070	−0.834153	0.002207	1.057780	...	−0.216479	...	0.663833
PSV(T, ξ=5%)	4.00	−6.735449	1.776420	−0.716986	0.001572	1.042894	...	−0.163145	...	0.709761

Vertical Component

Ground-Motion	Period				Attenuation Equation Coefficients					
Parameter, $Y^{V,T}$	T [sec]	$p_1^{V,T}$	$p_2^{V,T}$	$p_3^{V,T}$	$p_4^{V,T}$	$p_5^{V,T}$	$p_6^{V,T}$	$p_7^{V,T}$	$p_8^{V,T}$	$\sigma_{\ln Y}^{V,T}$
PGA	...	−1.725546	0.764676	−1.548369	18.364196	−0.067773	...	0.285830	...	0.611885
PSV(T, ξ=5%)	0.04	0.526387	0.759216	−1.635060	88.127107	−0.363091	...	0.373243	...	0.676089
⋮	0.10	1.213682	0.945844	−1.766289	11.354476	−0.041997	...	0.503098	...	0.688235
⋮	0.15	1.813103	0.719528	−1.407318	24.071591	−0.166183	...	0.398727	...	0.654138
⋮	0.20	1.524304	0.783045	−1.372194	42.942093	−0.226298	...	0.326083	...	0.667097
⋮	0.30	0.064487	0.781080	−0.972995	11.989361	−0.084220	...	0.361985	...	0.570768
⋮	0.40	−0.956925	0.939824	−0.942038	1.182603	0.289582	...	0.346593	...	0.557090
⋮	0.50	−2.410384	1.145846	−0.898898	0.091114	0.700216	...	0.370380	...	0.512922
⋮	0.60	−2.719244	1.097141	−0.757253	0.025803	0.743329	...	0.477149	...	0.564777
⋮	0.80	−2.465013	1.092663	−0.798560	0.016309	0.891525	...	0.416272	...	0.565420
⋮	1.00	−2.582774	1.108626	−0.767066	0.012798	0.915573	...	0.235089	...	0.550268
⋮	1.50	−4.140309	1.330392	−0.706613	0.003076	1.158884	...	0.041385	...	0.601047
⋮	2.00	−4.136549	1.366826	−0.766809	0.012379	1.006751	...	−0.119997	...	0.663141
⋮	3.00	−6.962224	1.810674	−0.799058	0.010925	1.065098	...	−0.156364	...	0.762751
PSV(T, ξ=5%)	4.00	−7.663303	1.787413	−0.650318	0.006922	1.017589	...	−0.115178	...	0.843241

Equation Set (16)

$$\ln Y^{c,T} = p_1^{c,T} + p_2^{c,T} M + p_3^{c,T} \ln\left(R + p_4^{c,T} \exp\left(p_5^{c,T} M\right)\right) + p_6^{c,T} S + p_7^{c,T} F + p_8^{c,T} D$$

Y ≡ ground-motion parameter—either peak ground acceleration (PGA), or peak 5 percent-damped pseudo-spectral velocity (PSV); units of PGA: [PGA] = g; units of PSV: [PSV] = cm/sec
M ≡ moment magnitude, M_w
R ≡ closest distance from site to fault rupture surface in km
S ≡ site classification code: $S = 0$ for site class B, $S = 1$ for site class C
F ≡ fault-type code: $F = 0$ for strike-slip, $F = 1$ for reverse
D ≡ depth to basement in km

Horizontal Component

Ground-Motion Parameter, $Y^{H,T}$	Period T [sec]	Attenuation Equation Coefficients $p_1^{H,T}$	$p_2^{H,T}$	$p_3^{H,T}$	$p_4^{H,T}$	$p_5^{H,T}$	$p_6^{H,T}$	$p_7^{H,T}$	$p_8^{H,T}$	$\sigma_{\ln Y}^{H,T}$
PGA	...	−2.722823	1.105448	−1.683807	0.425417	0.602958	...	0.183172	0.024488	0.400847
PSV(T, ξ=5%)	0.04	−0.453568	1.049550	−1.701597	0.531022	0.566631	...	0.198691	0.027820	0.399926
⋮	0.10	2.906963	1.136391	−2.222362	1.154496	0.511344	...	0.152023	0.026946	0.454405
⋮	0.15	4.343899	0.897721	−2.040535	2.539610	0.373475	...	0.177455	0.002064	0.447224
⋮	0.20	4.693018	1.134157	−2.302479	3.463922	0.384564	...	0.193536	0.015694	0.456061
⋮	0.30	2.068472	1.071210	−1.641261	0.841904	0.493745	...	0.227100	0.000130	0.412342
⋮	0.40	0.601977	1.068338	−1.317495	0.101083	0.731723	...	0.318640	0.015198	0.456408
⋮	0.50	0.004364	1.133078	−1.265281	0.201827	0.607581	...	0.326197	0.033414	0.437589
⋮	0.60	−0.538696	1.144968	−1.175065	0.243775	0.525161	...	0.287624	0.047093	0.441287
⋮	0.80	−2.111858	1.431323	−1.207824	0.017393	0.969773	...	0.220262	0.048159	0.443601
⋮	1.00	−2.591393	1.521160	−1.192724	0.013925	1.038309	...	0.074162	0.047710	0.442444
⋮	1.50	−3.325758	1.446800	−0.921095	0.010806	0.991039	...	−0.142566	0.061650	0.472638
⋮	2.00	−3.596462	1.384646	−0.752811	0.006434	0.946916	...	−0.377579	0.065902	0.465185
⋮	3.00	−5.665602	1.634462	−0.702852	0.002569	1.010255	...	−0.307991	0.070062	0.497140
PSV(T, ξ=5%)	4.00	−6.133363	1.575226	−0.534287	0.001843	0.882245	...	−0.182212	0.085524	0.559842

Vertical Component

Ground-Motion Parameter, $Y^{V,T}$	Period T [sec]	Attenuation Equation Coefficients $p_1^{V,T}$	$p_2^{V,T}$	$p_3^{V,T}$	$p_4^{V,T}$	$p_5^{V,T}$	$p_6^{V,T}$	$p_7^{V,T}$	$p_8^{V,T}$	$\sigma_{\ln Y}^{V,T}$
PGA	...	0.669394	0.644169	−1.888426	31.869138	−0.095439	...	0.103491	−0.016777	0.623173
PSV(T, ξ=5%)	0.04	3.434138	0.525762	−1.939816	136.682583	−0.373788	...	0.102450	−0.014754	0.651286
⋮	0.10	3.956864	0.910670	−2.270291	12.072915	0.055295	...	0.200860	−0.014682	0.693841
⋮	0.15	4.726885	0.552329	−1.806007	29.716172	−0.105575	...	0.229435	−0.003107	0.657990
⋮	0.20	3.911835	0.500999	−1.520666	118.213507	−0.343504	...	0.173085	−0.030268	0.679890
⋮	0.30	3.362888	0.490733	−1.311406	65.800181	−0.260923	...	0.178855	−0.015658	0.491104
⋮	0.40	1.365266	0.720016	−1.159498	11.266933	−0.019657	...	0.132407	−0.027266	0.480460
⋮	0.50	−0.486943	0.844271	−0.915951	9.014459	−0.081244	...	0.262286	−0.033728	0.433697
⋮	0.60	−0.595461	0.780898	−0.799571	2.048703	−0.004686	...	0.396638	−0.044864	0.428560
⋮	0.80	−1.051411	0.879716	−0.829975	0.011837	0.864018	...	0.326888	−0.044304	0.419317
⋮	1.00	−1.922788	0.987203	−0.709449	0.006926	0.893816	...	0.164202	−0.068869	0.431408
⋮	1.50	−3.225348	1.114051	−0.559256	0.001821	0.991820	...	−0.109495	−0.033227	0.519725
⋮	2.00	−3.991431	1.294437	−0.696769	0.010816	0.985673	...	−0.272321	0.024126	0.546003
⋮	3.00	−4.708215	1.361602	−0.623787	21.502256	−0.119324	...	−0.361965	0.062479	0.619146
PSV(T, ξ=5%)	4.00	−5.626069	1.365882	−0.467435	12.966326	−0.248231	...	−0.202523	0.068878	0.744878